POLITECNICO DI TORINO

Doctorate School
Doctorate in Metrology: Measurements Science and Technique - XIV Cycle

Doctoral Thesis

Timing Experiments with Global Navigation Satellite System Clocks

Supervisors:
Prof. Elio Bava (Polytechnic University of Turin)
Dott.ssa Patrizia Tavella (INRIM)
Dott.ssa Ilaria Sesia (INRIM)

Author:
Alice Cernigliaro

March 2012

Contents

List of Figures

List of Tables

Acknoledgments

First, I would like to thank Ilaria Sesia for the precious role she covered in my training, for her patience and availability to give me advice and teaching me.
I wish to express my gratitude to Dr. Patrizia Tavella, who was able to find the time to give answer to all my doubts.
A special thanks goes to my family: without their strong affection and continuous support I would never be arrived here today, writing this thesis.
Finally, I cannot forget to thank Manuel, who always encouraged me, supported me, and has constantly been present.

Introduction

The science of timekeeping is crucial in many different applications around the world: precise time is fundamental in communication systems, electrical power grids, financial networks, astronomy, atmospheric studies, aviation...
One of the most significative applications in which time and frequency metrology has an essential role are Global Navigation Satellite Systems (GNSS). Any satellite navigation system indeed, is based on the transmission of signals from a constellation of satellites: processing these signals it is possible to estimate the position of a user, provided that the time of transmission is indicated with extremely high accuracy. In fact, being the distance measured from a time, any error in the measure of time will be directly mapped into an error in the user position, which has to be kept below its specified limits. Signals travel at the speed of light, therefore small fractions of seconds have to be measured accurately.
In order to determine the user position, the time when the signal left the satellite and when it arrived at the receiver have to be known precisely.
The positioning accuracy is widely determined by the clocks quality. It is why all the satellites need to fly very accurate atomic clocks: fundamental for their excellent stability.
An agreement between the European Community and the European Space Agency (ESA) gave rise to a new European satellite system: Galileo.
At present, the Galileo system is still under development, through the cooperation of many research laboratories and industries located all over Europe.
The *Istituto Nazionale di Ricerca Metrologica* (INRiM) is deeply involved in the Galileo project, mainly concerning the activities related to the experimental phases, such as the generation of an experimental reference time scale for the system and the metrological characterization of atomic clocks employed onboard satellites.
The first contribution of INRIM to the Galileo project was on 2000, during the first experimental phase named Galileo System Test Bed V1, whose main objective was the realization of the Experimental Galileo System Time, the time scale for the Galileo system.
During my years of doctorate at INRIM, I participated at the activities on the Galileo project: I was involved in the second experimental phase, the *GIOVE Mission*. In particu-

lar, I was in charge of the characterization of the clocks on board the first two experimental satellites, GIOVE-A and GIOVE-B. For this purpose, I contributed to the analysis of the experimental results, to the development of specific statistical algorithms, and to the realization of some software routines for clock characterization. In the last year, I had the possibility to participate to the implementation of the Galileo *Time Validation Facility*, the infrastructure in charge of the timing activities in the frame of the In Orbit Validation phase, for the launch of the first satellites of the Galileo system. In this project my role is the responsibility of the clock validation activity.
The Galileo Time Validation Facility has been developed and installed at INRIM and it is now operating continuously, in real time with completely automated process, ensuring the generation of the timing products necessary in the current phase of the Galileo project.
The present thesis reports the activities and part of the analysis performed in these years of doctorate, concerning the timing experiments as support to Global Navigation Satellite Systems, in particular in the frame of the experimental phases of the Galileo project.
In Chapter 1 the fundamentals of satellite navigation systems are summarized, as well as the basic concepts of time and frequency metrology, reviewing the main definitions and the functioning of atomic clocks and time scales.
Chapter 2 describes the main satellite navigation systems currently operative: the American Global Positioning System, and the architecture of the European Galileo system.
Chapter 3 presents the activity of metrological characterization of satellite clocks, carried out in these years of doctorate: some representative results are reported, together with the description of the software realized for the analysis.
In Chapter 4 some analysis on GNSS clocks are reported.
It has to be remarked that, because of the confidentiality agreement established between INRIM and the European Space Agency, the experimental results related to the Galileo clocks cannot be reported, unless they have been already published in articles or conferences. Hence, the results illutrated in ths thesis, are related to GPS public data, or they are results already presented by ESA at international conferences, or they have been obtained through simulations.

Chapter 1

Time and Frequency Metrology in Satellite Navigation Systems

Time and frequency metrology has an essential role in satellite navigation systems: clocks accuracy and stability determine the quality of the positioning service.
For this reason, the use of atomic clocks is fundamental in these applications.
Moreover, Global Navigation Satellite Systems have a double scope: they allow to determine

1. the location of a user or a specific place, in terms of latitude, longitude and height coordinates
2. the exact time, in terms of the international time scale known as UTC (Universal Time Coordinated)

1.1 Fundamentals of Satellite Navigation

The determination of the position of user, even mobile, is allowed by a proper use of the signals broadcast by a constellation of satellites.
Navigation is a *real time* process: it must be possible to estimate instantaneously user's *Position, Velocity and Time* (PVT). The receiver position can be determined measuring the *Time of Arrival* (TOA): the time for a signal transmitted by a satellite at a known location to reach the user's receiver [1].
Global navigation satellite systems (GNSS) -such as GPS and the future Galileo- are spherical positioning systems. In a spherical positioning system the receiver evaluates the TOA of the signal incoming from a set of transmitters placed at known locations: the propagation time is proportional to the absolute distance between the receiver and each satellite of the constellation. The locus of possible positions is a sphere centered in the transmitter

and with radius equal to the distance from the transmitter itself (R_i).
To estimate the distance R_i between the i-th satellite of the constellation and the receiver, the time has to be multiplied by the speed of light: assuming that the receiver clock and the satellite transmitter are perfectly synchronized, the distance is given by:

$$R_i = c \cdot \tau$$

where c is the speed of light in vacuum and τ is the TOA.
The precise user position is then obtained using a procedure called *Trilateration*: the receiver location is the result of the intersection of at least three of the spheres mentioned above. The second point given by the intersection can be easily rejected, being in the deep space.

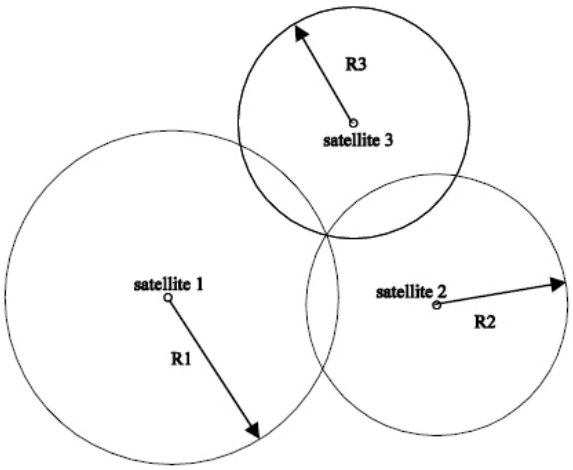

Figure 1.1: Spherical Positioning System

The hypothesis of synchronization between satellite clocks and user receiver is not realistic. In fact, while satellite clocks are very stable and are kept synchronized among them and aligned to the reference time scale (see section 1.2.3 for details on time scales), the user clock, realized with low cost and complexity, is most likely not aligned to the satellite clocks.
The misalignment between the satellite and the user time scales produces a bias ϵ in the measure of the distance.
Figure 1.2 shows the effect of the receiver clock bias on the trilateration procedure: it can be observed that an error in the measure of time originates an error on the positioning.

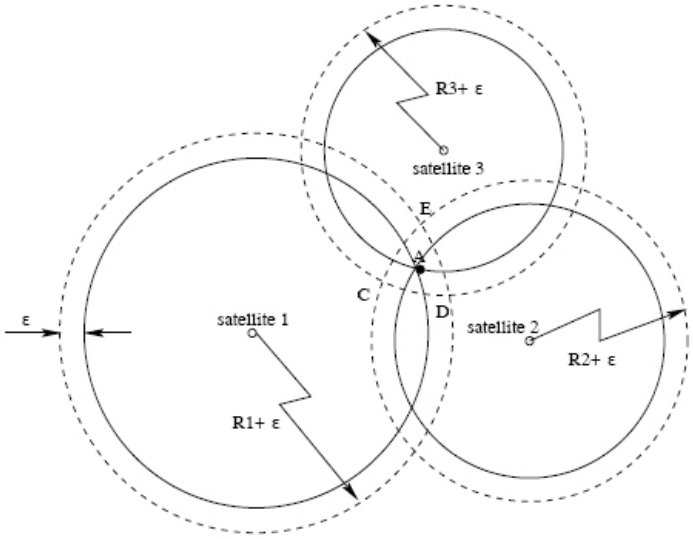

Figure 1.2: Effect of the receiver clock bias on the positioning

Since it is not possible to perfectly measure the time of arrival τ but there is a bias, the receiver does not measure the geometrical distance but a *pseudorange* ρ, defined as the sum of the true distance R_i from the i-th satellite and a term ϵ due to the time scale misalignment:

$$\rho_i = R_i + \epsilon \tag{1.1}$$

Defining the the clock synchronization bias of the user δt_u, Eq. 1.1 can be written as [1]:

$$\rho_i = R_i + \epsilon = R_i + c \cdot \delta t_u$$

To estimate the user position it is then necessary the use of a further satellite, since the unknowns in the system are at least four.
Introducing the user coordinates x_u, y_u, z_u, and the coordinates of the satellites x_{S_i}, y_{S_i}, z_{S_i}, which are transmitted in the navigation message, the user location and the bias δt_u, representing the misalignment between the user clock and the satellite clock, can be obatined solving the following equations [1]:

$$|\rho_1| = \sqrt{(x_{S_1} - x_u)^2 + (y_{S_1} - y_u)^2 + (z_{S_1} - z_u)^2} + c \cdot \delta t_u$$
$$|\rho_2| = \sqrt{(x_{S_2} - x_u)^2 + (y_{S_2} - y_u)^2 + (z_{S_2} - z_u)^2} + c \cdot \delta t_u$$

$$|\rho_3| = \sqrt{(x_{S_3} - x_u)^2 + (y_{S_3} - y_u)^2 + (z_{S_3} - z_u)^2} + c \cdot \delta t_u$$
$$|\rho_4| = \sqrt{(x_{S_4} - x_u)^2 + (y_{S_4} - y_u)^2 + (z_{S_4} - z_u)^2} + c \cdot \delta t_u$$

It has to be remarked that, in order to estimate the receiver position, at least the signal of four satellites has to be tracked.

1.1.1 Impact of Measurement Errors on the User Position

GNSS accuracy in the user position depends on several factors, in particular on the quality of pseudorange measurements and satellite ephemeris[1]. The uncertainty on the pseudorange value is called *User Equivalent Range Error* (UERE)[1].
The inpact of the UERE on the final user position depends also on the geometry of satellites in view, i.e their dislocation in the sky.

1.1.1.1 Pseudorange Errors

A single pseudorange, for a generic satellite S_j, is represented by:

$$|\rho_j| = \sqrt{(x_{S_j} - x_u)^2 + (y_{S_j} - y_u)^2 + (z_{S_j} - z_u)^2} + c \cdot \delta t_u$$

If each error source is modelled as an independent Gaussian random variable with zero mean and standard deviation σ_i, the uncertainty on the pseudorange value can be defined as:

$$\sigma_{UERE} = \sqrt{\sum_i \sigma_i^2}$$

Ranging errors are grouped into the six following classes [3]:

1. *Ephemeris data*: Errors in the transmitted location of the satellite
2. *Satellite clock*: Error in the transmitted clock, including SA[2] for GPS
3. *Ionosphere*: Errors in the pseudorange caused by ionospheric effects not perfectly compensated
4. *Troposphere*: Errors in the pseudorange caused by tropospheric effects not perfectly compensated

[1] a set of orbit parameters used to calculate the location and orientation of satellites
[2] Selective Availability: intentional disturb to limit the accuracy of GPS civil use

5. *Multipath*: Errors caused by reflected signals in the receiver antenna

6. *Receiver*: Errors in the receiver's measurement of range, caused by thermal noise, software accuracy etc.

Table 1.1 reports a quantitative example (on GPS) of the impact of the different error sources in the positioning [3] for a single frequency receiver:

Error Source	**Positioning Error** (1σ)
Ephemeris Prediction	2.1 m
Satellite Clock	2.1 m
Ionosphere	4.0 m
Troposphere	0.7 m
Multipath	1.4 m
Receiver	0.5 m

Table 1.1: Example of the Impact of the Different Error Sources in the Positioning (GPS), single frequency receiver

The different error sources are described in the subsequent paragraphs.

1.1.1.1.1 Ephemeris Error

Ephemeris errors occur when the navigation message does not transmit the correct satellite location [3]. Since the navigation message contains the predictions of satellite position, the errors tend to grow with time from the last upload from the control station. Ephemeris errors are slowly changing with time, and are closely correlated with the satellite clock.

1.1.1.1.2 Satellite Clock Error

As previously pointed out, all satellites carry atomic clocks to control all timing operations, including the signal generation and broadcast. Although these clocks are highly stable, a little deviation from the reference time scale is possible. It is experimentally observed that in GPS this deviation can be up to 10 ns from GPS Time: as a consequence a ranging error of the order of 3 meters (1σ) may occur.
To compensate for these errors the *Master Control Station* (MCS) evaluates and transmits clock correction parameters to all the satellites, which have to broadcast them to the user

through the navigation message.
The estimated terms to be used to evaluate the corrective parameter δ_t are reported in the navigation message and usually are part of a polynomial model, as in the following example:

$$\delta_t = a_{f_0} + a_{f_1}(t - t_{oc}) + a_{f_2}(t - t_{oc})^2 + \Delta_{t_r}$$

Where t_{oc} is the clock data reference time, t is the current time, and Δ_{t_r} is the correction for the relativistic effects.
a_{f_0}, a_{f_1} and a_{f_2} are the coefficients of the polynomial correction to be implemented.

1.1.1.1.3 Ionosphere Error

The atmosphere causes some small but non negligible effects. In fact, when the satellite signal passes through the atmosphere, it encounters a number of propagation effects, whose magnitude depends on the elevation angle of the signal path and on the atmospheric environment where the user is located [3].
These effects include the ionospheric group delay and scintillation.
The ionosphere is a region of ionized gases, and varies significantly from day to day, depending on the solar conditions and it experiences also large diurnal fluctuations. The ionization is mainly caused by the radiation of the Sun. The ionosphere presence changes the signal propagation velocity ν, according to the refractive index $n = c/\nu$. The refractive index n, varies along the propagation path r: n(r). The refractive index of the ionosphere, varies with the frequency because of the ionized gases.
The effects which can be caused on the satellite signal are the following:

- a combination of *group delay* and *carrier phase advance*, which varies with the paths and the electron density through which the signal traverses the ionosphere
- the ionospheric *scintillation* which, at some latitudes, can cause the receiver signal amplitude and phase to fluctuate rapidly with time

The ionosphere is characterizaed by the *Total Electron Content* (TEC), defined as *the number of electrons in a tube of 1 m^2 cross section from receiver to satellite.*
The delay $\Delta\tau$ introduced by the ionosphere on the satellite signal varies inversely with the squared frequency, and causes an error I_ρ on the pseudorange:

$$I_\rho = \frac{40.3 \cdot TEC}{f^2}$$

Where f is the signal frequency.
The ionospheric delay can be compensated using different methods depending on the receiver type: single frequency or multiple frequency receivers.

Since the ionosphere is a dispersive medium, its effect depends on the frequency: hence, using double frequency receivers, the delay can be estimated and compensated. Being ρ_1 and ρ_2 the pseudoranges measures at two different frequencies f_1 and f_2, they can be expressed in terms of the iono-free pseudorange ρ:

$$\rho_1 = \rho + \frac{40.3 \cdot TEC}{f_1^2}$$

$$\rho_2 = \rho + \frac{40.3 \cdot TEC}{f_2^2}$$

Solving for ρ and TEC the set of equations, we obtain:

$$\rho = \frac{f_1^2}{f_1^2 - f_2^2}\rho_1 + \frac{f_2^2}{f_1^2 - f_2^2}\rho_2$$

Multiple frequency receiver are therefore able to compensate for the error introduced by the ionosphere presence.
Single frequency receivers can compensate for this error source modelizing the ionosphere using the parameters broadcast from satellites. Two widely used models for the ionosphere are the *Klobuchar model* and the *NeQuick model*.

1.1.1.1.4 Troposphere Error

Another deviation from the vacum speed of light is caused by the troposphere [3]. The speed of light of radio waves undergo variations due to temperature, pressure and humidity changings which causes the alteration of the tropospheric refractive index.
The troposphere is a zone of dry gases and water vapour extended up to 50 km from the Earth surface. It is non-dospersive for frequencies up to 15 GHz.
Refractivity is often modelled using dry and wet components: the dry layer extends to a height of about 40 km and generates about the 90% of the tropospheric delay, the wet component extends to a height of about 10 km.
The dry component can be predicted very accurately. The wet component, on the contrary, is more difficult to predict, due to the uncertainties in the atmospheric distribution. The tropospheric delay also depends on the user height, since the dry and wet component refractivities depend on the atmospheric conditions at the user height.
Different models for tropospheric delay compensation are presented in literature: the classical ones are the *Hopfield* model and the *Kaplan* [4] model. Both models provide an estimation of the dry and wet components of the troposphere, which can be used at the receiver to compenste for the error introduced by the delay.

1.1.1.1.5 Multipath Error

The multipath error is caused by the reflected signals (from buildings, vehicles, etc.) which

enter on the front end of the receiver and which mask the real correlation peak, needed to decode the satellite signal [3], or generating its distortion, degrading the pseudoranges. It is one of the major error sources. Such effects tend to be more pronounced near large reflecting surfaces and, in some cases, more than 15 m of ranging error can be reached.
Multipath effects can be mitigated using the combination of antenna cut-off angle and antenna location: the antenna should be placed above the highest reflector to prevent reflected waves above the horizon.
A second approach is the used of the so called *narrow correlator* receivers, which tend to minimize the multipath impact.

1.1.1.1.6 Receiver Error

In the receivers, the dominant source of pseudorange measurement error is the thermal noise. In addition, there are the error sources due to hardware and software resolution, and to the oscillator stability.

1.2 Atomic Clocks and Time Scales

1.2.1 Basic Definitions

A precision oscillator generates a voltage which generally can be expressed as [5], [6]:

$$V(t) = [V_0 + a(t)] \sin[2\pi\nu_0 t + \phi(t)] \tag{1.2}$$

where:

V_0 : nominal amplitude of the signal
ν_0 : nominal frequency of the signal
$a(t)$: random amplitude variations
$\phi(t)$: random phase variations

It can be assumed that the amplitude fluctuations $a(t)$ are negligible around V_0.
The nominal frequency ν_0 at which the standard is designed to work, by definition, does not vary with time. All phase variations around the nominal accumulated phase $2\pi\nu_0 t$ are denoted with $\phi(t)$.

The oscillator istantaneous frequency can be written as:

$$\nu(t) = \nu_0 + \frac{1}{2\pi}\frac{d}{dt}\phi(t) \tag{1.3}$$

From Eq. 1.2 and Eq. 1.3 the following quantities can be defined:

Normalized Frequency Deviation
The normalized frequency deviation $y(t)$ is a dimensionless quantity defined as the fractional deviation of the free running frequency $\nu(t)$ from its nominal value ν_0:

$$y(t) = \frac{\nu(t) - \nu_0}{\nu_0} \tag{1.4}$$

Conceptually $y(t)$ represents the relative offset from the ideal. Even though it is a conceptual value, in practice $y(t)$ is very useful since it is a small number compared to $\nu(t)$, and it allows comparisons among sources at different frequencies easily.
In this thesis, the term *frequency* in Chapter 3 and 4 will always refer to the nomarlized frequency.

Time Deviation
Integrating the normalized frequency offset $y(t)$ yields the time deviation $x(t)$, which has the dimensions of a time:

$$x(t) = \int_0^t y(t')dt' \tag{1.5}$$

The time deviation can be written as a function of the phase deviation:

$$x(t) = \frac{\phi(t)}{2\pi\nu_0} \tag{1.6}$$

Since time deviation $x(t)$ and phase deviation $\phi(t)$ are directly proportional, sometimes the two terms are used intercheangeably.

In the discrete time domain, being the normalized frequency offset the time derivative of the time offset, we can write:

$$y_i = \frac{1}{\tau_0}[x_{i+1} - x_i] \tag{1.7}$$

Where τ_0 is the minimum data spacing, x_i and x_{i+1} are two consecutive time offset samples.

Clock Model

In general, a model for a clock is:

$$x(t) = x_0 + y_0 t + \frac{1}{2} D t^2 + \epsilon(t) \tag{1.8}$$

Where x_0 is initial phase offset (also called synchronisation error), y_0 is the initial frequency offset (also called syntonisation error), D is the *frequency drift* and $\epsilon(t)$ represents the random variations (environmental perturbations, noise deviations etc.).
It has to be remarked that the model in Eq. 1.8, even if quite general and useful, does not apply in all cases. In fact, some oscillators present significant frequency-modulation sidebands, in others the frequency drift D is not constant...For Cesium Beam oscillators for example, a better model is setting $D = 0$.
Taking the derivative of the model in Eq. 1.8 yields to a linear model on the frequency, represented in Eq. 1.9:

$$y(t) = y_0 + Dt + \dot{\epsilon}(t) \tag{1.9}$$

1.2.2 Atomic Clocks

A key feature of GNSS is time keeping. One of the most critical technologies for GNSS developers is the realization and employment of accurate timing standards, ensuring that all satellites clocks remain as much as possible synchronized and permitting user receivers to operate with low cost clocks.
The only devices presenting the required characteristics of accuracy and stability needed to ensure the high accuracy positioning of GNSS systems are atomic clocks. In any navigation system atomic clocks are used onboard satellites as well as in the control segment.
Atomic Frequency Standards are devices characterized by excellent performances of frequency stability, accuracy and reproducibility. This is a consequence of the fact that the

output frequency of the standard is the result of the inherent property of an atom. Hence, in principle, all standards using the same atom should have the same frequency [7].
The basic resonant system is an atom or a molecule experiencing transitions between two well defined energy levels inside the hyperfine structure of their ground state [8].
A given atomic or molecular transition occurs at a well defined frequency ν_0, such that, being $(E_2 - E_1)$ the energy difference between two atomic or molecular levels

$$h\nu_0 = E_2 - E_1$$

where h is the Planck's constant.
Such transition can be used to build a frequency and time reference, which will produce the same frequency or time scale.
Atomic clocks are atomic frequency standards under continuous operation, which deliver signals at time intervals of one second or submultiples of one second.
The current definition of the *second* is based on atomic clocks: in 1967 it was agreed, during the 13^{th} General Conference of Weights and Measures (CGPM), that *the second is the duration of 9 192 631 770 periods of the radiation correponding to the transition between the two hyperfine levels of the ground state of the cesium-133 atom* [9].
In any atomic frequency standard atoms or molecules are not completely free and are not at rest inside the device. Therefore it could happen that the transition frequency is slightly shifted from the nominal frequency expected in ideal conditions: the degree of conformity of a measured frequency to its definition is named *accuracy* [10]. Since the accuracy is related to the offset from an ideal value, frequency accuracy is usually stated in terms of the frequency offset [11].
The *Frequency stability* is defined as *the spontaneous and/or evironmentally-caused frequency change of a signal within a given time interval* [11]. It is therefore a measure of the degree to which the frequency stays constant after the oscillator is set in operation. The concept of stability and the statistics used to compute the frequency stability will be treated in Section 3.2.2.1
Atomic frequency standards of various type are available commercially, finding a large number of applications: navigation and time keeping, but also basic research, geophysical exploration, radio astronomy, communications,tracking systems, etc.
The atomic frequency standard to be used for a specific application is chosen taking into account factors such as frequency stability, accuracy, weight, size, power consumption, etc. In particular, for space applications, it is extremely advantageous to have small, lightweigthed clocks, whose power consumption is moderate. In addition, in navigation systems it is really important the clock frequency stability.
The classical atomic frequency standards used in navigation are illustrated in this section:

hydrogen masers, cesium beam and rubidium frequency standards.

1.2.2.1 Rubidium Atomic Frequency Standards (RAFS)

Rubidium oscillators operate at the resonance frequency of the Rubidium atom Rb-87 and use the Rubidium frequency to control a Quartz oscillator [10].
A scheme of Rubidium clocks functioning is illustrated in Fig. 1.3:

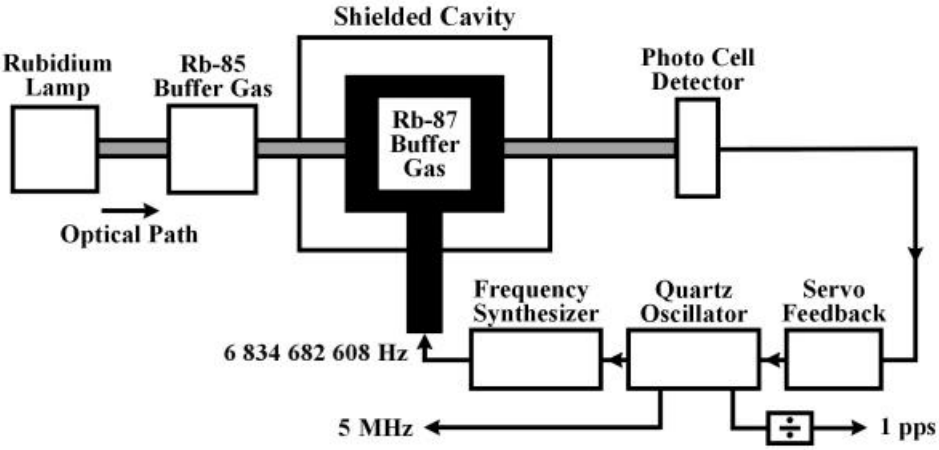

Figure 1.3: Rubidium Atomic Frequency Standards Scheme [10]

An optical beam from the Rubidium lamp pumps the Rb-87 buffer gas atoms in a particular energy state. The frequency synthesizer produces microwaves which induce transitions to a different energy state: the absorption of the optical beam by the Rb-87 buffer gas is increased.
The output of the photo cell detector, which measures the portion of beam absorbed, is used to tune a quartz crystal, which drives the synthesizer, oscillator to a frequency such that the amount of light absorption is maximized. The quartz oscillator is then locked to the resonance frequency of rubidium.
Rubidium oscillators are the less expensive atomic frequency standards: they present a long-term stability much better than the one of quartz oscillators, they are smaller, more reliable, and less expensive than cesium oscillators. They are largely employed in satellite navigation systems [12].
Frequency stability at 1 s is typically $1 \cdot 10^{-11}$ and at 1 day it is at the level of $1 \cdot 10^{-12}$.

The long-term stability is limited by shifts in the resonance frequency, mainly due to the collisions of the rubidium atoms with other buffer gas molecules and aging effects in the lamp system.

1.2.2.2 Cesium Beam Frequency Standards

The first cesium 133 beam tube resonator was built in 1952. In 1955 the National Physical Laboratory (NPL) in England built the first cesium-beam clock used as a calibration source: the frequency of the hyperfine transition was determined with reference to the available astronomical time scale [8]. In 1958 the cesium hyperfine transition was determined in terms of the previously defined Ephemeris second [13]: the result of this measurement was the basis of the present definition of the second [11]. Since the SI second is defined from the resonance frequency of the cesium atom (^{133} Cs), cesium beams can be primary frequency standards.
A scheme of a cesium beam frequency standard is illustrated in Fig. 1.4:

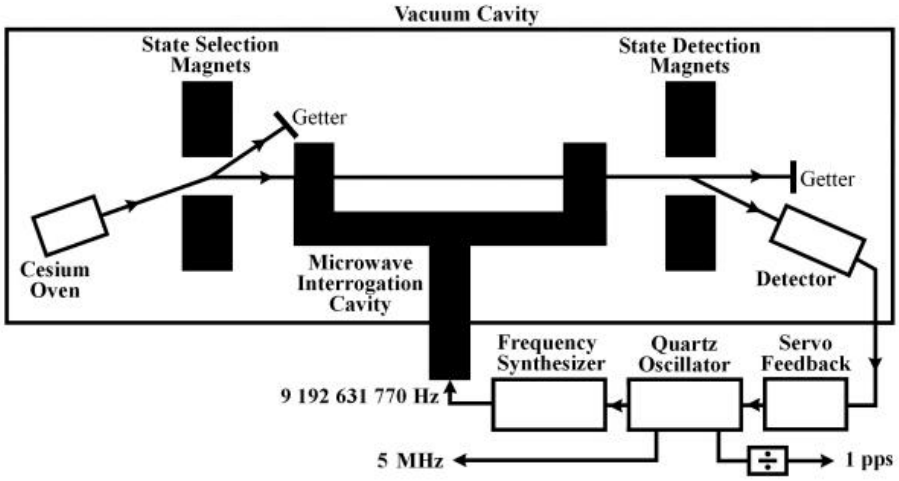

Figure 1.4: Cesium Beam Frequency Standard Scheme [10]

In cesium oscillators, the ^{133} Cs atoms are heated to a gaseous state in an oven [10]. Atoms from the gas leave the oven in a high-velocity beam that travels through a vacuum tube towards a couple of magnets. Only atoms of a particular magnetic energy state pass through the gate consituted by the magnets and go into a microwave cavity. In such cavity, the cesium atoms are exposed to a microwave frequency derived from a quartz oscillator:

if the microwave frequency matches the resonance frequency of cesium, the cesium atoms change their magnetic energy state. Then, the atomic beam passes through another magnetic gate near the end of the tube. Only the atoms which changed their energy state when passing through the microwave cavity are allowed to proceed to the detector located at the end of the tube. On the contrary, the atoms which didn't change their stare are deflected away. The detector produces a feedback signal that continually tunes the quartz oscillator: the number of atoms reaching the detector is maximized. Then, the standard output frequencies are derived from the locked quartz oscillator.
The impact in science and technology of cesium beam frequency standards and clocks is very high [8]: they realize the definition of the second, they are used in tests of the theory of relativity, and they are employed on board satellites in satellite navigation systems such as GPS.
The frequency stability at 1s is typically $5 \cdot 10^{-12}$ and the noise floor, around $1 \cdot 10^{-14}$, is reached at about 1 day.

1.2.2.3 Hydrogen Masers

MASER is the acronym of Microwave Amplification of Stimulated Emission of Radiation. Hydrogen masers are implemented in two different ways: the *active maser*, which is an oscillator, and the *passive maser*, which acts as an amplifier [7]. *Active* atomic frequency standards are those frequency standards which are able to oscillate at the atomic resonance frequency. On the contrary, in the *Passive* atomic frequency standards the atomic resonance has to be stimulated by an electromagnetic signal at the proper frequency, which is produced by an auxiliary frequency generator [8]. Hydrogen maser are the most elaborate and expensive frequency standards commercially available.
A schematic representation of an hydrogen maser is illustrated in Fig. 1.5 [10]:

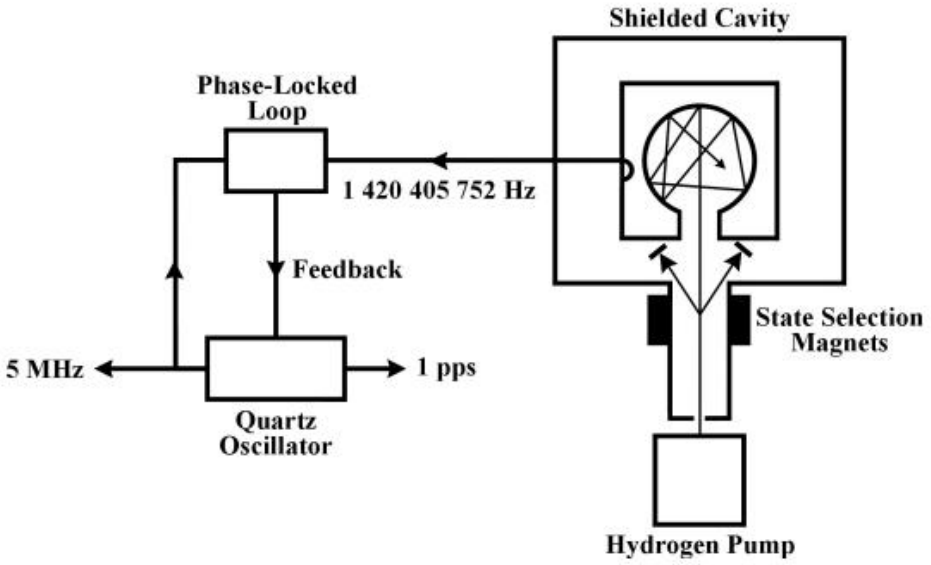

Figure 1.5: Hydrogen Maser Scheme [10]

These clocks operate at the resonance frequency of the hydrogen atom: 1420405752 Hz. Precisely, the atomic transition involved is the F=1, $m_F = 0 \leftrightarrow F = 0, m_F = 0$ transition in the hyperfine structure of atomic hydrogen in the gorund state, with a frequency near to 1420 MHz [8]. The hydrogen atoms are separated in two groups according to the direction of the electron spin, paraller or antiparallel, relative to the applied field. If a non homogeneous magnetic field is applied, a force is developed and the two groups of atoms are deflected in different directions and the state selection can be performed.
The atoms which pass through the magnetic gate enter in a storage bulb surrounded by a tuned, resonant cavity [10]. Inside such bulb, some atoms drop to a lower energy level, releasing photons at the maser microwave frequency which stimulate other atoms to drop their energy level, and they in turn release additional photons... In the bulb a self-sustaining microwave field is created. The tuned cavity around the bulb helps to redirect photons back into the system to mantain the oscillation. As long as new atoms are pumped in the system, a microwave signal locked to the hydrogen atom resonance frequency is generated. A quartz oscillator is locked to the resonance frequency of the hydrogen.
The cavity resonator can also be loaded with dielectric material: in such circumstances the quality factor Q of the cavity is not sufficient to achieve continuous oscillation, but the cavity volume is reduced. In order to relax the requirements of the cavity Q, the maser

can be operated in *passive mode* [7]. For passive operation, microwave energy close to the hyperfine frequency is injected inside the cavity through a coupling loop: such energy creates a field in the cavity, which is absorbed by the atomic ensemble [7].
At present, the hydrogen maser is the atomic frequency standard with the best overall frequency stability for τ larger than a few seconds [8].
the short term frequency stability ($\tau < 100$ s) is determined by the additive white phase noise in the microwave cavity, while the long term frequency stability ($\tau > 100$ s) is limited by the flicker frequency noise.
However, when measured for more than a few days or weeks, the hydrogen maser's performance might be worse than those of cesium oscillators: the stability decreases because of changes in the cavity's resonance frequency over time [10].
Hydrogen Masers are generally used to monitor atomic time scales produced by commercially available cesium beam frequency standards, to evaluate cesium clocks employed in laboratories, to perform tests on the theories of relativity, and, recently, have also been employed in navigation systems.

1.2.3 Time Scales

Time scales are the instrument to date events.
Uniform time scales can be realized using a reference signal generated by a frequency standard. A time scale shall be reliable, stable, accurate and accessible [14].
The *reliability* of a time scale is closely related to the reliability of the clocks whose measurements are used for its construction; at the same time, redundancy is needed. In the case of the international reference time scale, a large number of clocks are required.The *frequency stability* of a time scale represents its capability to maintain a fixed ratio between its unitary scale interval and its theoretical counterpart. One means of estimating the frequency stability of a time scale is the Allan variance [15] (see Section 3.2.2.2.1), which is the 2-sample variance designed for the statistical analysis of time series, and depends on the sampling interval.
The frequency *accuracy* of a time scale represents the ability of its unitary scale interval to reproduce its theoretical counterpart. After the calculation of a time scale on the basis of an algorithm which ensures the required frequency stability, the frequency accuracy can be improved by comparing the frequency (rate) of the time scale with that of primary frequency standards, and by applying, if necessary, frequency (rate) corrections.
Finally, the *accessibility* of a time scale represents its ability to provide a way of dating events for everyone, worldwide.

1.2.3.1 TAI

The international reference time scale is the *Temps Atomique International* (TAI), realized at the *Bureau International des Poids et Mesures* (BIPM), averaging data from the clocks monitored in 62 laboratories [14]. It was officially adopted in 1971.
TAI is an integrated time scale built by accumulation of seconds, without steps. Ideally, the phenomenon giving origin to a time scale should be reproducible with a constant frequency. In practice, this is not exacltly the case: the realizations of the second of the International System of Units (SI) [9] differ from the ideal duration specified in its definition. The BIPM, in the process of time scale construction, tries to reduce these differences [14].
An integrated time scale, such as TAI, requires the following elements:

1. a periodic phenomenon;
2. a definition of the unit, derived from the frequency of the phenomenon;
3. realizations of the unit, that is frequency standards, called clocks if they operate continuously;
4. an algorithm of calculation adapted to the required characteristics of the scale.

The instability of TAI, estimated today as $0.4 \cdot 10^{-15}$ for averaging times of 20 days to 40 days, is obtained by processing clock and clock comparison data at 5 days intervals over a monthly analysis, with a delay to publication of about 15 days after the last date of data reported in the official document called *BIPM Circular T* [17], [16] . In the very long-term, over a decade, the stability is maintained by primary frequency standards and is limited by the accuracy at the level of parts in 10^{15}, assuming constant performances.
The uncertainty of clock comparisons currently is between a few tens of nanoseconds and a nanosecond for the best links, a priori sufficient to allow a comparison of the best atomic standards over integration times of a few days.

1.2.3.2 UTC

The Universal Time Coordinated (UTC) is generated at the Bureau International des Poids et Mesures (BIPM). It takes about one month to collect all of the data and to perform the calculations to generate TAI and UTC times [18]. In order to obtain a realtime estimate of UTC, there are 50 timing centers around the world that generate their own current estimate of UTC: the so-called UTC(k), where the k denotes the particular timing center. The italian realization of UTC, UTC(IT), is maintained at the time and frequency laboratory of the National Institute of Metrological Research (INRIM).
By international agreement all of the timing centers have been given a goal to keep their

UTC(k)s within 100 ns of UTC.
The BIPM then generates a monthly bulletin, the Circular T, which reports the time differences of each of the UTC(k)s with respect to UTC for the previous month.
A time scale built accumulating atomic seconds has the disadvantage to be not in agreement time of Earth rotation.
UTC is a compromise between a continuous time scale, in which the second is determined by a physical phenomenon, and the apparent rotation of the celestial bodies.
UTC is kept in agreement with the Earth rotation by the insertion of leap seconds. The insertion of a leap second is determined by the International Earth Rotation Service (IERS), which operates out of the Paris Observatory and which collects Earth rotation data from numerous observatories and radio telescopes around the globe. The need for leap seconds is related to the tidal deceleration of the Earth's rotation [19].

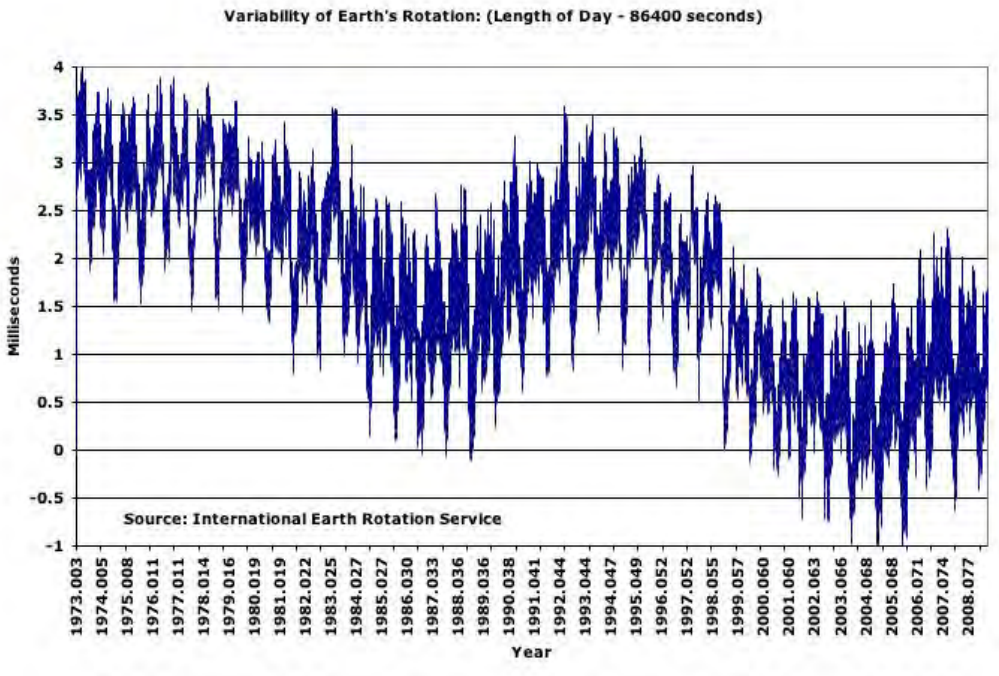

Figure 1.6: Variability of Earth's Rotation [20]

By international agreement, a leap second may be introduced at the end of any month. However, the preferred dates are at the end of June and the end of December when required. They are introduced when necessary to keep UTC within 0.9 seconds of Earth time (UT1).

Since 1972, UTC differs from TAI by an integer number of seconds: at the end of June 2012, the difference between UTC and TAI will be 35 s.

1.2.3.3 GPS Time

The reference time scale for the GPS system is GPS Time [3]. It is based on atomic standard time, and the time broadcast from satellites is continuous, without the introduction of leap seconds, differently from UTC. Leap seconds are not inserted since it would throw the P-code receivers out of lock at the time when they are introduced. However, GPS is maintained within $1\mu s$ of UTC(USNO) time (modulo 1s), the local realization of UTC realized at the United States Naval Observatory. Besides, the correction parameters to align GPS Time to UTC(USNO) are broadcast in the navigation message: thus, the GPS provides an important time transfer function. The information in the navigation message provides also notice to the user of any delta time in the recent past or in the near future due to leap seconds and the week number at which that leap second becomes effective.
GPS Time was set in 1980 to have zero seconds difference from UTC.

1.2.3.4 Galileo System Time

The reference time scale for the Galileo system will be the *Galileo System Time (GST)*. It will be the reference time for all the internal operations of the European satellite navigation system, such as the prediction of Galileo satellite clocks, and will be also useful as reference time for external users having access to GST through the Galileo signal in space. In fact in principle, the Galileo system time can be used in many applications provided that it is stable enough and hence predictable, as TAI and UTC [21].
The GST time scale, being designed for navigation purposes, will be a continuous time scale without the introduction of leap seconds and will have a well defined offset from UTC, which will be published in the BIPM Circular T [17] .
The Galileo System Time will be generated at a specific element of the Galileo Mission Segment, called Precise Timing Facility (PTF) [22].
Galileo System Time will be based on an ensamble of high performance atomic clocks [23], mantained at the precision timing station of the system, the PTF, and it will be routinely compared to the local realizations of UTC, the UTC(k) of the European laboratories k, using the Two-Way Satellite Time and Frequency Transfer (TWSTFT) [24] and GPS Common View (CV) [25], [26] time transfer techniques.
Besides, the data collected from the PTF will be used in near real-time to improve the accuracy of the prediction of UTC-GST in the period when the definitive values are not available, before the new issue of the BIPM Circular T.

As GPS, GST will be a continuous time scale, without introduction of leap seconds and it will be steered to UTC [27], modulo 1 s. The idea is that GST offset from UTC is kept below 50 ns.
For convenience, the start epoch of the Galileo time scale is the same as GPS, in order to favour the interoperability between the two systems [28].

Chapter 2

Satellite Navigation Systems Description

Different satellite navigation systems are currently available or under development: the United States system GPS and the Russian GLONASS are fully operational since several years, while the European Galileo is being implemented. Besides, also India and China are developing their own navigation systems, named IRNSS and Compass respectively.
This Chapter will describe in detail only the GPS and the future Galileo.

2.1 The Global Positioning System

The Global Positioning System (GPS) was developed by the U.S department of Defense (DoD). In 1973 the Navy and the Air Force systems joined and formed NAVSTAR, which is the official name of GPS, meaning Navigation Satellite Timing And Ranging Global Positioning System.
The first GPS satellite was launched in 1978 and the system reached the full operational capability in 1995 [2].

2.1.1 GPS Services

GPS is constituted by two level of services: a military service (Precise Positioning Service, PPS) and a civil serice (Standard Positioning Service, SPS). The **Precise Positioning Service** is an accurate positioning, velocity and timing service which is available only to authorized users: it is primarily intended for military purposes [29]. Authorized users, designated by the U.S Department of Defense, include the U.S military users, NATO military users and few other selected users.

The PPS positioning accuracy reaches the 16 meters Spherical Error Probable (SEP) (3-D 50 %) and the UTC time transfer accuracy is at the level of 100 ns (1σ). Access to PPS is controlled by two features using cryptographic techniques: *Selective Availability* (S/A) and *Anti-Spoofing* (A-S). Selective availability operates introducing pseudorandom errors in the satellite signal. The Anti-Spoofing feature is activated in all satellites to prevent potential spoofing[1] of the ranging signals. The technique encrypts the P-code into the Y-Code (see Section 2.1.3).
The **Standard Positioning Service** is a less accurate positioning and timing service, available to all users. The Selective Availability is set to provide a 100 m horizontal accuracy (2σ) and to achieve approximately 337 ns (2σ) UTC time transfer accuracy [29]. The SPS is primarly intended for civilian purposes.

2.1.2 GPS Architecture

The GPS consists of three segment: the Space Segment, the Control Segment and the User Segment.
The Space segment is composed of about 30 operational satellites (31 at the time of writing this thesis) [30], placed on 6 different orbital planes, inclined at 55° to the Equator, at an altitude of approximately 20300 Km from the Earth [3]: this altitude gives two orbital periods per sideral day (semisynchronous) and is a compromise among user visibility, the need to pass over the continental U.S ground/upload stations periodically, and the cost of the spacecraft launches. This configuration ensured a system robust enough to tolerate occasional satellite outages, providing a mimimum of 6 satellites in view at the same time.
GPS satellites can be divided, at the time of writing this thesis, in 5 different blocks [30], according to the time they were launched and to the Space Vehicle technology: Block II, Block IIA, Block IIR, Block IIR-M, Block IIF.
Satellites of Block II and IIA are the first and the second series, respectively, of full scale operational satellites developed by Rockwell International, and were launched between 1989 and 1997. Each space vehicle contains four atomic clocks: two Cesium (Cs) and two Rubidium (Rb). Block IIR satellites were launched starting from 1997, and each contains three Rubidium clocks. Block IIR-M and IIF satellites are more recent: launching of the Block IIFs bagan in May 2010.
The Control Segment consists in the Master Control Station (MCS), located at the Schriever Air Force Base in Colorado, monitor stations and ground control stations transmitting information to the satellites.

[1] A GPS spoofing attack attempts to deceive a GPS receiver by broadcasting a slightly more powerful signal than the one received from GPS satellites, structured to resemble a normal GPS signal. These spoofed signals are modified in order to cause the receiver to determine its position erroneously.

The Control Segment has also the capability to degrade intentionally the accuracy of the C/A code (the Coarse/Acquisition Code) for civil use, by desynchronizing the satellite clock, or by incorporating small errors in the broadcast of ephemeris by means of the *Selective Availability*: the magnitude of these ranging errors results in horizontal positioning errors of about 50 m.
The Selective Availability was shut down on May 2000, but it can be restored in any moment by the DoD, if necessary, either on a global or regional basis.
The User Segment consists on the receivers and antennae receiving the GPS signal on Earth, for civil and military use. The communication between the Space and the User segment is unidirectional, while the ground control stations are equipped with antannae enabling bidirectional communication.

Figure 2.1: GPS Control Segment [2]

2.1.3 GPS Signal

The GPS ranging codes, used to modulate the carrier phase with a binary modulation, are named C/A and P(Y) [31].

2.1.3.1 C/A Code

The C/A code consists of a 1023 bit pseudorandom noise (PRN) code with a clock rate of 1.023 MHz, repeated every 1ms [29]. The short lenght of such sequence is designed to enable a receiver to rapidly acquire the satellite signal, which helps the receiver transition to the longer P-Code. A different PRN, selected from a set of Gold Codes, is assigned to each GPS satellite. The Gold Codes are used to minimize to cross-correlation among

different codes, avoiding to mistake one code with another. The C/A code is transmitted only on L1 frequency. It is not encrypted.

2.1.3.2 P(Y) Code

The P-Code is a 10.23 MHz PRN code sequence. The P-Code is normally encrypted into the Y-Code to protect users from spoofing. Since the satellites have the capability to transmit either the P or the Y code, it is also referred to as the P(Y)-Code. Satellites transmit the P(Y)-Code on both L1 and L2 frequencies. On L1, the P(Y)-Code is 90 degrees out of carrier phase with the C/A Code.

2.1.4 GPS Frequency Plan

The frequency bands currently allocated to the GPS system are reported in Table 2.1:

Band	Bandwidth (MHz)	Center Frequency (MHz)
L5	24 [1164-1188]	1176.45
L2	20 [1217-1130]	1227.60
L1	24 [1563-1587]	1575.42

Table 2.1: GPS Frequency Plan

GPS signal is currently transmitted on two radio-frequency links: L1, at 1275.42 MHz, and L2, at 1227.60 MHz. These frequencies are coherent with the 10.23 MHz clock on board the GPS satellites. In fact, the two frequencies can be related to the clock frequency as:

$$f_{L1} = 1575.42MHz = 154 \cdot f_0$$
$$f_{L2} = 12275.60MHz = 120 \cdot f_0$$

Where $f_0 = 10.23$ MHz is the nominal frequency as it appears to an observer on the ground. To compensate for the relativistic effects the output of the satellite frequency standard (as it appears from the spacecraft) is a 10.23 MHz offset by a $\frac{\Delta f}{f_0} = -4.467 \cdot 10^{-10}$. Hence, the signal received by a GPS receiver is at the desired frequency. In addition, satellite and receiver motion produce a Doppler shift: at L1 frequency it is about $\pm$ 5kHz.
The GPS modernization program include an additional signal for civil use: the L5 frequency band, centered at 1176.45 MHz.

2.2 The Galileo System

In the 1990s the European Union saw the need for Europe to have its own global satellite navigation system. In 1999 the European Commission and the European Space Agency (ESA) approved and funded the Galileo project, an independent European system, under civilian control [32].
Galileo will be inter-operable with GPS and GLONASS[2]: its coming online will allow positions to be determined accurately for most places on Earth, even in high rise cities where buildings obscure signals from satellites low on the horizon. This is because the overall number of satellites available from which to take a position will be more than doubled.
Galileo satellites will be placed in orbits at greater inclination to the equatorial plane than GPS: Galileo will achieve better coverage at high latitudes. This will make it particularly suitable for operation over northern Europe, an area not well covered by GPS.

2.2.1 Architecture

Galileo is conceived to be a stand-alone global system, but interoperable with other services, such as GPS. The Galileo system will comprise *global*, *regional* and *local* components [34]. The global component is the core of the system, consisting of the satellites, the ground control and the ground mission segments. Galileo's regional component may comprise a number of External Region Integrity Systems (ERIS), implemented and operated by organisations, countries or groups of countries outside Europe to obtain integrity services independent of the Galileo system, in order, for example, to satisfy legal constraints relating to system guarantees. Local components may be deployed for enhancing the performance of Galileo locally. These will enable higher performance, such as the delivery of navigation signals in areas where the satellite signals cannot be received.
The architecture of the Galileo System is divided in three functional segments, as illustrated in Fig. 2.2:

- The Space Segment
- The Ground Segment
- The User Segment

[2]Global'naja Navigacionnaja Sputnikovaja Sistema: the Russian Satellite Navigation System

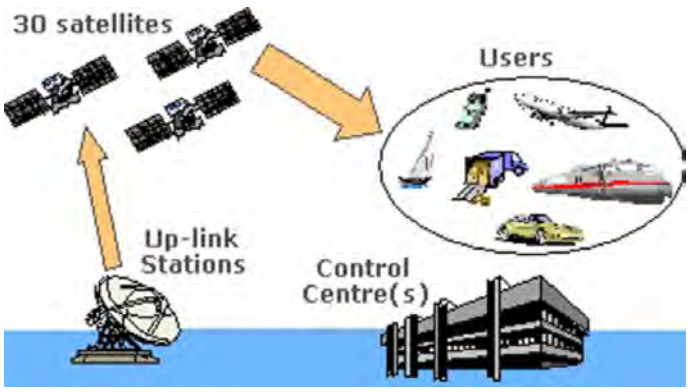

Figure 2.2: Galileo Segments [32]

2.2.1.0.1 The Space Segment

The fully deployed Galileo system consists of 30 satellites (27 operational + 3 active spares), positioned in three circular Medium Earth Orbit (MEO) planes at 23 222 km altitude above the Earth, and at an inclination of the orbital planes of 56 degrees to the equator. Nine satellites will be spread around each plane, taking about 14 hours to orbit the Earth. Each plane has one additional dormant spare, able to be moved to any of the other satellite positions within its plane. The spare satellite in each orbit plane ensures that in case of failure the constellation can be repaired quickly by moving the spare to replace the failed satellite. This could be done in a few days, rather than waiting for a new launch to be arranged which could take many months.

Several constellations were studied for optimisation of the space segment. The retained constellation is based exclusively on satellites in MEO orbit, which ensures a uniform performance both in terms of accuracy and availability, and which offers greater robustness in crippled mode (satellite failure). The GALILEO satellite constellation is furthermore well suited for high latitude countries and offers an improved visibility in towns and cities [35]. The altitude of the satellites has been chosen to avoid gravitational resonances so that, after initial orbit optimisation, station-keeping manoeuvres will not be needed during the lifetime of a satellite [32]. The position constraints for individual satellites are set by the need to maintain a uniform constellation, for which it is specified that each satellite should be within $\pm$ 2° of its nominal position relative to the adjacent satellites in the same orbit plane and should be within 2° of the orbit plane.

The satellites will use largely proven technologies. The body will rotate around its Earth-pointing (yaw) axis for its solar wings to rotate and point towards the Sun (generating peak power of 1600 W). A basic box structure will group the payload and platform elements. The launch mass is about 700 kg each.

The satellites are designed to be compatible with a range of launchers providing multiple and dual launch capabilities.

Satellite Components

Each Galileo satellite is equipped with several antennae and sensors [32].

The L-band[3] antenna transmits the navigation signals in the 1200-1600 MHz frequency range.

The SAR (Search and Rescue) antenna picks up distress signals from beacons on Earth and transmits them to a ground station for forwarding to local rescue services.

The C-band[4] antenna receives signals containing mission data from Galileo Uplink Stations. This includes data to synchronise the on-board clocks with a ground-based reference clock and integrity data which contains information about how well each satellite is functioning. The integrity information is incorporated into the navigation signal for transmission to users.

Two S-band[5] antennae are part of the telemetry, tracking and command subsystem. They transmit housekeeping data about the payload and spacecraft to ground control and, in turn, receive commands to control the spacecraft and operate the payload. The S-band antennae also receive, process and transmit ranging signals that measure the satellite's altitude to within a few metres.

The infrared Earth sensors and the Sun sensors both help to keep the spacecraft pointing at the Earth. The infrared Earth sensors do this by detecting the contrast between the cold of deep space and the heat of the Earth's atmosphere. The Sun sensors are visible light detectors which measure angles between their mounting base and incident sunlight.

The laser retro-reflector allows measurement of the satellite's altitude to within a few centimetres by reflecting a laser beam transmitted by a ground station. The laser retro-reflector is used only about once a year, as altitude measurements via S-band antenna ranging signals are otherwise accurate enough.

The space radiators are heat exchangers that radiate waste heat, produced by the units inside the spacecraft, to deep space and thus help to keep the units within their operational temperature range.

Critical Technology: Galileo Satellite Clocks

Two on board atomic clocks have been developed for Galileo:

[3] L-band: from 1 to 2 GHz

[4] C-band:from 4 to 8 GHz

[5] S-band: from 2 to 4 GHz

1. a Rubidium Atomic Frequency Standard

2. a Passive Hydrogen Maser

In parallel, a system for generating navigation signals has been developed, with a navigation signal generator, a navigation antenna and associated equipment [32].
The spacecraft has four clocks, two of each type. At any time, only one of each type is operating. Under normal conditions, the operating maser clock produces the reference frequency from which the navigation signal is generated. If the maser clock fails, however, the operating rubidium clock will take over instantaneously and the two reserve clocks will start up. If the problem with the failed maser clock is unique to that clock, the second maser clock will take over from the rubidium clock after a few days when it is fully operational. The rubidium clock will then go on stand-by or reserve again. In this way, by having four clocks, the Galileo spacecraft is guaranteed to generate a navigation signal at all times.
The European Space Agency has chosen the rubidium and hydrogen maser clocks as they are very stable over a few hours and because their technology can fly onboard the Galileo satellites. If they were left to run indefinitely, though, their timekeeping would drift, so they need to be synchronised regularly with a network of even more stable ground-based reference clocks. These will include clocks based on the caesium frequency standard, which show a far better long-term stability than rubidium or hydrogen maser clocks. The clocks on the ground will also generate a worldwide time reference called Galileo System Time.
The clocks on-board the satellites are the first of their type to be developed and built in Europe. Similar clocks are available in the US and in Russia (for example those flown on the GPS and Glonass satellites), but technological independence is part of mastering Europe's own navigation system.
The passive hydrogen maser clock was actually the first one of its type ever to fly. It has been built by the Observatoire de Neuchatel in co-operation with Officine Galileo of Italy, the former being responsible for the overall development and in particular for the so-called physics package, the latter being in charge of the electronics. A similar arrangement applies for the rubidium clock for which Temex Neuchâtel Time assumes overall responsibility and Astrium Germany contributes the electronics.
The first two flight models of the rubidium clock are in orbit on board GIOVE-A, the first Galileo satellite. Two flight models of the passive hydrogen maser are flying on GIOVE-B since April 2008. Both clocks have shown their reliability and two of each model will be embarked on board the four satellites of the subsequent In Orbit Validation phase.
In addition, each Galileo satellite is provided with other equipment, such as the Clock Monitoring and Control Unit (CMCU) and the Navigation Signal Generation Unit (NSGU).

The clock monitoring and control unit provides the interface between the four clocks and the navigation signal generator unit. It passes the signal from the active master clock to the NSGU and also ensures that the frequencies produced by the master clock and the active spare are in phase, so that the spare can take over instantly should the master clock fail.
The navigation signal generator, frequency generator and up-conversion units are in charge of generating the navigation signals using input from the clock monitoring unit and the up-linked navigation and integrity data from the C-band antenna. The navigation signals are converted to L-band for broadcast to users.
The remote terminal unit is the interface between all the payload units and the on-board computer.

2.2.1.0.2 The Ground Segment

The core of the Galileo ground segment will be the two Galileo Control Centres (GCCs). Each will manage control functions supported by a dedicated Ground Control Segment (GCS), and mission functions supported by a dedicated Ground Mission Segment (GMS). The GCS will handle satellite housekeeping and constellation maintenance, while the GMS will handle the navigation and timing system. A network of ground stations consisting of sensor stations, control centres and uplink stations will support satellite operations. A global network of nominally thirty network of Galileo Sensor Stations (GSSs) will continuously monitor the satellites [34]. The prime element of the GSS is the Reference Receiver. GSS data will be disseminated to the Galileo Control Centres continuously through a comprehensive communications network using satellites and terrestrial connections, with each link duplicated for redundancy. The GMS processing facilities in the GCCs will process the data and produce the navigation and integrity messages up-linked to Galileo satellites via a network of Up-Link Stations (ULSs), installed at five sites, each of which will host a number of 3-metre antennae, operating at C-band. The navigation signals are generated aboard the Galileo satellites and broadcast to users in the L-band. The satellite constellation will be controlled from the GCS facilities installed in the GCC, and supported by a worldwide network of Telemetry and Telecommand S-band stations.
In details, the GCC will consist of the [36]:

- Orbit Synchronization and Processing Facilities (OSPF)
- Precise Time Facilities (PTF)
- Integrity Processing Facilities (IPF)
- Mission Control Facility (MCF)

- Satellite Control Facility (SCF)
- Services Product Facility (SPF)

The GMS will use the GSS network in two independent ways. The first is the Orbitography Determination and Time Synchronisation (ODTS) function, which will provide batch processing every ten minutes of all the observations of all satellites over an extended period and calculates the precise orbit and clock offset of each satellite, including a forecast of predicted variations (SISA - Signal-in-Space Accuracy) valid for the next hours. The results of these computations for each satellite will be up-loaded into that satellite nominally every 100 minutes using a scheduled contact via a Mission Up-link Station.
The second use of the GSS network is for the Integrity Processing Function (IPF), which will provide instantaneous observation by all GSSs of each satellite to verify the integrity of its signal. The results of these computations, for the complete constellation, will be up-loaded into selected satellites and broadcast such that any user will always be able to receive at least two Integrity Messages.
The Integrity messages will comprise two elements. The first is as an *Integrity Flag*, which warns that a satellite signal appears to exceed its tolerance threshold. This flag will be generated, disseminated and broadcast with the utmost urgency, so that the *Time-to-Alert*, being the period between a fault condition appearing at a user's receiver input and the Integrity Flag appearing, there will be no more than six seconds, and will be re-broadcast a number of times. The second element of the Integrity Message comprises Integrity Tables, which will be broadcast regularly to ensure that new users or users who have missed recent signal (for example when travelling through a tunnel) will be able to reconstitute the system status correctly.
The ODTS operation thus monitors the long-term parameters due to gravitational, thermal, ageing and other degradations, while the IPF monitors short-term effects, due to sudden failure or change.

2.2.1.0.3 The User Segment

The user receivers and terminals will need to satisfy market requirements [37]:

- Competitive performance and costs compared with the existing systems
- Potential for change and integration of the services (eg. communications)
- Possibility of multi-model use (interoperability)

2.2.1.1 Galileo Services

Four navigation services and one service to support Search and Rescue operations have been identified to cover the widest range of users needs, including professional users, scientists, mass-market users, safety of life and public regulated domains [32].
The following Galileo satellite-only services will be provided worldwide and independently from other systems by combining Galileo signals-in-space:

1. The Open Service (OS): it results from a combination of open signals, free of user charge, and provides position and timing performance competitive with other GNSS systems.

2. The Safety-of-Life Service (SoL): it improves the open service performance through the provision of timely warnings to the user when it fails to meet certain margins of accuracy (integrity). It is envisaged that a service guarantee will be provided for this service.

3. The Commercial Service (CS): it provides access to two additional signals, to allow for a higher data throughput rate and to enable users to improve accuracy. The signals are encrypted. It is envisaged that a service guarantee will be provided for this service.

4. The Public Regulated Service (PRS): provides position and timing to specific users requiring a high continuity of service, with controlled access. Two PRS navigation signals with encrypted ranging codes and data will be available.

5. The Search And Rescue Service (SAR): The Galileo support to the search and rescue service represents the contribution of Europe to the international COSPAS-SARSAT co-operative effort on humanitarian Search and Rescue activities. Galileo is to play an important part of the Medium Earth Orbit Search and Rescue system (MEOSAR). Galileo satellites will be able to pick up signals from emergency beacons carried on ships, planes or persons and ultimately send these back to national rescue centres. From this, a rescue centre can know the precise location of an accident. At least one Galileo satellite will be in view of any point on Earth so near real-time distress alert is possible. In some cases, feedback could be sent back to a beacon, something which is only made possible by Galileo.

2.2.1.2 Galileo Frequency Plan

Galileo receivers receive the signals broadcast by the Galileo satellites and process them to compute position. Through this processing, the receivers extract measurements giving

an indication of the distance from the user to the satellite [32].
They also decode the Galileo navigation data, which contain fundamental pieces of information for computing the user position such as the position of the satellites and the satellite clock errors as determined by the Galileo ground segment and up-linked regularly to the Galileo constellation.
The frequencies used by the satellites are within the 1.1 to 1.6 GHz band; a range of frequencies particularly well suited for mobile navigation and communication services.
Each Galileo satellite will broadcast 10 different navigation signals making it possible for Galileo to offer the open (OS), safety-of-life (SOL), commercial (CS) and public regulated services (PRS).
A distinction is made between signals containing navigation data (the data channels) and signals carrying no data (pilot channels), which carry a short sequence of bit used for data synchronization and signal tracking.
All the satellites transmit at the same frequency, that is, the Galileo signal at L1 is broadcast at 1575.42 MHz from any satellite. To allow the receivers to distinguish which satellites the signals are coming from and to allow the receivers to measure the time it took the signal to travel from the satellite to the receiver (the basic measurement used for position determination), a code is added to the signal. This code is different for each satellite and its design is one of the many arts involved in making a good satellite navigation system.
When a receiver attempts to acquire a satellite signal, it compares the code of the received signal with a local replica stored on the receiver. When the two codes match, the receiver channel is open, otherwise the receiver tries with another code corresponding to another satellite, as long as a match is not found.
The different frequency bands used by the Galileo system are illustrated in Fig. 2.3:

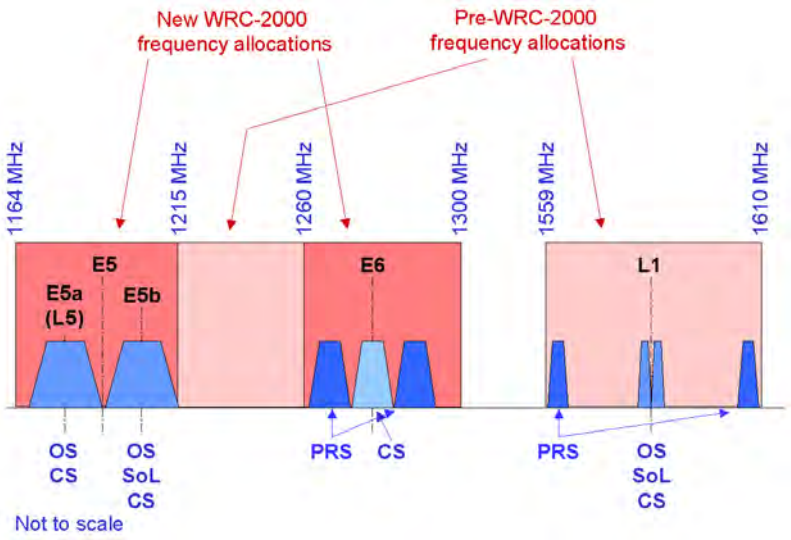

Figure 2.3: Galileo Frequency Plan [32]

As it can be observed on the previous diagram, the different Galileo services can use different frequency bands.

The *open services* are realized by using the signals at L1, E5a and E5b, whether data or pilot. Several combinations are also possible, such as a dual frequency service based on using L1 and E5a (for best ionospheric error cancellation) or single frequency services (at L1, E5a, E5b or E5a and E5b together) in which case the ionospheric error is removed using a model, and even triple frequency services using all the signal together (L1, E5a and E5b), which can be exploited for very precise, centimetric applications.

The *safety-of-life services* are based on the measurements obtained from the open signal and use the integrity data carried in special messages designated for this purposed within the open signals. The safety-of-life service is like a data channel within the open signals.

The *commercial service* is realized with two additional signals in the 1278.75 MHz band plus also the capability to include commercial data within the open signals.

The *Public Regulated Service* is realized by two signals, one in the 1575.42 MHz band and the other in the 1278.75 MHz band. These signals are encrypted, allowing the implementation of an access control scheme.

Finally, the distinctive shape of the spectrum of the signals is due to the special modulation adopted for Galileo. This modulation has been chosen to avoid interference with other satellite navigation systems within the same band, which is indeed the case of GPS at L1. The modulation adopted is called BOC(1,1), meaning Binary Offset Carrier[6] of rate (1,1).

[6]modulation in which the signal is multiplied by a rectangular sub-carrier, equal or higher than the

This kind of modulation allows GPS and Galileo signals to occupy the same frequency while avoiding mutual interference. This makes building receivers that use both GPS and Galileo simpler, because GPS and Galileo use the same frequency.

2.2.2 History and Future Plan

In preparation for the development of the Galileo system, the European Space Agency launched in 2000 the development of an experimental ground segment - Galileo System Test Bed Version 1. This was followed in 2003 by the development of two experimental satellites, the Galileo In-Orbit Validation Element (GIOVE).

2.2.2.1 Galileo System Test Bed-V1

Within the GSTB-V1 project [32], tests of Galileo orbit determination, integrity and time synchronization algorithms were conducted with the GPS satellites and an experimental ground segment consisting of a worldwide network of sensor stations collecting high quality GPS observables at one hertz, an Experimental Precision Timing Station, located at the INRIM Time Laboratory -formerly Istituto Elettronico Nazionale (IEN)-, providing the reference time scale synchronised to universal time and international atomic time (UTC/TAI), and a Processing Centre located at the European Space Agency (ESA-ESTEC) in The Netherlands. The latter was used for the generation of navigation and integrity core products based on Galileo-like algorithms.
Tests conducted with GSTB-V1 proved that it is possible to broadcast orbit determination and time synchronization data with high accuracy (better than 50 cm) and with low update rate (two hours), as it was envisaged for the Galileo system.

2.2.2.2 The First Galileo Satellites: Galileo In-Orbit Validation Element

Within the GIOVE project, two experimental satellites were developed that make up the first step in the in-orbit validation of the Galileo system. This task will be completed with the deployment of the four In-Orbit Validation satellites.
The objectives of these two experimental satellites were [32]:

- to secure the Galileo frequency filings allocated within the International Telecommunications Union (ITU)
- to characterise the orbits to be used by the in-orbit validation satellites

basic chip rate, in order to shift the main lobes of the resulting spectrum, thus avoiding the interference with the BPSK modulated signal

- to test some of the critical technologies, such as the atomic clocks

The first experimental satellite, GIOVE-A, was manufactured by Surrey Space Technology Limited (SSTL). The second one, GIOVE-B, was made by European Satellite Navigation Industries: a European consortium named ESNIS, including Alcatel Space Industries (F), Alenia Spazio (I), Astrium GmbH (D), Astrium Ltd (UK) and Galileo Sistemas y Servicios (E).
These two satellites were developed in parallel to guarantee that one of them was in-orbit by December 31^{st} 2005, the deadline defined by ITU regulations. The capabilities of the two satellites are similar. The smaller satellite, GIOVE-A, carries a rubidium clock and transmits an experimental signal through two separate channels at a time. The larger satellite, GIOVE-B, embarks an additional passive hydrogen maser clock and will transmit an experimental signal through three separate channels.
GIOVE-A, was launched with a Soyuz launcher from the Baikonur Cosmodrome on December 28th 2005. It carried two RAFS clocks.
The second GIOVE satellite, GIOVE-B, was launched from the Baikonour cosmodrome in Kazakhstan on April 27^{th} 2008 [33]. Its main objective were to maintain frequency filing, provide in-orbit validation of the Galileo payload units, specifically the Passive Hydrogen Maser (PHM), and the Solid State Power Amplifiers (SSPAs), which were not present on GIOVE-A, measure the medium earth orbit (MEO) radiation environment, and continue the Signal In Space experimentation.
GIOVE-B signals in space are fully representative of the operational Galileo system, in terms of radio frequency and modulations, as well as chip rates and data rates.
The experience gathered with both test beds V1 and V2 has being transferred to the development of the In-Orbit Validation system and will contribute to the success of the Galileo mission.

2.2.2.3 IOV: The First Four Satellites of the Constellation

The first four Galileo satellites to be launched in the frame of the In Orbit Validation (IOV) phase are fully representative of the 30 satellites of the Galileo constellation. Each will broadcast precise time signals, ephemeris and other navigation and commercial data [34].
The first two of the four IOV satellites were launched on October 21^{st} 2011. Two more are scheduled for launch in 2012.
Following the IOV phase, the Full Deployment phase will consist on the launch of 26 satellites and the completion of the ground segment, an extensive network of stations and local and regional service centres.

The role of INRIM in Galileo continued also in this phase. In fact, in order to support the Galileo IOV system validation, INRIM has been commissioned to the development and installation of the so called *Time Validation Facility*, in charge of driving and assessing performances of the system from the timing point of view.

Chapter 3

Metrological Characterization of Space Clocks

3.1 Scenario Description

The so called satellite *orbits* and *clocks*, that are respectively the satellite position and the time difference between the clock on board the spacecraft and a timing reference, are determined through a network algorihm which processes the data collected by different ground stations.
A set of ground stations worldwide distributed and provided with GNSS receivers acquire the Satellite Signal-In-Space. The raw data collected by each station are then converted in RINEX[1] format [38].
In addition, also the satellite telemetry and telecommand data are collected, containing measures of the different sensors located on board satellites, measuring eg. temperature.
The International GNSS Service (IGS) is a voluntary federation of more than 200 worldwide agencies providing resources such as satellite tracking stations, data centers, analysis centers, generating precise products for GNSS, in near real time [39]. IGS products are conceived as a support for Earth science research, scientific and engineering applications, and education. The IGS collects, archives, and distributes GNSS observation data sets. Such data sets are used by the IGS to generate the data products which are made available to interested users through the Internet.
IGS products are public and can be freely retrieved from the IGS Web Site.
At present IGS products are generated just for two navigation systems: the GPS and the Russian GLONASS. Future GNSS will be incorporated when operational.
Among the IGS products there are GPS satellite clock information.

[1] standard files used in GNSS

Figure 3.1: International GNSS Service (IGS) Network [40]

The IGS data containing the clock estimates are routinely used at INRIM for the timing activities. Moreover, I largerly made use of these data during the years of doctorate and most of the results presented in this thesis were obtained processing and analysing IGS products.

In the Galileo project, the technique used to generate the clock solutions is called *Orbit Determination & Time Synchronization* (ODTS). It is a batch least squares algorithm which processes iono-free satellite code code and phase combinations, for GIOVE and GPS satellites [41] (see also Section 2.2). The algorithm is analogous to the one used by IGS.

The ODTS solves for orbits, clocks, troposphere and Inter-System Bias[2] (ISB), following a dedicated strategy in order to deal with different effects, such as ionosphere, troposphere, relativity etc.

A total of 11 dynamic parameters are estimated by the algorithm for each satellite: position velocity and five coefficients of the simplified Solar Radiation Pressure[3] (SRP) model.

Together with the dynamic parameters, the main products from the ODTS process are estimated orbits for GIOVE and GPS satellites, and estimated phase offsets with respect to the reference clock, for all satellites and ground stations. These data are generated in clock-RINEX format, with a five-minute sampling interval.

[2]differential delay of the signals of two different GNSS systems in a multi-GNSS receiver.

[3]model based on the estimate of five coefficients that best fit the orbit.

The ODTS clock estimates represent the basis for the clock characterization activity. In the frame of the INRIM participation to the Galileo project, in which I have been taking part during these years of doctorate, the ODTS clock estimates have been the input of the analysis of satellite and ground station clocks.
The ODTS is one module of the E-OSPF software installed at Processing Centre (GPC), in charge of producing the information used to update the navigation message.
The other module of the E-OSPF software is the IONO.
The clock estimate as seen through the ODTS algorithm is not the *pure* clock as tested on the ground, but an *apparent* clock, as seen through the complete on board signal generation chain, the space propagation path, the receiver network, the system noise, and the ODTS algorithm itself.
Table 3.1 summarizes the ground stations employed in the frame of the GIOVE Mission, the so called Galileo Experimental Sensor Station (GESS), reporting their geographical location [41], [42]:

GIEN	INRIM, Turin	Italy
GKIR	Kiruna	Sweden
GKOU	Kourou	French Guyana
GLPG	La Plata	Argentina
GMAL	Malindi	Kenya
GMIZ	Mizusawa	Japan
GNNO	New Norcia	Australia
GNOR	ESA, Noordwijk	The Netherlands
GOUS	Dunedin	New Zeland
GTHT	Tahiti	French Polynesia
GUSN	USNO, Washington	USA
GVES	Vasleskarvet	Antartica
GWUH	Wuhan	China

Table 3.1: Galileo Experimental Sensor Station in the GIOVE Mission

The so called *Depth of Coverage* (DOC) indicates the number of ground stations in view of the satellites of a particular GNSS system: a DOC-1 area implies that a satellite is in view of at least one station, while a DOC-2 area means that at least two stations can access the satellite, etc.
In the early experimental phases of the Galielo project, despite the limited number of ground stations, the geographical area with DOC-2 have been minimized.

3.2 Clock Behaviour Characterization

This Section will describe the main methodologies for characterization of atomicd clocks and their implementation in a robust software developed at INRIM for institutional purposes, and also used in the framework of the European project Galileo, for the characterization of satellite clocks.
Different types of atmic clocks are employed on GNSS satellites. As expected, each clock technology has different features with respect to the others and, most importantly, the space clocks behaviour is different from the one observed on the same type of clocks measured on ground or in timing laboratories. This is due to the clock technology itself, which is differently designed to work on ground or in space, but also to the different operational environment and to the complex space-to-ground measurement system: because of these aspects, unexpected phenomena can be noted on the observed apparent clock. Data from satellite clocks, indeed, often present missing data and outliers [43], as well as periodic fluctuations [63], [44]. All these aspects may complicate the analysis, since clock data from timing laboratories, regularly used by INRIM in institutional activities, are equally spaced and usually do not present outliers.
In fact, often space clocks data may be unavailable since the system ground stations could experience problems in data collection or satellites could be not transmitting for maintenance operations or faults ... Clock estimates have to be regularized as for the stability analysis necessarily equally spaced data are needed.
Moreover, frequently space clock data present outliers, which have to be identified and removed to allow a representative analysis of clock performances. Often these outliers may be caused by steps intentionally introduced in the clock phase offset for operations such clock synchronizations[4], or may be due to the processing of satellite raw data while generating the clock solution.
Therefore often, for space clock applications, the typical methods and techniques for clock characterization currently in use in timing laboratories are not sufficient: in fact, the spatial environment where clocks operate as well as the strict requirements of reliability and integrity needed for the navigation systems, require the development of new approaches and algorithms, more suitable for GNSS applications [45].
To overcome these limitations and to allow a proper analysis of typical GNSS data, INRIM developed the *Clock Analysis Tool*, a software tool for clock characterization optimized to deal with atomic clocks for space applications. For this purpose, an existing software used for clock characterization in INRIM laboratories has been adapted to fulfill GNSS needs:

[4] Generally, in time and frequency metrology, *synchronization* is an operation to have two or more clocks with the same apparent time reading [6]

it has been enhanced and extended including new routines for the monitoring such as the Dynamic Allan Deviation (DADEV) and Dynamic Hadamard Deviation (DHDEV), commonly used for GNSS satellite clock characterization [46].
My contribution in the period of doctorate consisted indeed in the upgrade of the tools used for clock characterization, with the implementation and the integration of new features in the existing routines, in order to obtain a complete software to produce most of the necessary products needed to characterize the clock behaviour.
Moreover, collecting the algorithms and software usually employed in the INRIM clock characterization activities, and adapting them adding new features, I was in charge of the development of an automatic software to be used for the characterization of clocks and time scales, to be used in the frame of the project named Galileo Time Validation Facility (see Section 2.2.2).

The methodologies adopted in such activity of clock characterization can be divided in four main areas, as illustrated in the following scheme [45]:

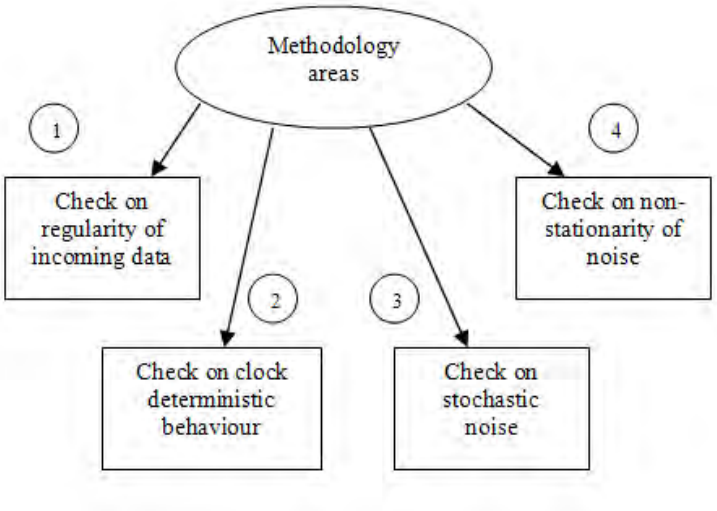

Figure 3.2: Clock characterization methodologies

1. *Check on regularity of incoming data*: before any analysis is performed it is necessary to establish the possible presence of data gaps or outliers[5].

[5] values that appear unusually too large or too small and out of place when compared with the other data values

2. *Check on clock deterministic behaviour*: this activity is devoted to the evaluation of the deterministic behaviour of the clock estimates, particularly in terms of frequency drift (see Section 3.2.1.1).

3. *Check on stochastic noise*: this activity consits in the evaluation of clocks' frequency stability, in terms of Allan Deviation and Hadamard Deviation (see Section 3.2.2).

4. *Check on non-stationarity of noise*: the study on clocks' non-stationary noise is performed through the Dynamic Allan Deviation

3.2.1 Deterministic Behaviour

The clock parameters considered to assess the deterministic behaviour are basically

- the clock *time offset* (also indicated as *phase offset*)
- the clock *normalized frequency offset*
- the clock *frequency drift*

As described in [11], the clock phase offset is the time difference between the lectures of two clocks, while the normalized frequency offset is the difference between the realized value and the reference frequency value, normalized with respect to the reference frequency.
Clock phase and frequency offset have been defined in Section 1.2.1. In the particular context of this thesis, the clock phase offset is the difference between the clock on board the satellite and the reference time scale maintained on the ground, or, in some cases between two ground clocks. The frequency offset is the time derivative of the phase offset. The frequency generated by atomic clocks does not remain constantly in agreement with its nominal value: deterministic and stochastic perturbations cause the variation of clocks frequency stability and accuracy.

3.2.1.1 Frequency Drift

The main deterministic effect in atomic clocks is the *frequency drift*, that is a systematic variation of the frequency generated by the clock [11], [47]. It may be due to intrinsic changes in the clock itself, to the ageing or to environmental factors.
It has been observed that, in general, older clocks have drifted further, but this is not always the case.
Drift is a well known and significant characteristic of Rubidium atomic clocks. On the contrary, the Cesium clocks' frequency drift is very close to zero [48].
Uncorrected frequency drift can be a significant source of error for precise time keeping

systems, especially in satellite navigation systems, in which the Rubidium Atomic Frequency Standards (RAFS) are widely used due to their low weight and moderate power consumption.
The origin of the frequency drift is still not well understood: some hypothesis and experimental studies can be found in literature. From those studies can be derived some general characteristics for the drift of Rubidium Atomic Frequency Standards [49]:

- the sign of the drift coefficient can be variable
- drift magnitude and sign are typically stable over a period of roughly three months

There are several possible mechanisms which can induce the frequency drift in atomic clocks; in Hydrogen Masers for example, the collisions of the Hydrogen atoms with the container walls of the clock produce a significant shift of the hyperfine resonance frequency [8]. However, in Rubidium gas cell standards this is an unlikely cause of drift, since the glass walls of resonance cell are generally bare.
Another common and plausible cause of frequency drift in atomic clocks is the temperature sensitivity: in Rb clocks the resonance frequency can be subjected to a shift due to the buffer gas temperature changes [49].
From a mathematical point of view (see Eq. 1.9) the drift is the derivative of the clock frequency: the noisiness of the drift depends on the length of the period over which the drift has been evaluated [48].

3.2.1.1.1 Frequency Drift Estimation and Removal

As described in Section 1.1, the user's position in GNSS is established processing the predicted values of satellite orbit and clock, contained in the navigation message. To predict the on-board clock signal, in order to transmit its parameters to the users, it is necessary to model and characterize the clock behaviour, estimating the clock stochastic components as well as the clock deterministic components, such as the frequency drift. If the frequency drift is not taken into account in the clock prediction, or if it is not correctly estimated, it is a huge problem for precise time keeping applications, such as the positioning.
Actually, the frequency drift evaluation and the monitoring of its evolution over time is extremely important in GNSS applications, to ensure the adequacy of the timing system to the integrity requirements of the positioning service. It is fundamental to routinely monitor the satellite clock drift, in order to verify that the clock is performing as expected.
In addition, sometimes it could be necessary to analyse the clock phase or frequency having

removed any deterministic behaviour, in order to allow a better observation of the stochastic components affecting the clock signal.
The clock frequency drift can be predicted and removed, using well established features. Different techniques are proposed in literature for frequency drift estimation: it can be estimated through a quadratic regression on clock phase, through a linear regression on clock frequency, computing the simple mean of first difference of frequency ,using a Kalman filter, where the drift term is one element in the state vector ... [50], [51], [52]. The appropriateness of a specific technique is critically dependent on the oscillator model and on the noise present in the signal.
The purpose of this thesis work is not to develop new techniques for drift estimation and removal, nor to discuss the advantages and disadvantages of the different existing methods, but simply to describe the methodology adopted in INRIM activities and on whose implementation and improvement I contributed in these years of doctorate.
The system used in INRIM routine activities for frequency drift evaluation consists in the estimate of the coefficients of a quadratic least squares fit on clock phase data [53].
This solution has been adopted since from our experience on experimental data coming from the Galileo project or from the analysis performed on GPS data, as satellite clock data often present jumps, gaps, and outliers, we considered better to evaluate the fit coefficients on clock phase data, being the clock frequency seemingly more affected by these phenomena. However, in our operations, the clock drift has been estimated several times using a linear model on the frequency data, carefully choosing a period without particular events which could corrupt the estimate.
In the following a brief theoretical description of the clock drift estimation using a least squares approach [54] is reported, considering both a parabolic fit on clock phase data and a linear fit on clock frequency. First, for sake of completeness, it is reported also the generalization to an m^{th} degree fit. Typically, when the frequency drift is evaluated on clock phase data of Rubidium Atomic Frequency Standards m=2 is needed, while for cesium clocks m=1 can be a good choice.
It has to be remarked that in the following description only the clock deterministic behaviour is considered, since the random deviation affecting the clock phase and frequency are evaluated separately in a subsequent step of the clock characterization (see Section 3.2.2).

Problem description

As described in Section 1.2.1, a typical representation of the clock output is a quadratic model of the clock phase offset (Eq. 1.8) or a linear model of the clock frequency offset (Eq. 1.9). In both cases the frequency drift D is the quantity to be estimated: the estimate

of the clock frequency drift is therefore transduced in a ordinary least squares problem.

Fitting a polynomial of m^{th} degree

The fitting problem, for a general function of degree m of the measures z_i, can be expressed in matrix notation as [54]:

$$\hat{z}_{LS} = V \cdot \hat{p} + r \tag{3.1}$$

that is

$$\begin{bmatrix} \hat{z}(t_1) \\ \hat{z}(t_2) \\ \vdots \\ \hat{z}(t_N) \end{bmatrix} = \underbrace{\begin{bmatrix} 1 & t_1 & t_1^2 & \cdots & t_1^m \\ 1 & t_2 & t_2^2 & \cdots & t_2^m \\ \vdots & \vdots & \vdots & \cdots & \vdots \\ 1 & t_N & t_N^2 & \cdots & t_N^m \end{bmatrix}}_{V} \cdot \underbrace{\begin{bmatrix} \hat{a}_0 \\ \hat{a}_1 \\ \hat{a}_2 \\ \vdots \\ \hat{a}_m \end{bmatrix}}_{\hat{p}} + \begin{bmatrix} r_0 \\ r_1 \\ r_2 \\ \vdots \\ r_m \end{bmatrix} \tag{3.2}$$

Where $\hat{z}_{LS}$ is a column vector containing the least squares estimates for the general measures z, V is the Vandermonde matrix [55], $\hat{p}$ is the vector with the $m+1$ fit coefficients, and r is the column vector with the fit residuals, defined as:

$$r = z - \hat{z}_{LS} \tag{3.3}$$

that is the vector of the differences between the real measures and the correspondent estimated values.

The least squares solution to this problem consists in the minimization of the squared residuals r^2: for the projection theorem [56] r^2 is minimized when $\hat{z}$ is the projection of z in the subspace generated by the columns of V. Assuming that the measures z_i are independent and identically distributed with variance σ^2, and hence the covariance matrix of the residuals is simply $\Psi = \sigma^2 I_N$ [57] (where I_N is the identity matrix of dimension N), the vector with the fit coefficients $\hat{p}$ can be estimated using Eq. 3.4:

$$\hat{p} = \left(V^T \cdot V\right)^{-1} \cdot V^T \cdot \hat{z} \tag{3.4}$$

Where the symbol T represents the transposition of a matrix.

The covariance matrix of the coefficients is then:

$$\Gamma_{\hat{p}} = \sigma^2 \cdot \left[V^T \cdot V\right]^{-1} \tag{3.5}$$

In the more general case, without the assumption of uncorrelated residuals, the vector of the estimated coefficients $\hat{p}$ and the correspondent covariance matrix $\Gamma_{\hat{p}}$ can be obtained using Eq. 3.6 and Eq. 3.7 respectively:

$$\hat{p} = \left(V^T \cdot \Psi^{-1} \cdot V\right)^{-1} \cdot V^T \cdot \Psi^{-1} \cdot \hat{z} \tag{3.6}$$

$$\Gamma_{\hat{p}} = \left[V^T \cdot V\right]^{-1} \cdot V^T \cdot \Psi \cdot V \cdot \left[V^T \cdot V\right]^{-1} \tag{3.7}$$

Where Ψ is the covariance matrix of fit residuals.
It has been demonstrated that, in case of linear estimates and measures independent and identically distributed, the ordinary least squares method (whose solution is illustrated in Eq. 3.4) provides optimum estimates for the fit parameters. On the other hand, in case the covariance matrix of the residuals Ψ is general and unknown, the ordinary least squares is still a significant method for fit parameters estimate, but it is not optimum.
When the measures z_i are independent and identically distributed, the variance σ^2 can be estimated with the sample variance [58]:

$$\sigma^2 = \frac{\sum_{i=1}^{N} r_i^2}{N - (m+1)} \tag{3.8}$$

Where the denominator represents the degree of freedom of the problem, being the difference between the number of measures N and the number of unknowns.
Hence, Eq. 3.5 can be written as:

$$\Gamma_{\hat{p}} = \frac{\sum_{i=1}^{N} r_i^2}{N - (m+1)} \cdot \left(V^T \cdot V\right)^{-1} \tag{3.9}$$

QR Decomposition

The problem of the least squares fitting can be also approached in a different way, allowing not only to find the estimated fit coefficients but also to significantly reduce the computational cost of the method: it is a great advantage in the software implementations, especially when a large amount of data is considered. The *QR* decomposition, also named *Cholesky Decomposition* [57], consists in the decomposition of the $N \times m'$ Vandermonde matrix V, where $m' = m + 1$ is the number of unknowns, into the products of two matrix

$$V = Q \cdot R \tag{3.10}$$

such that Q is an $N \times m'$ orthogonal matrix

$$Q^T \cdot Q = I_{m'} \tag{3.11}$$

where $I_{m'}$ is the identity matrix of dimension m', and R is an $m' \times m'$ upper triangular matrix [6]. Thanks to this transformation, the inversion of $\left(V^T \cdot V\right)^{-1}$ required in Eq. 3.4 and Eq. 3.5 can be substituted with the equivalent operation $R^{-1} \cdot \left(R^{-1}\right)^T$, since it can be demonstrated that

$$\left(V^T \cdot V\right)^{-1} = R^{-1} \cdot \left(R^{-1}\right)^T \tag{3.12}$$

The result is that the computational cost of the solution to least squares problem is considerably reduced: the computational time is reduced.

Fitting a 2^{nd} degree polynomial on clock phase data

Given a set of clock phase measures $z_x(t)$, of the physical phenomenon described in Eq. 1.8, and neglecting the random deviations, the purpose is to evaluate the clock frequency drift finding the best estimate $\hat{x}(t)$ of the phase measures $z_x(t)$:

$$\hat{x}(t) = \hat{a}_2 t^2 + \hat{a}_1 t + \hat{a}_0 \tag{3.13}$$

which minimizes the sum of the squared difference between the N experimental data and respective estimated values:

$$\sum_{i=1}^{N} \left[z_x(t_i) - \hat{x}(t_i)\right]^2 = \sum_{i=1}^{N} \left[z_x(t_i) - \hat{a}_2 t_i^2 - \hat{a}_1 t_i - \hat{a}_0\right]^2 = min \tag{3.14}$$

In matrix notation the problem described in Eq. 3.13 becomes:

$$\begin{bmatrix} \hat{x}(t_1) \\ \hat{x}(t_2) \\ \vdots \\ \hat{x}(t_N) \end{bmatrix} = \underbrace{\begin{bmatrix} 1 & t_1 & t_1^2 \\ 1 & t_2 & t_2^2 \\ \vdots & \vdots & \\ 1 & t_N & t_N^2 \end{bmatrix}}_{V} \cdot \underbrace{\begin{bmatrix} \hat{a}_0 \\ \hat{a}_1 \\ \hat{a}_2 \end{bmatrix}}_{\hat{p}} \tag{3.15}$$

Applying the least squares method as per Eq. 3.4, the estimated coefficients are:

[6] a matrix with all zeros below the main diagonal, also called right triangular matrix

$$\hat{a}_0 = \frac{\sum_{i=1}^{N} z_{x_i} \left[\sum_{i=1}^{N} t_i^2 \sum_{i=1}^{N} t_i^4 - \left(\sum_{i=1}^{N} t_i^3 \right)^2 \right] - \sum_{i=1}^{N} z_{x_i} t_i \left[\sum_{i=1}^{N} t_i \sum_{i=1}^{N} t_i^4 - \sum_{i=1}^{N} t_i^2 \sum_{i=1}^{N} t_i^3 \right] + \sum_{i=1}^{N} t_i^2 z_{x_i} \left[\sum_{i=1}^{N} t_i \sum_{i=1}^{N} t_i^3 - \left(\sum_{i=1}^{N} t_i^2 \right)^2 \right]}{Den}$$

$$\hat{a}_1 = \frac{N \left(\sum_{i=1}^{N} t_i z_{x_i} \sum_{i=1}^{N} t_i^4 - \sum_{i=1}^{N} t_i^2 z_{x_i} \sum_{i=1}^{N} t_i^3 \right) - \sum_{i=1}^{N} t_i \left(\sum_{i=1}^{N} z_{x_i} \sum_{i=1}^{N} t_i^4 - \sum_{i=1}^{N} t_i^2 z_{x_i} \sum_{i=1}^{N} t_i^2 \right) + \sum_{i=1}^{N} t_i^2 \left(\sum_{i=1}^{N} z_{x_i} \sum_{i=1}^{N} t_i^3 - \sum_{i=1}^{N} t_i z_{x_i} \sum_{i=1}^{N} t_i^2 \right)}{Den}$$

$$\hat{a}_2 = \frac{N \left(\sum_{i=1}^{N} t_i^2 \sum_{i=1}^{N} t_i^2 z_{x_i} - \sum_{i=1}^{N} t_i^3 \sum_{i=1}^{N} t_i z_{x_i} \right) - \sum_{i=1}^{N} t_i \left(\sum_{i=1}^{N} t_i \sum_{i=1}^{N} t_i^2 z_{x_i} - \sum_{i=1}^{N} t_i^3 \sum_{i=1}^{N} z_{x_i} \right) + \sum_{i=1}^{N} t_i^2 \left(\sum_{i=1}^{N} t_i \sum_{i=1}^{N} t_i z_{x_i} - \sum_{i=1}^{N} t_i^2 \sum_{i=1}^{N} z_{x_i} \right)}{Den}$$

$$Den = N \left[\sum_{i=1}^{N} t_i^2 \sum_{i=1}^{N} t_i^4 - \left(\sum_{i=1}^{N} t_i^3 \right)^2 \right] - \sum_{i=1}^{N} t_i \left[\sum_{i=1}^{N} t_i \sum_{i=1}^{N} t_i^4 - \sum_{i=1}^{N} t_i^3 \sum_{i=1}^{N} t_i^2 \right] + \sum_{i=1}^{N} t_i^2 \left[\sum_{i=1}^{N} t_i \sum_{i=1}^{N} t_i^3 - \left(\sum_{i=1}^{N} t_i^2 \right)^2 \right]$$

Then, the clock frequency drift can be obtained as twice the quadratic term:

$$D = 2 \cdot \hat{a}_2 \tag{3.16}$$

Fitting a 1^{st} degree polynomial on clock frequency data

Given a set of clock frequency measures $z_y(t)$, of the physical phenomenon described in Eq. 1.9, and neglecting the random deviations, the purpose is to evaluate the clock frequency drift finding the best estimate $\hat{y}(t)$ of the normalized frequency measures $z_y(t)$:

$$\hat{y}(t) = \hat{a}_1 t + \hat{a}_0 \tag{3.17}$$

which minimizes the sum of the squared difference between the M experimental data and respective estimated values:

$$\sum_{i=1}^{M} [z_y(t_i) - \hat{y}(t_i)]^2 = \sum_{i=1}^{M} [z_y(t_i) - \hat{a}_1 t_i - \hat{a}_0]^2 = min \tag{3.18}$$

In matrix notation the problem described in Eq. 3.17 becomes:

$$\begin{bmatrix} \hat{y}(t_1) \\ \hat{y}(t_2) \\ \vdots \\ \hat{y}(t_M) \end{bmatrix} = \underbrace{\begin{bmatrix} 1 & t_1 \\ 1 & t_2 \\ \vdots & \vdots \\ 1 & t_M \end{bmatrix}}_{V} \cdot \underbrace{\begin{bmatrix} \hat{a}_0 \\ \hat{a}_1 \end{bmatrix}}_{\hat{p}} \tag{3.19}$$

Applying the least squares method as per Eq. 3.4, the estimated coefficients of the linear fit are:

$$\hat{a}_0 = \frac{\sum_{i=1}^{M} z_{y_i} \sum_{i=1}^{M} t_i^2 - \sum_{i=1}^{M} t_i \sum_{i=1}^{M} t_i z_{y_i}}{M \sum_{i=1}^{M} t_i^2 - \left(\sum_{i=1}^{M} t_i\right)^2}$$

$$\hat{a}_1 = \frac{M \sum_{i=1}^{M} t_i z_{y_i} - \sum_{i=1}^{M} t_i \sum_{i=1}^{M} z_{y_i}}{M \sum_{i=1}^{M} t_i^2 - \left(\sum_{i=1}^{M} t_i\right)^2}$$

The clock freqeuncy drift is then

$$D = \hat{a}_1 \tag{3.20}$$

Use of Barycentric Coordinates

An interesting trick to be used when implementing a least squares solution on a set of experimental data is the use of barycentric coordinates for the abscissae axis. In fact, by moving in barycentric coordinates, the formulae to be used for fit coefficients estimation

significantly simplify.
Considering the coefficients of the quadratic and linear fit obtained solving the systems of equations illustrated in Eq. 3.15 and Eq. 3.19, it can be observed that the formulae for their estimation contain several summations of the coordinates t_i. In order to obtain a simpler formulation for the polynomial coefficients (and for the related uncertainties, as illustrated in Section 3.2.1.1.2) it is therefore suitable to set the origin of the axis at the barycenter of the time, so that all the terms $\sum_{i=1}^{N} t_i^{\alpha}$, in which α is odd, cancel out.
The new set of coordinates is obtained by subtracting to each coordinate the coordinate of the barycenter t_B, that is the mean value of the abscissae:

$$t_B = \frac{1}{N}\sum_{i=1}^{N} t_i \tag{3.21}$$

Barycentric coordinates are then given by:

$$\bar{t}_i = t_i - t_B \tag{3.22}$$

With this axis traslation, the best estimates of the clock phase measures illustrated in Eq. 3.13 become:

$$\hat{x}(\bar{t}) = \hat{a}_2\bar{t}^2 + \hat{a}_1\bar{t} + \hat{a}_0 \tag{3.23}$$

where the coefficients of the quadratic fit are:

$$\hat{a}_0 = \frac{\sum_{i=1}^{N} z_{x_i} \sum_{i=1}^{N} t_i^2 \sum_{i=1}^{N} t_i^4 - \sum_{i=1}^{N} t_i^2 z_{x_i} \left(\sum_{i=1}^{N} t_i^2\right)^2}{Den}$$

$$\hat{a}_1 = \frac{N \sum_{i=1}^{N} t_i z_{x_i} \sum_{i=1}^{N} t_i^4 - \sum_{i=1}^{N} t_i z_{x_i} \left(\sum_{i=1}^{N} t_i^2\right)^2}{Den}$$

$$\hat{a}_2 = \frac{N \sum_{i=1}^{N} t_i^2 \sum_{i=1}^{N} t_i^2 z_{x_i} - \left(\sum_{i=1}^{N} t_i^2\right)^2 \sum_{i=1}^{N} z_{x_i}}{Den}$$

Where

$$Den = \sum_{i=1}^{N} t_i^2 \left[N \sum_{i=1}^{N} t_i^4 - \left(\sum_{i=1}^{N} t_i^2\right)^2 \right]$$

Analogously, the best estimate of the clock frequency measures in Eq. 3.17 can be written as

$$\hat{y}(\bar{t}) = \hat{a}_1\bar{t} + \hat{a}_0 \tag{3.24}$$

with coefficients:

$$\hat{a}_0 = \frac{\sum_{i=1}^{M} z_{y_i}}{M}$$

$$\hat{a}_1 = \frac{\sum_{i=1}^{M} t_i z_{y_i}}{\sum_{i=1}^{M} t_i^2}$$

It can be easily observed that, using barycentric coordinates, the expressions of the polynomial fit have been noticeably simplified.

3.2.1.1.2 Evaluation of the Uncertainty on Frequency Drift Estimate

One of my contributions to the clock characterization activity performed at INRIM, consisted in the evaluation of the uncertainty on the frequency drift estimate on clock data and the correspondent software implementation.

The uncertainty related to each term of the polynomial fit can be derived from the covariance matrix $\Gamma_{\hat{p}}$ obtained using Eq. 3.7, assuming that the clock measures are independent and identically distributed, with variance σ^2, defined in Eq. 3.8.

In order to minimize the computational complexity of problem, the uncertainty evaluation is implemented using the Cholesky Decomposition of the Vandermonde matrix V. Therefore, considering the equality in Eq. 3.12 and substituting σ^2 with its definition, the uncertainty of the coefficients can be evaluated using Eq. 3.25:

$$\Gamma_{\hat{p}} = \frac{R^{-1} \cdot (R^{-1})^T \cdot \sum_{i=1}^{N} r_i^2}{N - (m+1)} \tag{3.25}$$

Where R is the upper triangular matrix resulting from the Cholesky decomposition of V, N is the number of experimental measurements (in this context either clock phase or normalized frequency mesures) and m is the degree of the fitting polynomial.

Quadratic fit on clock phase data

In case the clock frequency drift is evaluated through a quadratic fit on N clock phase data $z_x(t)$, the variance $\sigma_{\hat{x}}^2$ of the best estimate $\hat{x}(t)$ can be evaluated through the law of propagation of the uncertainty, described in [59] and reported in Eq. 3.26 for our specific case:

$$\begin{aligned}
\sigma_{\hat{x}}^2 &= \left(\frac{\partial z_x}{\partial a_0}\right)^2 \sigma_{a_0}^2 + \left(\frac{\partial z_x}{\partial a_1}\right)^2 \sigma_{a_1}^2 + \left(\frac{\partial z_x}{\partial a_2}\right)^2 \sigma_{a_2}^2 \\
&\quad + 2 \cdot \left[\frac{\partial z_x}{\partial a_0} \cdot \frac{\partial z_x}{\partial a_1} \sigma_{a_0,a_1} + \frac{\partial z_x}{\partial a_0} \cdot \frac{\partial z_x}{\partial a_2} \sigma_{a_0,a_2} + \frac{\partial z_x}{\partial a_1} \cdot \frac{\partial z_x}{\partial a_2} \sigma_{a_1,a_2}\right] \\
&= 1^2 \cdot \sigma_{a_0}^2 + t^2 \cdot \sigma_{a_1}^2 + t^4 \cdot \sigma_{a_2}^2 + 2 \cdot \left[1 \cdot t \cdot \sigma_{a_0,a_2} + 1 \cdot t^2 \cdot \sigma_{a_0,a_2} + t \cdot t^2 \cdot \sigma_{a_1,a_2}\right] \\
&= \sigma_{a_0}^2 + t^2 \cdot \sigma_{a_1}^2 + t^4 \cdot \sigma_{a_2}^2 + 2 \cdot \left[t \cdot \sigma_{a_0,a_1} + t^2 \cdot \sigma_{a_0,a_2} + t^3 \cdot \sigma_{a_1,a_2}\right]
\end{aligned} \tag{3.26}$$

Where the variance terms σ_i^2 and the covariance terms $\sigma_{i,j}$ are derived from the covariance matrix $\Gamma_{\hat{p}}$, obtained applying Eq. 3.25 and reported in Eq. 3.27.

In particular, the uncertainties of the parabolic fit coefficients σ_{a_2} , σ_{a_1} and σ_{a_0}, can be directly derived as the square root of the elements of the main diagonal.

$$\Gamma_{\hat{p}} = \frac{\sigma^2}{Den} \cdot \begin{bmatrix} M_{11} & M_{11} & M_{12} \\ M_{21} & M_{22} & M_{23} \\ M_{31} & M_{32} & M_{33} \end{bmatrix} = \begin{bmatrix} \sigma_{a_0}^2 & \sigma_{a_0,a_1} & \sigma_{a_0,a_2} \\ \sigma_{a_1,a_0} & \sigma_{a_1}^2 & \sigma_{a_1,a_2} \\ \sigma_{a_2,a_0} & \sigma_{a_2,a_1} & \sigma_{a_2}^2 \end{bmatrix} \tag{3.27}$$

Where σ^2 is the sample variance defined in Eq. 3.8, that is, in this context:

$$\sigma^2 = \frac{\sum_{i=1}^{N} (z_{x_i} - \hat{x}_i)^2}{N - (m+1)} \tag{3.28}$$

$$M_{11} = \sum_{i=1}^{N} t_i^2 \sum_{i=1}^{N} t_i^4 - \left(\sum_{i=1}^{N} t_i^3 \right)^2$$

$$M_{12} = \sum_{i=1}^{N} t_i^3 \sum_{i=1}^{N} t_i^2 - \sum_{i=1}^{N} ti \sum_{i=1}^{N} t_i^4$$

$$M_{13} = \sum_{i=1}^{N} t_i \sum_{i=1}^{N} t_i^3 - \left(\sum_{i=1}^{N} t_i^2 \right)^2$$

$$M_{21} = \sum_{i=1}^{N} t_i^2 \sum_{i=1}^{N} t_i^3 - \sum_{i=1}^{N} t_i \sum_{i=1}^{N} t_i^4$$

$$M_{22} = N \sum_{i=1}^{N} t_i^4 - \left(\sum_{i=1}^{N} t_i^2 \right)^2$$

$$M_{23} = \sum_{i=1}^{N} t_i \sum_{i=1}^{N} t_i^2 - N \sum_{i=1}^{N} t_i^3$$

$$M_{31} = \sum_{i=1}^{N} t_i \sum_{i=1}^{N} t_i^3 - \left(\sum_{i=1}^{N} t_i^2 \right)^2$$

$$M_{32} = \sum_{i=1}^{N} t_i^2 \sum_{i=1}^{N} t_i - N \sum_{i=1}^{N} t_i^3$$

$$M_{33} = N \sum_{i=1}^{N} t_i^2 - \left(\sum_{i=1}^{N} t_i \right)^2$$

$$Den = N\left[\sum_{i=1}^{N} t_i^2 \sum_{i=1}^{N} t_i^4 - \left(\sum_{i=1}^{N} t_i^3\right)^2\right] - \sum_{i=1}^{N} t_i \left[\sum_{i=1}^{N} t_i \sum_{i=1}^{N} t_i^4 - \sum_{i=1}^{N} t_i^3 \sum_{i=1}^{N} t_i^2\right] + \sum_{i=1}^{N} t_i^2 \left[\sum_{i=1}^{N} t_i \sum_{i=1}^{N} t_i^3 - \left(\sum_{i=1}^{N} t_i^2\right)^2\right]$$

Then, the uncertainty on the frequency drift estimate, can be immediately obtained as:

$$\sigma_D = 2 \cdot \sigma_{a_2} \tag{3.29}$$

If barycentric coordinates are used, the covariance matrix becomes:

$$\Gamma_{\hat{p}} = \frac{\sigma^2}{Den} \cdot \begin{bmatrix} \sum_{i=1}^{N} t_i^2 \sum_{i=1}^{N} t_i^4 & 0 & -\left(\sum_{i=1}^{N} t_i^2\right)^2 \\ 0 & N\sum_{i=1}^{N} t_i^4 - \left(\sum_{i=1}^{N} t_i^2\right)^2 & 0 \\ -\left(\sum_{i=1}^{N} t_i^2\right)^2 & 0 & N\sum_{i=1}^{N} t_i^2 \end{bmatrix} \tag{3.30}$$

Where:

$$Den = \sum_{i=1}^{N} t_i^2 \left[N\sum_{i=1}^{N} t_i^4 - \left(\sum_{i=1}^{N} t_i^2\right)^2\right]$$

It can be noted that the variance and covariance terms have considerably simplified: the covariance between the linear term and the intercept as well as the covariance between the linear and the quadratic term canceled out.

Linear fit on clock frequency data

Analogously, if the clock frequency drift is evaluated through a linear fit on M clock normalized frequency data $z_y(t)$, the variance $\sigma_{\hat{y}}^2$ on the best estimate $\hat{y}(t)$ can be evaluated according to [59]: Eq. 3.31 reports the derivation for our specific case:

$$\begin{aligned} \sigma_{\hat{y}}^2 &= \left(\frac{\partial z_y}{\partial a_0}\right)^2 \sigma_{a_0}^2 + \left(\frac{\partial z_y}{\partial a_1}\right)^2 \sigma_{a_1}^2 + 2 \cdot \left[\frac{\partial z_y}{\partial a_0} \cdot \frac{\partial z_y}{\partial a_1} \sigma_{a_0,a_1}\right] \\ &= \sigma_{\hat{a}_0}^2 + t^2 \cdot \sigma_{\hat{a}_1}^2 + 2t\sigma_{\hat{a}_0,\hat{a}_1} \end{aligned} \tag{3.31}$$

Where the variance and covariance terms, reported in Eq. 3.32, are calculated from the covariance matrix $\Gamma_{\hat{p}}$, obtained applying Eq. 3.25:

$$\Gamma_{\hat{p}} = \frac{\sigma^2}{D} \cdot \begin{bmatrix} \sum_{i=1}^{M} t_i^2 & -\sum_{i=1}^{M} t_i \\ -\sum_{i=1}^{M} t_i & M \end{bmatrix} \tag{3.32}$$

Being:

$$\sigma^2 = \frac{\sum_{i=1}^{M} (z_{y_i} - \hat{y}_i)^2}{M - (m+1)}$$

and

$$Den = M \sum_{i=1}^{M} t_i^2 - \left(\sum_{i=1}^{M} t_i \right)^2$$

Using barycentric coordinates, the expression of the covariance matrix considerably simplifies, as showed in Eq. 3.33:

$$\Gamma_{\hat{p}} = \sigma^2 \cdot \begin{bmatrix} \frac{1}{M} & 0 \\ 0 & \frac{1}{\sum_{i=1}^{M} t_i^2} \end{bmatrix} \tag{3.33}$$

It can be noted that the covariances are now zeros.
Fig. 3.2.1.1.2 and Fig. 3.2.1.1.2 illustrate a linear fit executed on the frequency data of an Active Hydrogen Maser available in INRIM laboratories: in the first case, both the fit coefficients and the 2σ uncertainty have been evaluated using the values of $\sigma_{a_0}^2$, $\sigma_{a_1}^2$ and σ_{a_0,a_1} derived from Eq. 3.32, while on the other case the variance and covariance terms have been derived from Eq. 3.33:

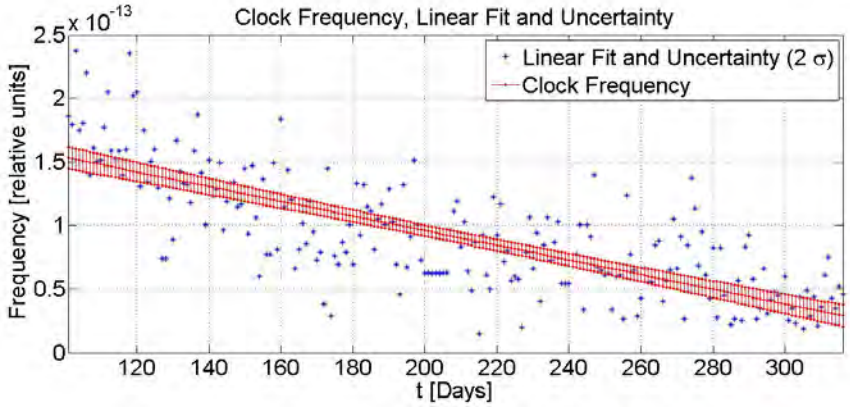

Figure 3.3: Clock Frequency, Linear Fit and Uncertainty: Ordinary Coordinates

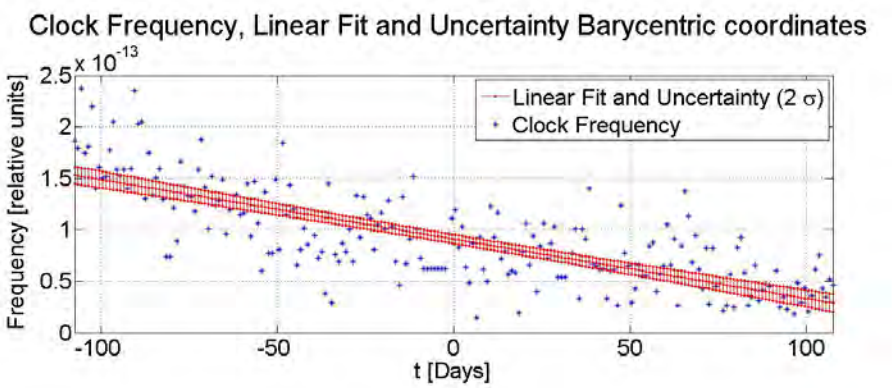

Figure 3.4: Clock Frequency, Linear Fit and Uncertainty: Barycentric Coordinates

The aim of Fig. 3.2.1.1.2 and Fig. 3.2.1.1.2 is to show that the choice of using barycentric coordinates is purely a matter of convenience in the implementation of the formulae, and does not impact the final result. In fact, by changing coordinates, if the variance is decreased then the covariance terms are increased and vice versa, as shown in Table 3.2, reporting the numerical results of the variance and covariance terms of the linear fit on frequency data illustrated in Fig. 3.2.1.1.2 and Fig. 3.2.1.1.2:

$\sigma^2_{i,j}$	Barycentric Coordinates	Ordinary Coordinates
$\sigma^2_{a_0}$ [rel.units^2]	$4.51 \cdot 10^{-30}$	$5.50 \cdot 10^{-29}$
$\sigma^2_{a_1}$[rel.units^2/day^2]	$1.16 \cdot 10^{-33}$	$1.16 \cdot 10^{-33}$
σ_{a_1,a_0} [rel.units^2/day]	0	$-2.42 \cdot 10^{-31}$

Table 3.2: Variances and Covariances on Linear Fit using Barycentric or Ordinary Coordinates

It can be observed that, while the variance on the linear term remains the same adopting barycentric coordinates (since the use of barycentric coordinates implies only a translation over the x-axis), the variance of the intercept decreases. On the contrary, the covariance between the two fit coefficients is increased if barycentric coordinates are used: on the whole, the uncertainty on the linear fit does not change.

3.2.1.1.3 Analysis of the Adequacy of the Algorithm for Drift Estimate

In this paragraph the method presented in Section 3.2.1.1.1 for clock frequency drift estimation and removal is applied to experimental data from the GPS system, showing the effectiveness of the method. In addition, an analysis of the residuals resulting from the drift removal is performed, in order to check the initial assumptions.
Considering for example the normalized frequency generated by the RAFS on board GPS satellite SVN 50, for the period from January 13^{th} to 17^{th} of year 2008, obtained processing the RINEX for clock files generated by the International GNSS Service (IGS) with the INRIM tool described in Section 3.2.4, it is possible to observe the linear drift producing a slight decrease of the normalized frequency in Fig. 3.5:

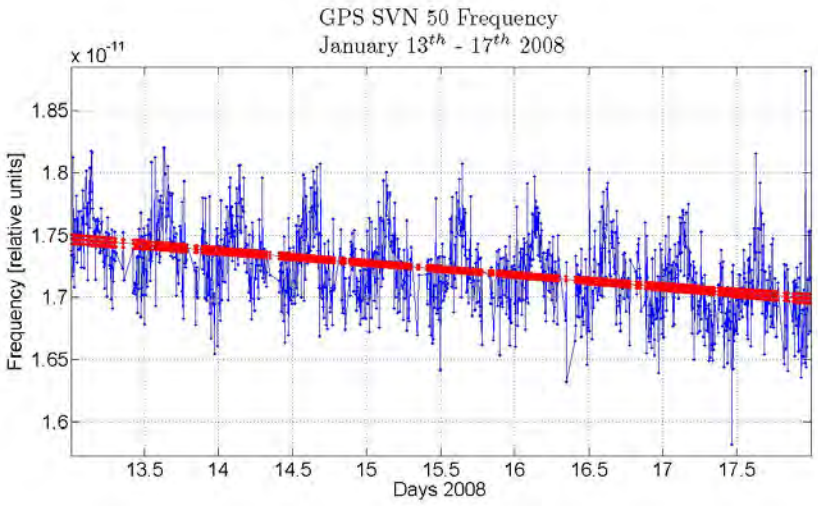

Figure 3.5: GPS Satellite SVN 50 (RAFS) Normalized Frequency Offset Affected by Linear Drift, January 13^{th} - 17^{th} 2008

The red lines represent the linear fit on clock normalized frequency data and its uncertainty. A coverage factor k=2 has been used to get the expanded uncertainty [59].
It is quite evident in Fig. 3.5 the presence of a sinusoidal pattern on the apparent clock frequency. In fact, as reported in this thesis (see section 4.2.2) and in literature (see [44], [63]), the estimated GNSS clocks on board satellites are often affected by periodic fluctuations. It is quite probable that the residuals resulting from the analysis after frequency drift removal could show a slight sinusoidal behaviour: the hypothesis of uncorrelated measurement errors could appear to be not confirmed. However, since the periodic contribution over the whole considered period can cancel out, being as positive as negative, the ordinary

least squares method described in Section 3.2.1.1.1 is used to quantify the frequency drift. The results for the fit coefficients and the respective uncertainties are reported in Table 3.3:

$a_1 \pm\sigma_{a_1}$ $[s/s]$	$a_0 \pm\sigma_{a_0}$ $[s]$
$-9.61 \cdot 10^{-14} \pm 6.04 \cdot 10^{-15}$	$1.87 \cdot 10^{-11} \pm 9.42 \cdot 10^{-14}$

Table 3.3: Linear fit coefficients and uncertainty

The linear coefficient a_1 is directly the estimate of the clock frequency drift.
The results reported in Tab. 3.3 were obtained under the assumption that the error terms have a normal distribution and are independent (with constant variance). To check the assumptions of independent errors and constant error variance, one approach is to plot the residuals, that is the differences between the experimental data and the estimated fit [60], and to observe their spread over time.
Fig. 3.6 illustrates a desirable plot for residuals: the spread is fairly constant over time and no particular pattern can be observed.

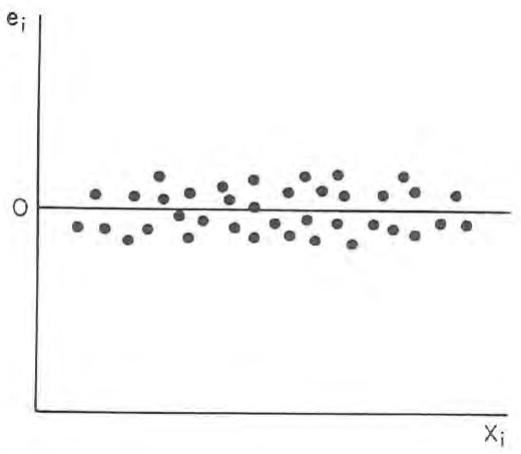

Figure 3.6: Example of Residuals in case of independent estimates and constant variance [60]

On the contrary, Fig. 3.7 and Fig. 3.8 show the distribution of residuals in case of an inappropriate use of the least squares regression: in Fig. 3.7 the residuals are not random distributed, while the residuals in Fig. 3.8 are the result of an analysis in which the hypothesis of constant variance of the measures is not satisfied.

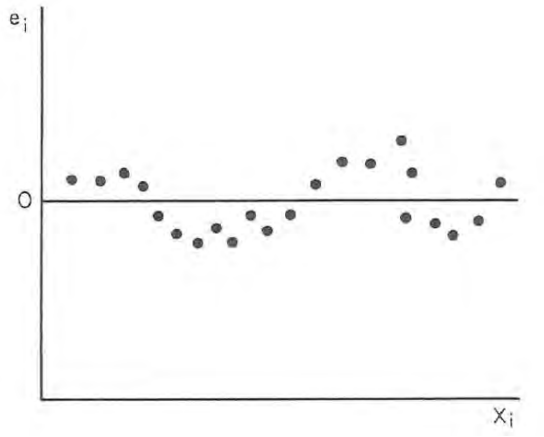

Figure 3.7: Example of non-random residuals [60]

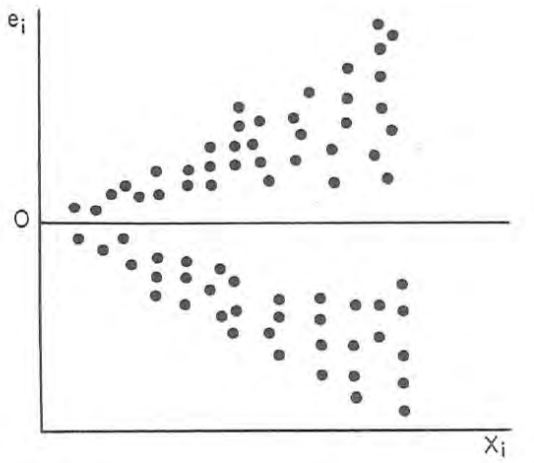

Figure 3.8: Example of non-constant variance [60]

Other examples of residuals are reported in [57]:

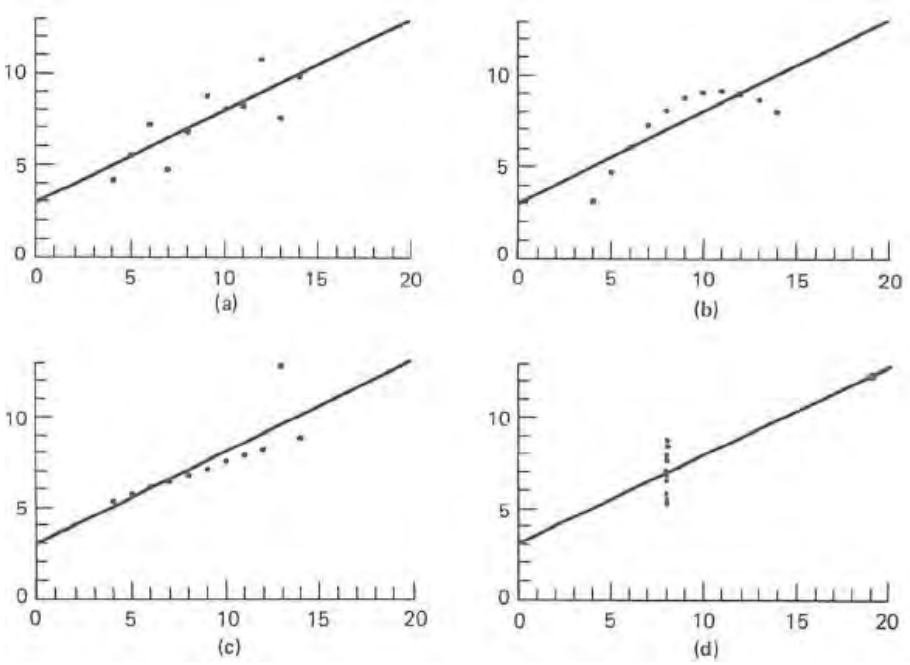

Figure 3.9: Four cases of hypothetical data sets [57]

The first example (a) shows the expected distribution of residuals when the simple linear regression model is appropriate to the input data. The second example (b) suggests that the analysis based on a simple linear regression is not correct: probably a quadratic polynomial would be a better choice for the fit on input measures.
The third case (c) is an example of the appropriateness of the simple linear regression for most of the data, except for one outlier. In such case the best solution is to remove the outliers from the data set before evaluating the fit, as routinely done by the INRIM analysis tool. The fourth example (d) illustrates again a not correct regression, but there is not enough information concerning the fitted model.
The residuals for the normalized frequency data set showed in Fig. 3.5 are illustrated in Fig. 3.10:

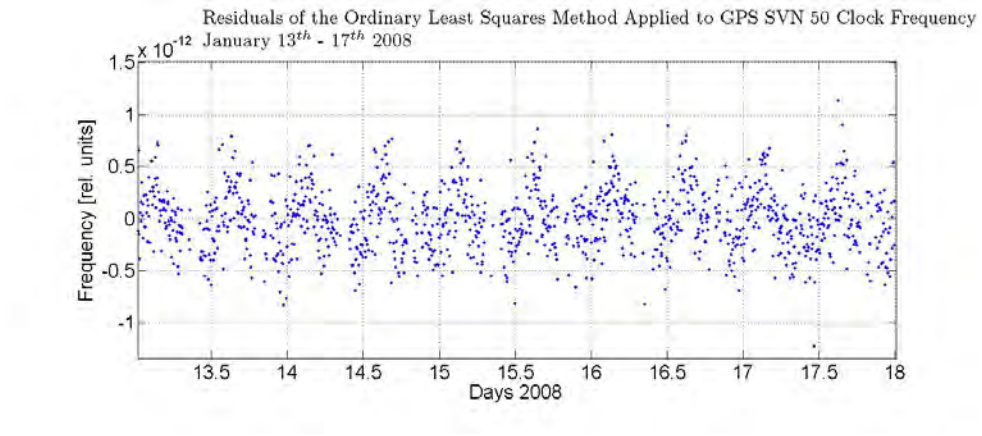

Figure 3.10: Residuals of the Ordinary Least Squares Method Applied to GPS SVN 50 Clock Normalized Frequency, January 13^{th}-18^{th} 2008

It can be noted that the hypothesis of constant variance is verified, since the spread of the residuals is rather constant over time. However a slight sinusoidal pattern can be observed: it could suggest that the hypothesis of random residuals has been violated and the analysis based on simple linear regression could be incorrect.
To check the actual correlation between residuals, the autocorrelation function, shown in Fig. 3.11, has been computed:

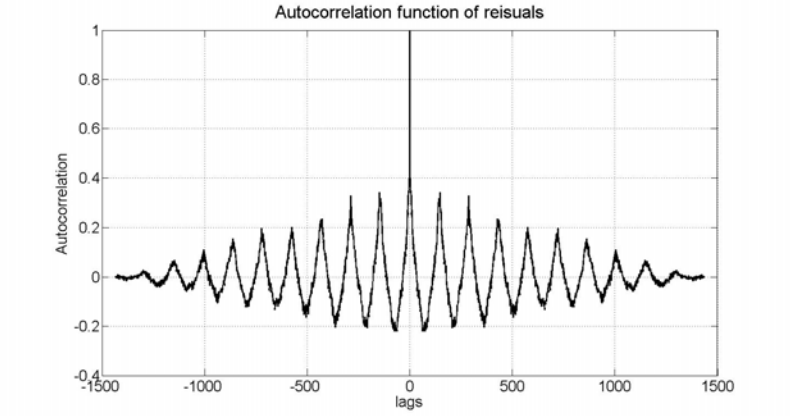

Figure 3.11: Autocorrelation function of residuals of the linear fit on the clock normalized frequency of GPS satellite SVN 50, from January 13^{th} to 18^{th} 2008

In the case of correlated observations the ordinary least squares algorithm does not represent the optimal solution for the estimate of the fit coefficients and the uncertainty

would be then underestimated. An alternative approach is to abandon the hypothesis of white noise and find a better model for the measurement errors.
Considering the measurement errors as a second order autoregressive process [61], [62], an estimate of the residuals covariance matrix Ψ can be obtained, and the generalized least squares formula Eq. 3.6 can be used to get the fit coefficients.
Applying Eq.3.6 to the experimental GPS clock normalized frequency data, the estimates of the frequency fit coefficients reported in Table 3.4 can be found:

$a_1 \ \pm\sigma_{a_1}\ [s/s]$	$a_0 \ \pm\sigma_{a_0}\ [s]$
$-8.25 \cdot 10^{-14} \pm 1.15 \cdot 10^{-14}$	$1.85{\cdot}10^{-11} \pm 1.94 \cdot 10^{-13}$

Table 3.4: Linear fit Coefficients and Uncertainty, Generalized Least Squares

As it can be observed in the example reported in Table 3.4, the apparent clock drift estimate and the value of its statistical dispersion are of the same order of magnitude. Actually, sometimes it may happen that the frequency drift and the respective uncertainty are comparable: it can be due to the excessive measurement noise affecting the experimental data. In such cases the clock drift estimate needs to be improved considering, for example, a larger observation period for the clock drift estimate.
In this paragraph, since the objective is the analysis of clock residuals, the period considered for the drift estimate has not been increased.
Comparing Table 3.3 and Table 3.4, it can be noted that the results of the fit on clock normalized frequency data are not considerably different: the use of the generalized least squares method instead of the ordinary least squares method did not introduce any improvement: the uncertainty on the fit coefficients is even increased with respect to the first estimates.
The residuals of the linear fit on clock frequency performed using the generalized least squares method still show a periodic fluctuation, as it can be observed in Fig. 3.12:

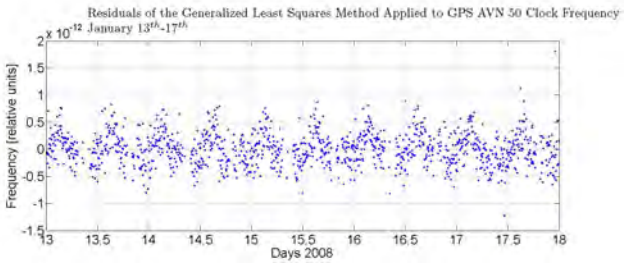

Figure 3.12: Residuals obtained using the generalized least squares method

This can be due to the fact that the measurement errors can not be modeled as a second order autoregressive process to refine the estimate of the frequency drift.
Actually, the sinusoidal fluctuation could be ascribed to some orbital effects, which affect the estimates of the clock [44]. The assumption of white noise over the frequency estimates was not uncorrected, in fact the ordinary least squares algorithm allows a proper evaluation of the clock frequency drift. The sinusoidal fluctuation on the residuals is not due to an erroneous model of the problem, but it is caused by orbital dynamics and environmental factors.
According to some studies on GPS satellite clocks, periodic signals have been detected superimposed to the random background, in all clock types: a clear relationship between such periodic signals and the orbital dynamics has been assessed.
The ordinary least squares could then be considered a proper method for the estimation of the frequency drift, since the periodic behaviour visible on the residuals is not the consequence of a bad model but it could be ascribed to orbital dynamics. However, even if the sinusoidal pattern observed on the apparent clock estimates is not due to the clock itself, it should not be present: the best solution would be to remove the periodic contribution from the apparent clock estimates before evaluating the frequency drift. Alternatively, the estimate of the apparent clock frequency drift could be estimated over an integer number of cycles of the periodic phenomenon. This is the solution we usually adopt.

3.2.1.1.4 Monitoring of Frequency Drift Evolution

As already mentioned, the clock frequency drift should be continuously monitored in order to verify if the clock is behaving as per manufacturer specifications. The GNSS operators could be interested in observing if potential deviations of the frequency drift from the nominal values are just a temporary status, with no impact on the navigation solution, or if they can be indicators of some malfunctioning, either on the clock itself or in the surrounding environment (ex. a fault in the thermal control, etc.). In this latter case some recovery actions shall be foreseen: the affected satellite shoud be identified as not reliable and its measures will not be used in the navigation solution, or the reference for signal generation on board the satellite should switch to the redundant clocks... In this context, in the frame of the GIOVE Mission, I periodically evaluated the clock frequency drift for GIOVE satellites over some selected periods and reported its entity on specific files to be exchanged with the European Space Agency and the other contractors involved in the project.
The frequency drift of GIOVE clocks is also estimated on a weekly basis, together with the other clock parameters, for the on board clock characterization activity.
The results produced are periodically collected and the evolution of the parameter over

time is showed through proper graphics.
As an example of the activity carried out, Fig. 3.13 reports the evolution of one of GPS satellites, PRN G05, launched on Space Vehicle 35 on August 30th 1993, flying a Rubidium Atomic Frequency Standard.

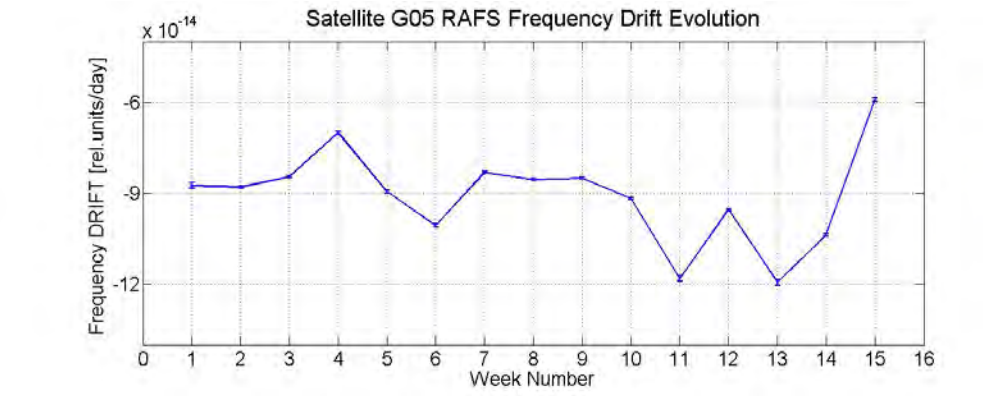

Figure 3.13: GPS Satellite G05 (RAFS) Frequency Drift Evolution, January-February 2008

Fig. 3.13 shows different measures of the frequency drift of the RAFS clock on board the satellite, as estimated processing the IGS RINEX for clock files with the INRIM tool for clock characterization, for several weeks. The frequency drift has been evaluated over different 5 days batches, indicated as *Week* in the x-axis of Fig. 3.13, from the beginning of January to the beginning of March of year 2008. The absolute value of the frequency drift of RAFS clocks is expected to stay below a certain threshold, according to the manufacturer specification. For that reason, it is important to monitor the drift behaviour so that in case it exceeds the specified threshold a warning can be raised, related to the observed anomaly.
It can be observed that the frequency drift estimate does not remain constant but experience some variations from one week to another. However, in the considered period, it remains well below the specifications.
For each estimate of the clock frequency drift, the correspondent uncertainty is also evaluated and reported in the evolution plot, as evident in the zoom in Fig. 3.14. However the uncertainty on the frequency drift for the clock on board GPS satellite G05, in the considered period, is typically very small, oscillating from one undredth to one thousandth of the drift estimate.
The implementation of the calculus of the uncertainty has been part of my tasks and has been performed applying the theory reported in Section 3.2.1.1.2.

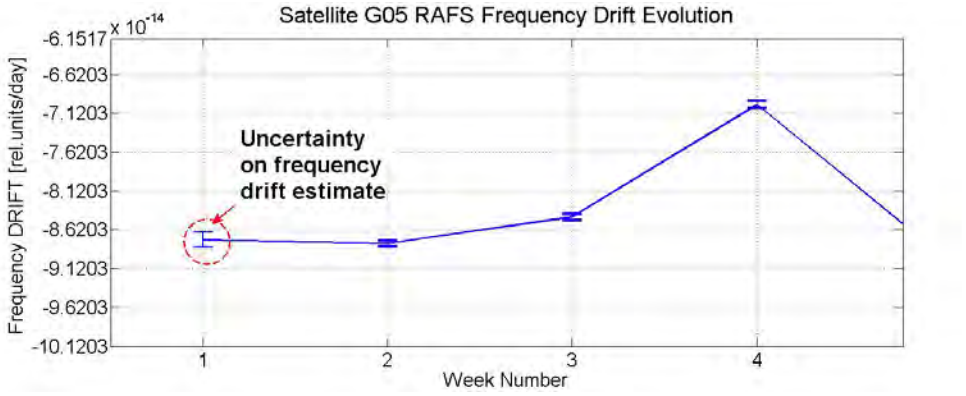

Figure 3.14: GPS Satellite G05 (RAFS) Frequency Drift Evolution, January-February 2008: Zoom on Uncertainty Bars

3.2.2 Stochastic Behaviour

The clock signal is affected by stochastic noises which produce random variations on the oscillator frequency.
It can be demonstrated that the frequency of high quality frequency sources can be perturbed by a superposition of independent noise processes [64].
Considering the one-sided spectral density $S_y(f)$ of the fractional frequency defined in Eq. 1.4, function of the Fourier frequency f, the noise processes perturbing the oscillator frequency belong to the five following types:

$$S_y(f) = h_\alpha f^\alpha \tag{3.34}$$

Where

$$\alpha = -2, -1, 0, 1, 2$$

Table 3.5 lists the noise types affecting the oscillators and summarizes their main features [65]. These noises can be studied either in the frequency or in the time domain. In this section the attention will be focused on the statistics for the analysis of clocks' stochastic behaviour in the time domain.

Noise type	Denomination	Description
$\alpha = -2$	Random walk of frequency	Limits the long term frequency stability. It is probably originated by environmental factors.
$\alpha = -1$	Flicker frequency noise	It is the source of the limitation of the log term frequency stability for all frequency sources.
$\alpha = 0$	White frequency noise	Result of the noise perturbation in the generation of the oscillation, due to white noise within the band width of the frequency-determining element of the frequency control system. Usually masked by other noise processes, such as flicker frequency noise and white phase noise.
$\alpha = 1$	Flicker phase noise	Mainly generated by transistors.
$\alpha = 2$	White phase noise	Predominates for f large enough. It the the result of the additive thermal or quantum noise.

Table 3.5: Noise types affecting frequency sources

3.2.2.1 The Concept of Stability

The stability of an oscillator is the characteristic that determines how well it can produce the same frequency over a given time interval [10]. Therefore *stability* indicates whether the frequency of an oscillator remains the same over a considered observation interval.

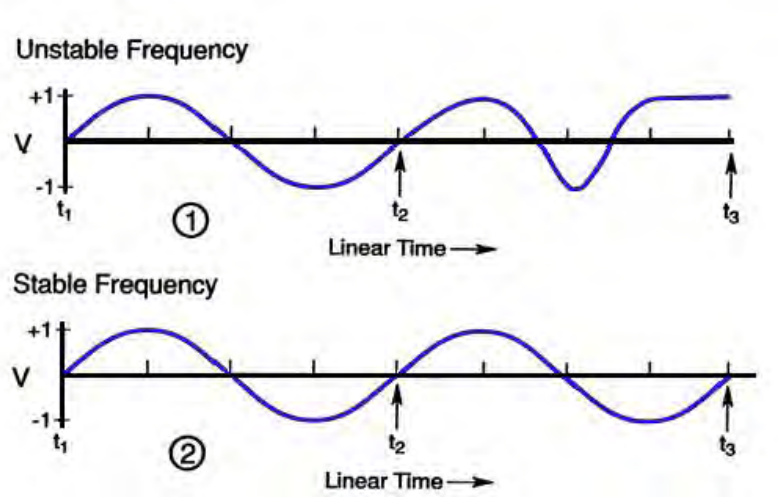

Figure 3.15: Frequency Stability Concept [10]

Manufacturers usually specify their oscillators in term of short term, long term, and environmental frequency stability [66]. Environmental stability reflects the effects of temperature, power supply variations, and other environmental factors which can influence the oscillator output. Long term stability involves a gradual drift in the oscillator output and includes the effect of aging, caused by a variety of electromechanical mechanisms. Short term stability is a function of noise signals within the oscillator and represents a phase modulation of the oscillator output.
The stability is usually specified by statistics such as the Allan variance and the Hadamard variance (see Section 3.2.2.2.1 and 3.2.2.2.3).

3.2.2.2 Statistics for Stability Evaluation

Clocks' stability could be assessed in the time domain by means of the classical standard deviation. However, it has been demonstrated that, for some kind of power law spectra encountered in precision oscillators, it is divergent: it does not converge to a well defined value and it is a function of data length [67]. As a consequence, the classical standard deviation is not convenient for clock characterization. An IEEE subcommittee recommended the power law spectra $S_y(f)$ in the frequency domain and the Allan variance $\sigma_y(\tau)^2$ in the time domain [68].

3.2.2.2.1 The Allan Variance

The Allan Variance (AVAR), or Two Sample Variance, $\sigma_y(\tau)^2$, is the most common time domain stability measure, and its convergence has been verified for the power law spectra of interest in precision oscillators.

The Allan Variance is defined as follows [5], [15]:

$$\sigma_y(\tau)^2 = \frac{1}{2} < (\Delta_y)^2 > \tag{3.35}$$

Where Δ_y^2 is the difference between adjacent (i.e no dead time exists between the measurements) fractional frequency measurements, between a pair of clocks or oscillators, sampled over a time interval τ. The brackets $<>$ indicate the infinite time average, or expectation value.

Analogously, the Allan Variance can be expressed in terms of time offset measurements:

$$\sigma_y(\tau)^2 = \frac{1}{2\tau^2} < (\Delta_x)^2 > \tag{3.36}$$

Where Δ_x is the second difference among three time offset measurements spaced by τ.

Fig. 3.16 illustrates a visual description of Allan Variance computation:

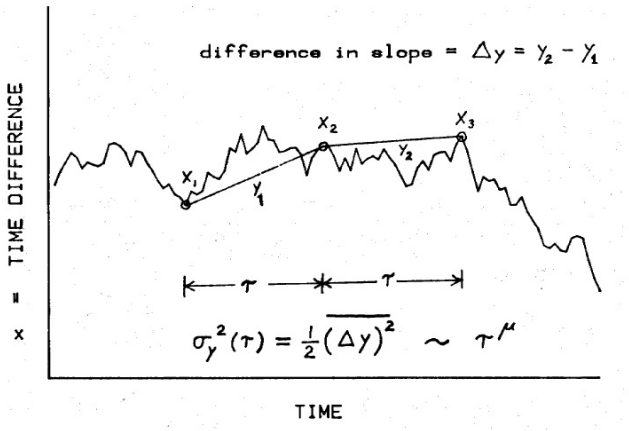

Figure 3.16: Visual description of Allan Variance computation [5]

Given a discrete set of N time offset differences x_i, taken from the measurable time difference between a pair of clocks, and given that the nominal spacing between adjacent

measureas is τ_0, the discrete set of M = N-1 fractional frequency measurements y_i can be obtained using Eq. 1.7.
The original data spacing τ_0, can be changed by the software to $\tau = n\tau_0$, in order to average n adjacent values of y_i, obtaining a new fractional frequency estimate y_i^τ, with sample time τ instead of τ_0.
For a finite data set of M values of y_i^τ, the Allan Variance can be calculated as a function of τ:

$$\sigma_y(\tau)^2 = \frac{1}{2(M-2n+1)} \sum_{k=1}^{M-2n+1} (y_{k+n}^\tau - y_k^\tau)^2 \tag{3.37}$$

where y_{k+n}^τ and y_k^τ are still adjacent fractional frequencies, each averaged over $\tau = n\tau_0$.
Alternately, considering directly the N time offset measurements x_i, it can be written:

$$\sigma_y(\tau)^2 = \frac{1}{2\tau^2(M-2n+1)} \sum_{k=1}^{N-2n} (x_{i+2n} - 2x_{i+n} + x_i)^2 \tag{3.38}$$

Eq. 3.37 is obtained from the first differences on frequency data, while Eq. 3.38 is obtained from the second differences on time data: the two equations are mathematically identical.
The Allan variance has the advantage, with respect to the ordinary variance, of converging to a value which is independent of the number of samples, for divergent noise types (such as flicker noise).
The slope of $\sigma_y(\tau)^2$ graph depends on the noise process which is considered, except for $\alpha = 1$ and $\alpha = 2$, for which the slope is the same.
The following proportionality exists:

$$\sigma_y(\tau)^2 \propto \tau^\mu$$

where μ is typically constant for a particular value of α.
For flicker frequency noise, on the contrary, the value of $\sigma_y(\tau)^2$ does not depend on τ: this kind of noise is also known as *flicker floor*.
There is the following correspondence between α and μ:

α	μ
-2	1
-1	0
0	-1
1	-2
2	-2

Table 3.6: Correspondence between α and μ

Often the square root of the Allan variance is used: $\sigma_y(\tau)$, the Allan deviation (ADEV). As already mentioned, observing the Allan variance graph (or similarly the Allan deviation graph), it is possible to identify the noise type present on the clock. Figure 3.17 shows the correspondence between the slope of the Allan curve and the noise type:

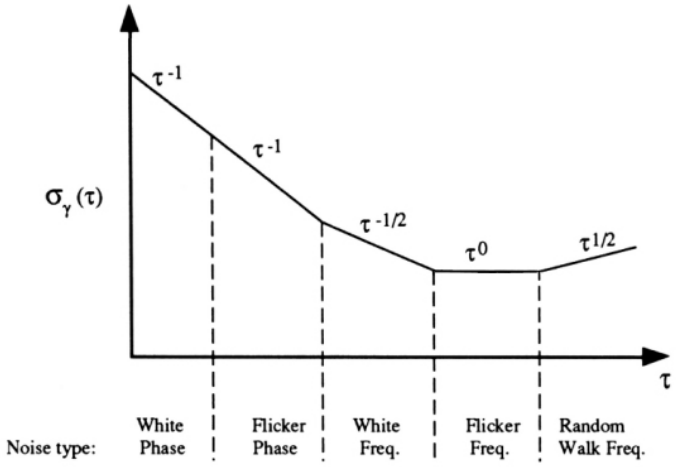

Figure 3.17: Correspondence between slope and noise type [69]

As it has been illustrated in the present paragraph, the frequency stability as well as the noise type affecting an oscillator can be assessed either in the frequency or in the time domain. From a statistical point of view, the spectral density of fractional frequency $S_y(f)$ carries more information than the frequency stability estimate evaluated in the time domain $\sigma_y(\tau)^2$ [64]. In fact, $\sigma_y(\tau)$ can be predicted if $S_y(f)$ is known, while the determination of $S_y(f)$ from $\sigma_y(\tau)$ is not possible. In telecommunication systems the knowledge of $S_y(f)$ is of interest, while $\sigma_y(\tau)$ is used mainly in systems in which time measurements or time synchronization are involved.

3.2.2.2.2 Modified Allan Variance

As shown in Table 3.6 and Fig. 3.17, it is not possible to distinguish between the flicker phase nose and the white phase noise: for both of them the slope of the Allan Deviation graph is $\mu = 2$.
The ambiguity can be solved using the so called *Modified Allan Variance*, defined as follows:

$$Mod\sigma_y(\tau)^2 = \frac{1}{2\tau^2 n^2 (N-3n+1)} \sum_{j=1}^{N-3n+1} \left(\sum_{i=j}^{n+j} (x_{i+2n} - 2x_{i+n} + x_i)\right)^2 \tag{3.39}$$

where n is the multiplicative factor of the original data sampling τ_0 to obtain $\tau = n\tau_0$, and N is the number of time offset measures.
Now, if $\sigma_y(\tau)^2 \propto \tau^{\mu'}$, then $\mu' = -\alpha - 1$ (for $1 \leq \alpha < 2$) or $\mu' = -\alpha$ (for α=2) .

3.2.2.2.3 The Hadamard Variance

One of the limits to the high spectral resolution of $\sigma_y(\tau)$ is the bandwidth of its transfer function, which is pretty large. A better resolution can be obtained using the Hadamard Variance (HVAR), whose general definition is reported in Eq. 3.40:

$$\sigma_H^2(p, T, \tau) =< (\overline{y}_1 - \overline{y}_2 + \overline{y}_3 - \overline{y}_4 .... - \overline{y}_p)^2 > \tag{3.40}$$

where p is the order, that is the number of samples used to compute the differences, T is the sampling time, τ is the measurement duration. If there are no dead times between subsequent measurements, as assumed in Section 3.2.2.2.1, then $\tau = T$.
Considering the case $p = 3$, the Hadamard Variance is expressed as:

$$\sigma_H^2 = \frac{1}{6\tau^2(N-3)} \sum_{i=1}^{N-3} [x_{i+3} - 3x_{i+2} + 3x_{i+1} - x_i]^2 \tag{3.41}$$

Considering the $M = N - 1$ normalized frequency data samples, the Hadamard variance can be written as:

$$\sigma_H^2 = \frac{1}{6(M-2)} \sum_{i=1}^{M-2} [y_{i+2} - 2y_{i+1} + y_i]^2 \tag{3.42}$$

By increasing the order p, the selectiveness of the transfer function's main lobe is increased. Differently from the Allan variance, the Hadamard variance is not affected by linear frequency drift.
Like the Allan variance, the Hadamard variance is usually expressed as its square-root, the Hadamard deviation (HDEV).
As for the Allan deviation, also for the Hadamard deviation there is a correspondence between the slope of the curve obtained as result of the analysis and the type of noise present, as shown in Fig. 3.18:

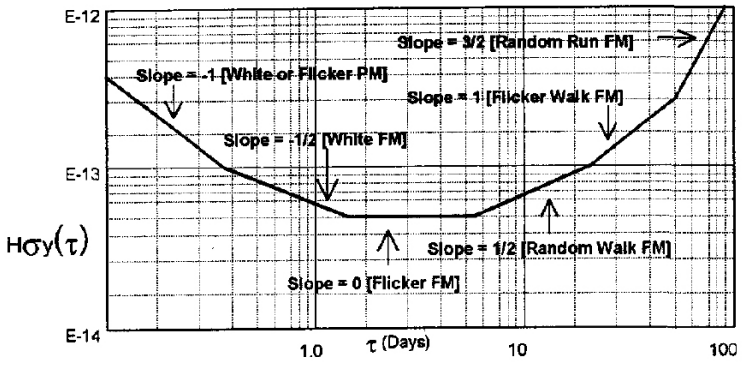

Figure 3.18: Noise types identified by the Hadamard deviation [70]

3.2.2.3 Monitoring of Frequency Stability Evolution

As for the clock frequency drift, also the clock frequency stability has to be continuously monitored, in order to compare the experimental results with the theoretical clock performances reported in manufacturer specifications and detect promptly any malfunctioning or suspicious behaviour which could prevent the target clock reliability.
As a routine operation, the frequency stability of GIOVE clocks is evaluated at INRIM, on a weekly basis, by means of the Allan and Hadamard deviation. The results produced in the frame of the GIOVE Mission are reported in the specific files for the European Space Agency. Again, periodically the results are collected and reported on the graphics showing the evolution of the parameter of interest, the Allan Deviation in this case. The same kind of analysis can be done on GPS satellites. An example of the monitoring activity of clock frequency stability is illustrated in Fig. 3.19, for the first weeks of year 2008 for GPS satellite G05:

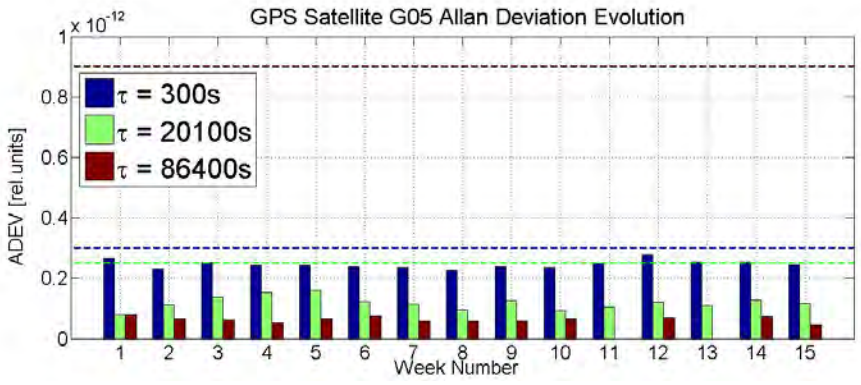

Figure 3.19: GPS Satellite G05 (RAFS) Frequency Stability (Allan Deviation) Evolution, January-February 2008

For each week, three values of Allan Deviation are reported: the short term stability (for averaging interval τ of 300 s), the medium term stability (for averaging interval τ of 20100 s) and the long term stability at 1 day (τ of 86400 s).
The correspondent specification lines can also be reported for each of the considered averaging intervals.
The Allan Deviation values reported in Fig. 3.19 have been obtained starting from IGS RINEX for clock files. The frequency stability has been evaluated on clock phase data affected by drift, after outliers filtering.
As it can observed in Fig. 3.19, for the considered period, the frequency stability of the RAFS on board GPS satellite G05 is always in agreement with the pure clock specifications.

3.2.3 Clock Sensitivity to Environment

One of the objectives of the experimental phase of the Galileo project named GIOVE Mission, was the characterization of the space environment at Medium Earth Orbit, which the final constellation of satellites will encounter.
Space weather has generally an impact on several areas of the spacecraft operation: it can even interfere with the on-board electronics. Many physical phenomena influence space weather: geomagnetic storms, ionospheric disturbances, etc [71].
It is hence important to monitor the space environment in which the satellite operate, in order to properly design the equipment and understand the observed data.

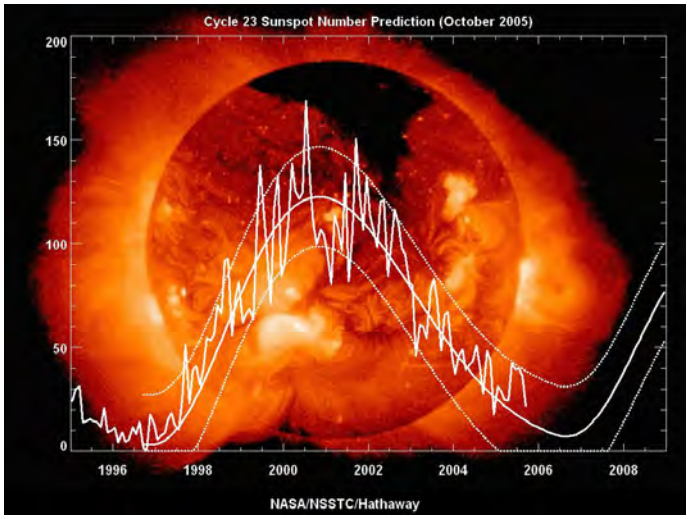

Figure 3.20: Solar Magnetic Activity Cycle [72]

One of the topics studied during my collaboration to the INRIM projects is the satellite clock sensitivity to the environmental parameters, such as temperature and solar radiation. Environmental parameters are measured through special sensors located on board satellites, and telemetry data are transmitted to the ground processing centres.
Satellites are generally carrying temperature sensors as well as radiation sensors, allowing the environment monitoring. For example, the payload of the first experimental satellite of the Galileo project, GIOVE-A, includes two radiation monitors, CEDEX and MERLIN [73]. The second Galileo experimental satellite, GIOVE-B, carries a SREM instrument [74]. Both satellites are provided with several temperature sensors, located at different strategic points of the satellite.
The aim of the study is to assess if the satellite apparent clock frequency is influenced by the environment temperature or solar radiation; especially in correspondence of possible anomalous behaviours observed on the satellite apparent clock, it is interesting to assess whether these phenomena could be related to the environmental conditions.
To this purpose, we periodically performed correlation analysis between the satellite apparent clock normalized frequency and temperature or radiation telemetry measures. The distribution of the quantities to be analyzed is observed and the correlation coefficient is quantified.
Fig. 3.21 illustrates some examples of possible distributions of sets of points x and y [75]: a strong positive correlation, a linear positive correlation, a weak negative correlation, and no correlation respectively.

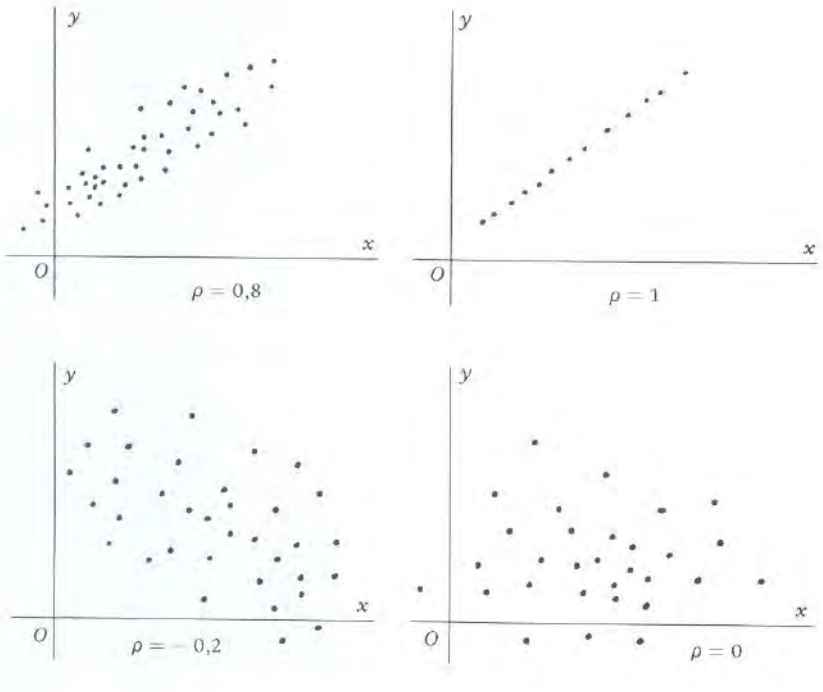

Figure 3.21: Examples of Distributions of Sets of Points

Besides the telemetry measures received from the satellites, another important source of information are the plot of the space environment [76], particularly those operated by the United States National Environmental Satellite, Data, and Information Service (NESDIS), by means of some geostationary satellites, named GOES (Geostationary Operational Environmental Satellite) [77]. Fig. 3.22 reports an example of proton flux measured on a period of 4 days, which has been used for our evaluations on the potential solar radiation influence on satellite clocks.

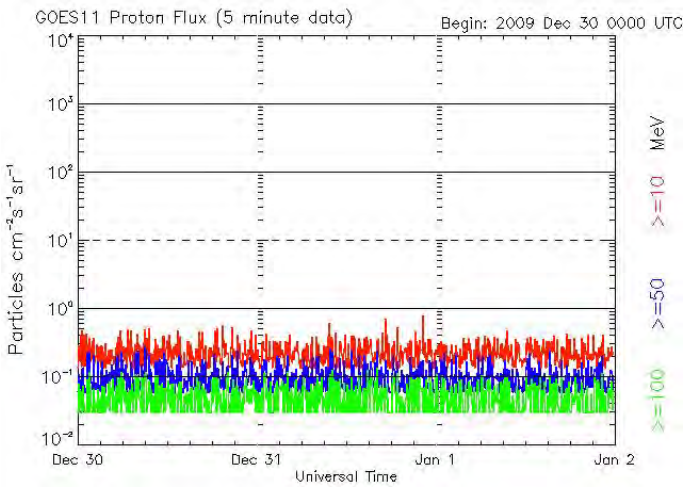

Figure 3.22: Proton Flux Observed from GOES 11 Satellite from December 30^{th} 2009 to January 2^{nd}[76]

3.2.4 Software Tool for Satellite Characterization and Monitoring

This Section illustrates the Software tool which I contributed to realize [78], [53], [45], and I gradually updated including some additional features, as the uncertainty evaluation on the frequency drift estimate (described in Section 3.2.1.1.2), the introduction of the system noise estimate, and the filtering of clock phase data .

As previously mentioned, the presented tool has been optimized in order to deal with typical satellite clock data. Nevertheless, it is actually suitable for all type of atomic clocks, not necessarily employed on board satellites, as for example the clocks employed in the ground stations of satellite navigation systems ground network, and it can be even used for the characterization of time scales.

The realized software has been checked with respect to other commercial software and the results were found in complete agreement.

Main products for the clock characterization tool are plots generated in an automatic way; such plots allow to monitor in an easy way the clock key parameters and to perform an accurate clock analysis.

To ease the procedure of analysis the tool has been provided with a graphical user interface, illustrated in Fig 3.23

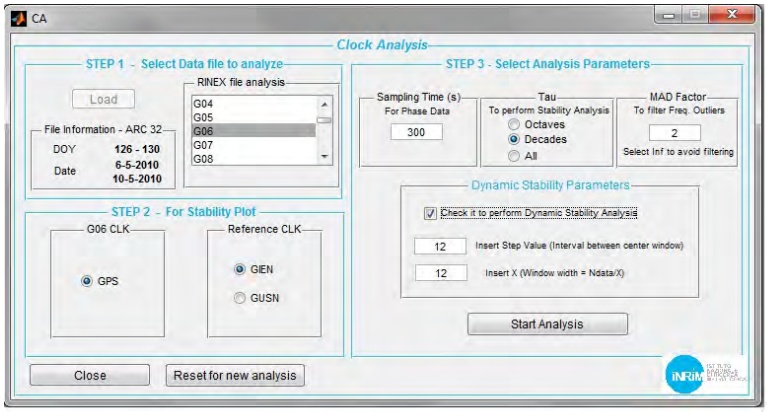

Figure 3.23: Graphical User Interface of the Software Tool for Clock Characterization

3.2.4.1 Data Pre-Processing

The clock estimates have to be extracted from standard files used in GNSS, the RINEX for clock files [38], and have to be converted in a proper format to be processed by the tool. For this purpose, the Graphical User Interface is provided with a menu in which the operator can select the satellite whose clock has to be analyzed.
The clock time offset between the extracted clock the reference clock indicated in the configuration file is then computed.
The satellite clock measures of interest are then extracted, the data are converted and then saved in a 2-column ASCII format. The tool is able to import also ASCII files which are already in the 2-column format, coming from some previous processing, not necessarily extracted from the RINEX files, ensuring the flexibility of the software to allow the analysis of different type of clocks coming from different sources (timing laboratories, IGS, etc.).
Once the data have been extracted, as a first step, the clock time offset estimates are pre-processed in order to identify and properly manage potential data gaps and outliers. In fact, often space clocks data may be unavailable due to some problems on the satellite transmission or on receiver data collection...Clock estimates have to be regularized as for the stability analysis equally spaced data are needed [5]. For this purpose, through an

appropriate algorithm, some neutral values called *Not A Number* (NaN in MATLAB® language) are inserted where data gaps are identified.

3.2.4.1.1 Outliers Filtering

Moreover, frequently space clock data present outliers, which have to be identified and removed to allow a representative analysis of clock performances. The solution adopted for outliers detection and filtering is based on a Median Absolute Deviation (MAD) [43]. The filter on input data can be enabled by the user through the proper panel on the graphical user interface, in which also the filter selectivity can be set according to the user's needs.
One of my tasks, besides some modifications on the use of the filtering algorithm inside the tool, was the implementation of a filter on clock time offset data, based on the outliers identified on clock frequency data with the Median Absolute Deviation approach. Hence, after the filtering on the frequency data set, on the basis of the information collected on the detected frequency outliers, a filtered clock time offset data set is generated eliminating (i.e substituting with *NaN*) those data producing a frequency outlier. In fact, since the clock frequency offset is the time derivative of the clock time offset, as per the discrete relationship illustrated in Eq. 1.7, if an outlier is identified on the $y_{i^{th}}$ frequency datum, then the $x_{i^{th}}$ and $x_{i+1^{th}}$ time offset data shall be filtered.

3.2.4.2 Deterministic Behaviour

Averaged frequency estimates are obtained from clock time offset data through a time derivative, as per Eq. 1.7.
Then, the main deterministic effect, the frequency drift, is evaluated in order to monitor its evolution over time and to remove such deterministic contribution from clock estimates when the aim is to observe only the clock stochastic behaviour. Details on frequency drift estimate are reported in Section 3.2.1.1.1.
Once the clock drift has been evaluated, it is removed from both phase and normalized frequency data by subtracting to the original data sets the estimated quadratic and linear fit respectively. Then the following analysis are performed on both data sets with and without frequency drift.
Clock time and normalized frequency offsets, as well as the respective residuals after drift removal, are displayed in the graphics generated by the tool, in order to allow the operator to observe the clock behaviour.
The values of the statistical dispersion of the polynomial coefficients of the fitted curve are reported on the graphics of both phase and normalized frequency clock data: this permits to have direct evidence of the frequency drift entity together with the level of accuracy

of the estimate. Details about the uncertainty of frequency drift estimate are reported in Section 3.2.1.1.2.

3.2.4.3 Stochastic Behaviour

The subsequent step in the clock characterization activity is the assessment of the clock stochastic behaviour. This is performed by means of the stability analysis (see Section 3.2.2.1 and 3.2.2.2).
Stability analysis is generally based on the assumption of using equispaced samples [5]. Since data from space vehicles are not always available, very often space clock data present long periods of missing values. The Clock Analysis Tool has been designed to extend the approach commonly used for the study of the frequency stability, to deal with the peculiar aspects of satellite clock data [45]. The frequency stability of space clocks is evaluated by means of two independent statistics: first the Allan Deviation is computed on the averaged frequency estimates, then the Hadamard deviation is also determined. Both statistics are evaluated for different observation intervals; the number of different observation intervals for frequency stability computation can be set by the user at the beginning of the analysis, through the proper panel on the graphical user interface.
To observe the stochastic behaviour of the clocks, it is of extreme importance to evaluate the clock frequency stability on a data set in which the drift has been properly removed.
In addition, if one is interested in the evolution of the clock stability over time, also the Dynamic Allan Deviation and the Dynamic Hadamard Deviation are computed if the option of dynamic stability has been selected. Both dynamic analysis are based on the estimate of the Allan and Hadamard Deviation respectively on a sliding window on input data, whose width can be set by the user at the beginning of the analysis [46].
The results of all the analysis performed by the Clock Analysis tool are automatically saved as ASCII files and images in an output folder purposely created during the tool execution. The user can also observe the graphics while they are generated so that he can have an immediate idea of the general clock behaviour; moreover, one can analyze the saved plots in order to deepen the analysis focusing on certain periods of data or on particular features. The analysis can be reset and repeated in any moment with different configuration parameters or input files.

3.2.4.4 System Noise Estimate

To evaluate the performances of satellite clocks, or similarly those of ground station clocks, it is extremely important to evaluate the system noise in order to understand the limit of observatbility allowed by the available infrastructure.

In the frame of the activity of GNSS clocks characterization, the system noise is evaluated as the relative stability of two Active Hydrogen Maser clocks: typically the one connected to the GIEN station located at INRIM and the one connected to the GUSN station located at the USNO. Indeed, the noise present on maser clocks, which are the most stable available nowadays, is considerably lower with respect to other clock technologies, for the observation interval of interest: the estimate of the offset which we obtain is then mainly affected by the measurement system noise, hence it can be considered the *system noise* [79]. Besides, the considered active hydrogen masers are more stable than the satellite clocks to be characterized (RAFS, PHM, Cesium clocks).
My contribution consisted in the implementation of the system noise estimate in the tool for clock characterization, in order to have the frequency stability of the system noise displayed together with the one of the clock being analysed.
To this purpose, from the RINEX for clock files containing satellite and station time offset estimates, the measures of the clocks to be used for system noise computation are extracted and the offset between the two is evaluated, obtaining the system noise estimate.
This functionality has been included in the INRIM tool for clock characterization, producing graphics as the one reported in Fig. 3.24, where the frequency stability of the RAFS clock on board GPS satellite G05, for the period from January 25^{th} to 29^{th} 2009, is reported together with the clock specifications and the system noise estimate, to be intended as the best frequency stability which one can obtain with the current infrastructure:

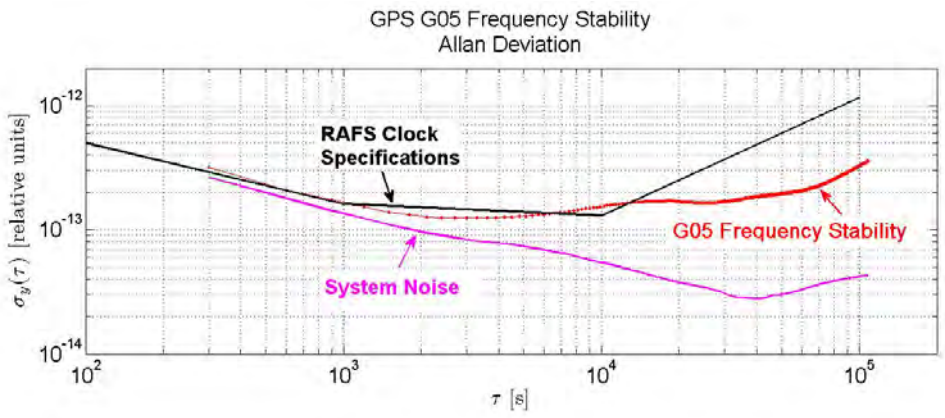

Figure 3.24: Example of Clock Frequency Stability with System Noise Estimate

As it can be noted from Fig. 3.24, the system noise estimate is not so distant from the clock specifications and the experimental clock stability. Even if the level of noise is

limited by the number of ground stations currently employeed in the Galileo infrastructure, it allows a proper characterization of tthe satellite clocks.

3.2.4.5 An Application to Experimental Data

Considering for example GPS satellite PRN G26, launched on July 7^{th} 1992 and carrying a RAFS, RINEX for Clock files generated by the International GNSS Service (IGS) for the period June 5^{th} - July 21^{st} 2010 have been processed with the INRIM tool described in Section 3.2.4, and the main results of the respective analysis for the considered satellite are reported, step by step, in the present section.
First, the clock deterministic behaviour is evaluated. Fig. 3.25 illustrates the time offset between the RAFS on board GPS satellite G26 and the reference time scale, IGS Time [39], once extracted from IGS RINEX files and pre-processed:

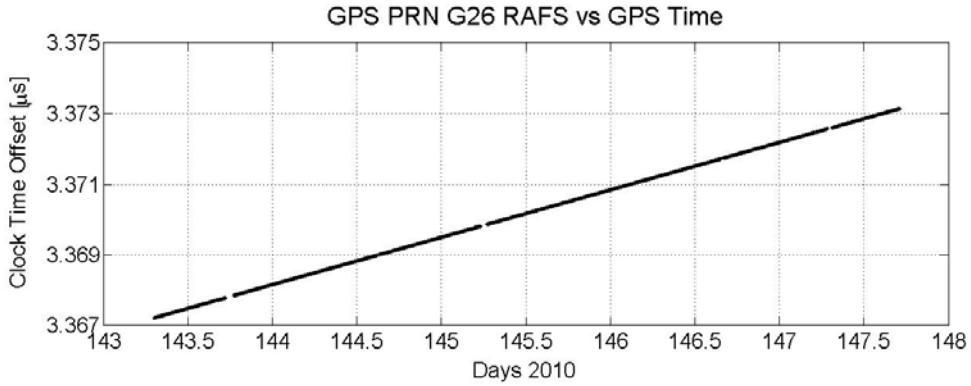

Figure 3.25: GPS Satellite G26 vs GPS Time: Apparent Clock Time Offset, June 5^{th} - July 21^{st} 2010

The estimate of the apparent clock normalized frequency offset is then produced, as depicted in Fig. 3.26, in which it can be observed the presence of a periodic fluctuation most likely consequence of orbit residuals in the clock solution, topic also discussed in Section 3.2.1.1.3, 4.1, and 4.2.1. Further, one can notice the presence of an outlier which is going to be removed with the filtering process (see next Fig. 3.26):

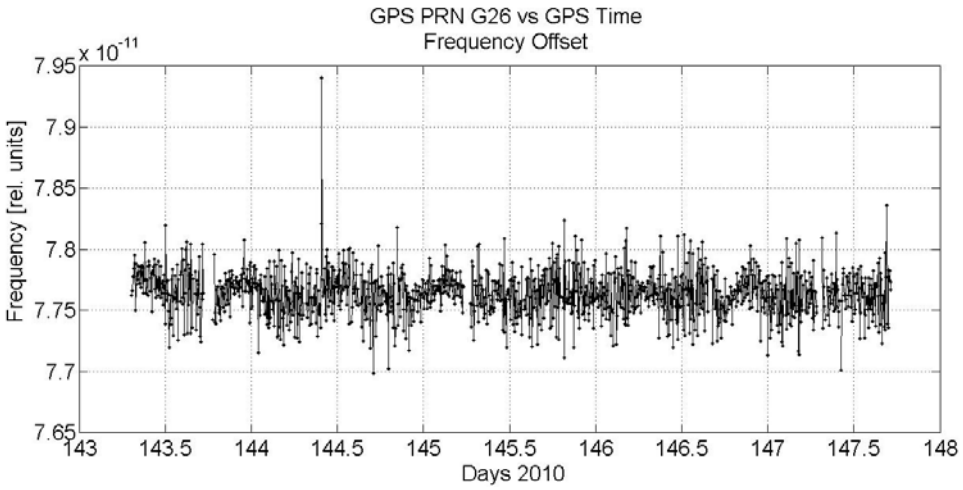

Figure 3.26: GPS Satellite G26 vs GPS Time: Apparent Clock Normalized Frequency Offset, June 5^{th} - July 21^{st} 2010

Secondly, the main deterministic effect, the frequency drift, is evaluated. Once the clock drift has been estimated, with the technique illustrated in Section 3.2.1.1, it is removed from both time and normalized frequency offset: the residuals are illustrated in Fig. 3.27 and Fig. 3.28, in which the coefficients of the estimated polynomial fit are also reported. For graphical purpose, the uncertainty on the fit coefficients is not reported on Fig. 3.27 title, but it is reported only on the ASCII file generated when the tool is executed.

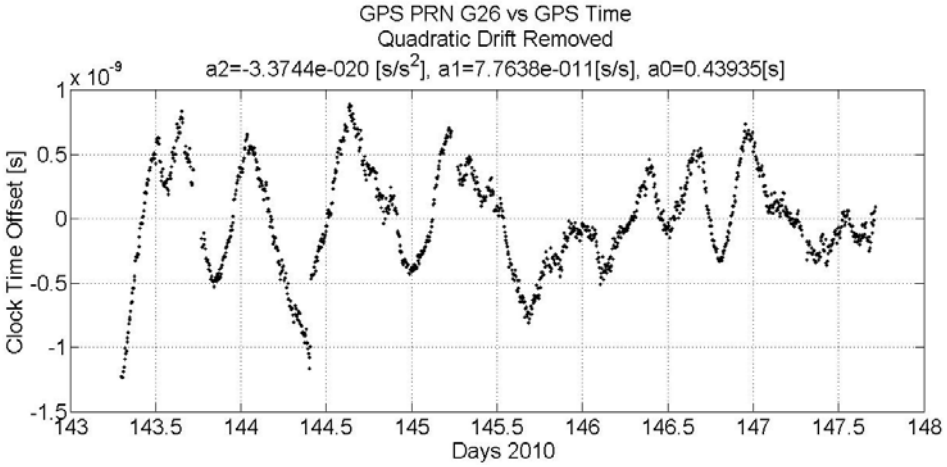

Figure 3.27: GPS Satellite G26 vs GPS Time: Apparent Clock Time Offset, After Quadratic Drift Removal, June 5^{th} - July 21^{st} 2010

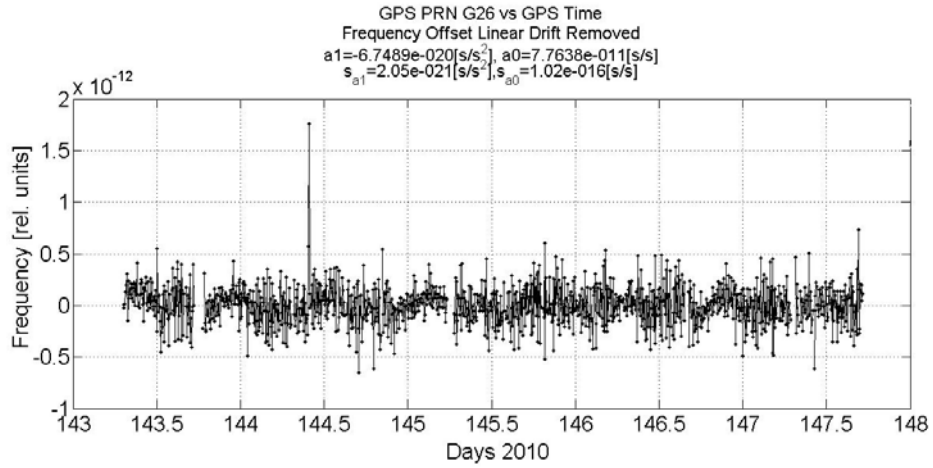

Figure 3.28: GPS Satellite G26 vs GPS Time: Apparent Clock Normalized Frequency Offset, After Linear Drift Removal, June 5^{th} - July 21^{st} 2010

Since the clock drift was not really pronounced, being at the level of $-5.8 \cdot 10^{-15}$ relative units/day, no substantial difference can be noted between the apparent clock frequency before (Fig. 3.26) and after (Fig. 3.28) drift removal, except the fact that the de-trended

frequency oscillates around the level of zero.
Fig. 3.29 shows G26 clock frequency after the outliers filtering: it can be noted that the outlier present on day 144 has been filtered.

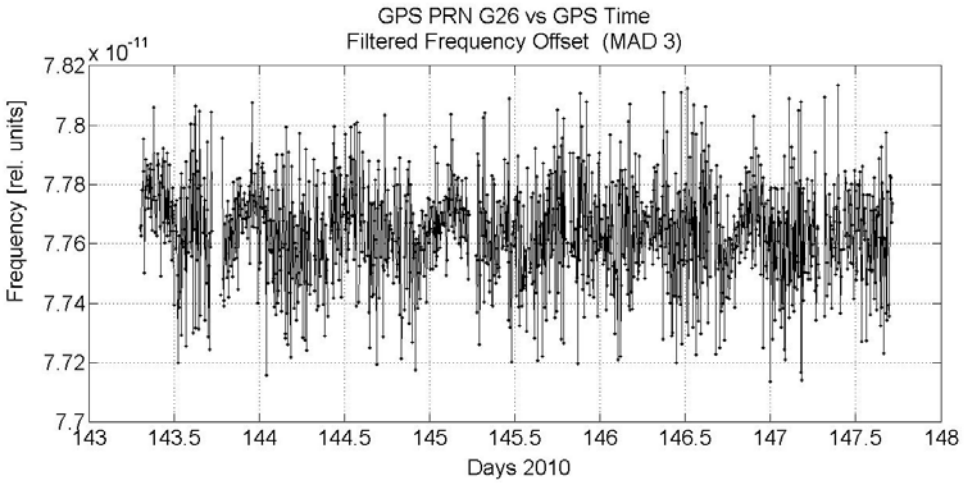

Figure 3.29: GPS Satellite G26 vs GPS Time: Apparent Clock Filtered Frequency Offset, MAD Factor=3,June 5^{th} - July 21^{st} 2010

Finally, the tool evaluates the clock stochastic behaviour. The Allan Deviation is computed in order to evaluate the frequency stability of the analysed clock. The number of averaging intervals τ for which the Allan Deviation is evaluated are set by the operator through the special panel in the graphical user interface. In the considered example, reported in Fig. 3.30, all the possible averaging intervals have been used. The result is the black curve in Fig. 3.30, reported together with the clock specifications (dashed line) and the system noise estimate (green line).
The periodicity observed on the clock frequency in Fig. 3.26 is evident in the bump visible on the Allan Deviation curve of both G26 apparent clock and the system noise estimate, around $\tau = 2 \cdot 10^4$ s.
The system noise, in the presented analysis, has been estimated as the offset between two IGS stations connected to an Active Hydrogen Maser: IRKT [80], located at Irkutsk (Russia) and IENG [81], located at Turin (Italy).

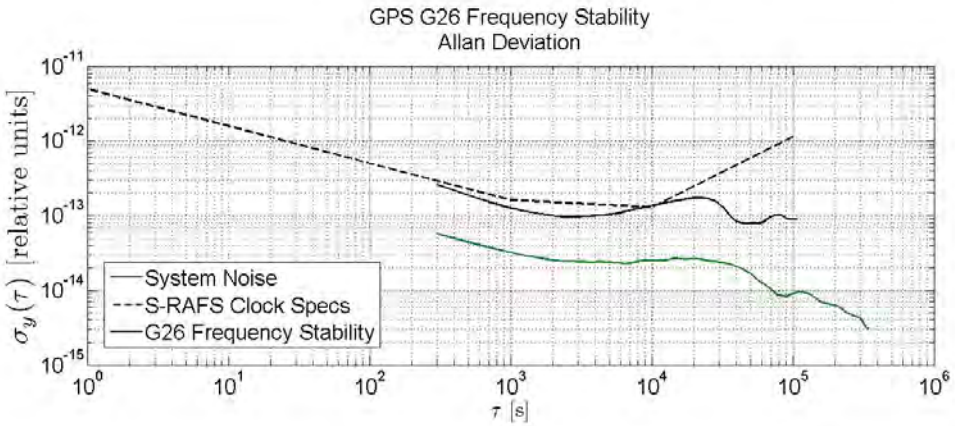

Figure 3.30: GPS Satellite G26 vs GPS Time: Apparent Clock Frequency Stability (Allan Deviation), June 5^{th} - July 21^{st} 2010

Observing Fig. 3.30 it can be noted that the system noise estimate, on the whole, is clearly below the system noise estimate reported in Fig. 3.24, as the IGS network has a considerable number of ground stations, while the level of the frequency stability of the RAFS clock on board GPS satellite G26 (Fig. 3.30) is not so different from the one of GPS satellite G05 (Fig. 3.24). The difference between the two system noise estimates is due to the different network used to generate the clock estimates from which the analysis of clock characterization has been peformed. In fact, in one case (Fig. 3.24) the clock estimates have been obtained processing the data collected from the Galileo Experimental Sensor Stations, whose number was quite limited (13), while in the other case (Fig. 3.30), the IGS network has been used, with more than 200 ground stations.

3.2.4.6 Activity for the Galileo In Orbit Validation Phase

As a support for the In Orbit Validation phase of the Galileo system, since 2010 INRIM is involved in the design and development of the Time Validation Facility: it is the infrastructure (hardware and software) conceived for the assessment of Galileo performances, from a timing point of view. The overall project is quite articolated and consists in different modules, and it is interfaced with several external entities. My personal contribution consisted in the development of the module dedicated to the generation of the timing products to be used for the validation of performances of space and ground clocks, as well as time scales. Starting from the available algorithms and routines developed in the previous years, it has

been necessary to realize a module which is suitable for the current phase of Galileo, able to generate the required timing products according to the project requirements.
The main work consisted in the automatization of the processing, in order to ensure continuous operation 24h/24, minimizing the operator intervention, and this is indeed the main innovation with respect to what was initially avaialble.
With the aim of ensuring a continuous operation, the module has been designed to be activated periodically, in a scheduled time slot: the RINEX for clock files used in navigation are processed, graphics and ASCII files containing the analysis results are produced, and the generated results are directly transmitted to the archive of the European Space Agency.
All the information needed for the processing are contained in a configuration file, which is updated by an operator whenever it is needed to set differently the value of certain parameters. In such file it is possible to set which satellites or ground station clocks will be analyzed, which will be the reference clock for the analysis, which ground stations will be used for the system noise estimate, the period to analyze...In addition, all the parameters which can be dynamically changed for the analysis are configured according to the objectives of the analysis: the selectiveness of the filter, the averaging intervals to be used for the stability analysis, I/O managing, etc.
Besides, the generation and managing of feedback information has been treated, with the generation of specific report files notifying to the users step by step what is happening and, above all, reporting potential warnings and alarms raised whenever the expected products are not generated, or for example identifying the situation in which the measures of a specific satellite are missing in certain input files...
The objective is to ensure a processing as much as possible transparent, in order to allow the operator to check the correct functioning of the machine and to identify any possible malfunctioning or unexpected event, permitting to repair the situation. Indeed, the presence of these reports has proved to be really important during the operational activities, since often allowed the understanding of peculiar situations, localizing the problem and hence making faster the problem fixing.
In addition, the possibility of managing a large number of configurable values has been fundamental, so that the realized infrastructure could be suitable for a large variety of situations, which often were not even initially foreseen.
The realized infrastructure is currently used to analyze the clocks on board the first two Galileo satellites, launched during the In Orbit Validation phase of the project (October 2011). Besides, it has been conceived to characterize the behaviour of the reference time scale of the Galileo system, the Galileo System Time (GST), as well as the single atomic clocks contributing to the realization of such time scale. Being the Galileo System Time not

currently available, the realized facility has been tested characterizing the italian realization of the Universal Time Coordinated (UTC), UTC(IT), with respect to the international time scale UTC, as available from the BIPM Circular T [17].
The realized module seems to be ready for the operational use in the frame of the assessment of Galileo timing system, but the final design and development is still in progress and under confidentiality agreement.

Chapter 4

Analysis and Experiments on GNSS Clocks

This chapter includes some analysis and tests performed on GNSS clocks during the years of doctorate. Some of these experiments were carried out in the frame of the experimental phases of the Galileo Project, as campaign activities expressely needed for the assessment of some particular topics.

4.1 Analysis on the Possible Influence of Ground Clocks' Behaviour on the On Board Clock Solution

As already mentioned, the estimate of the apparent clock on board satellites is obtained through a network algorithm which evaluates the solution of a least squares system involving all satellites and ground stations. Ground stations collect satellite measures each time the satellite passes over their location. Then, the estimate of the satellites clock behaviour for the whole day, evaluated with respect to a single reference, is obtained processing together the data collected by the different ground stations, during the different visibility periods of each space vehicle.
With the aim of evaluating the possible impact of the ground station clocks on the Orbit Determination and Time Synchronization algorithm, which produces the on board clock solution, an analysis on the satellite and ground station clocks has been performed for some selected periods.
The objective is to assess if any particular behaviour or malfunctioning on the ground station clock having in visibility for a certain time the satellite, could have some influence in the solution of that satellite clock, since this latter is obtained processing the measures of different stations. This analysis was motivated by the not nominal behaviour sometimes

observed on ground station clocks.
This test requires the knowledge of which ground stations are in view of the satellites: this information has been obtained by the use of the commercial tool STK (Satellite Tool Kit) [82] and by inspecting the IGS RINEX files containig the satellite clock estimates, or the special files of the orbits and clocks estimation process, containing the information on which station measures have been used to compute the on board clock estimates at the different time instants.
STK is a tool that allows users to perform complex dynamic simulations of real-world systems based on satellites. Among the various features that STK offers, the Access Tool allows to simulate satellite passes over a specific geographical point, and calculate the time intervals in which the satellite is in line of sight for a station located in such particular point.
This feature has been largely used in the analysis here presented, since it has been possible, given satellite orbits and ground station coordinates, to trace the satellite way, as illustrated in Fig 4.1, where GIOVE-A orbit is showed together with the location of some ground stations:

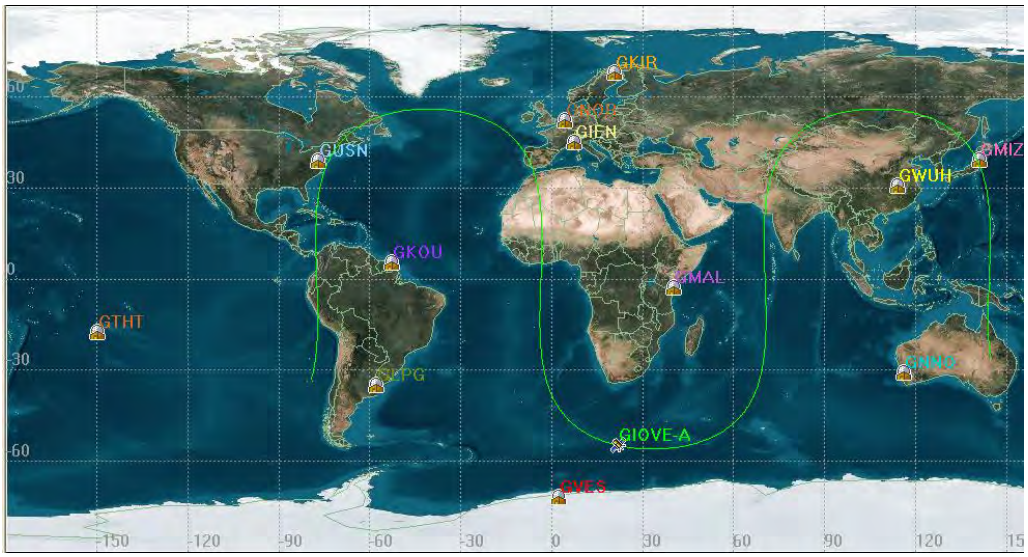

Figure 4.1: Example of Use of Satellite Tool Kit Access Tool Sotware

The analysis here reported are the result of simulations, in order not to show the original figures, since often satellite or station data are strictly confidential, especially when related to the Galileo project. The graphics showed in this thesis are therefore reported as significative examples with the aim of summarizing the activities carried out during the period of doctorate and, most of all, as an example of timing activities applied to a

concrete situation.
In the following two situations are reported:

1. On the first presented case, a non-nominal behaviour has been observed on the satellite apparent clock and the possible causes have been searched among the ground station clocks

2. On the second case, a non-nominal behaviour has been observed on a ground station clock and the possible impact on the satellite apparent clock estimate has been investigated.

4.1.1 Non-nominal Behaviour On Satellite Apparent Clock: Search of the Possible Cause Among the Ground Clocks

This section reports an example of a possible frequency change that can be observed in the frequency offset evolution of a GNSS satellite clock [48], [87]. An analyis on the ground station clocks has been performed with the aim of identifying any possible connection with the behaviour observed on the on board clock.
Fig. 4.2 reproduces a frequency change on the on board frequency of a generic GNSS satellite:

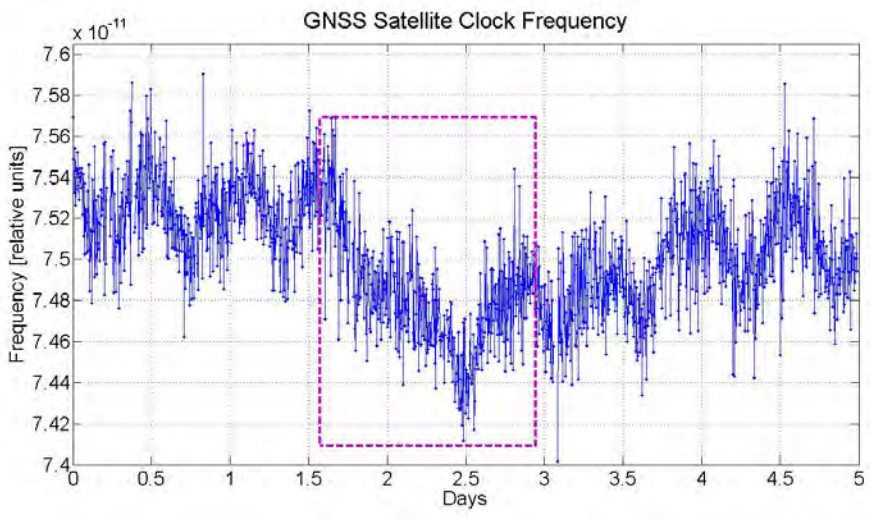

Figure 4.2: Example of Change in the On Board Clock Frequency

The change in the clock frequency between day 2 and 3 is highlighted with the dashed rectangle.

The aim of the investigation was to verify any possible correlation between the observed satellite clock behaviour with the ground station clocks of the network. As a first step, the frequency of the clock used as reference is analyzed, but no anomalies are identified.
Then, to determine whether one of the ground stations could have caused the change on the satellite frequency, the stations in view of the satellite during the anomaly were identified by the use of the STK Access Tool. Fig 4.3 shows the time intervals in which each of the considered ground stations were able to collect satellite data of the analysed satellite, around the period when the anomaly has been detected:

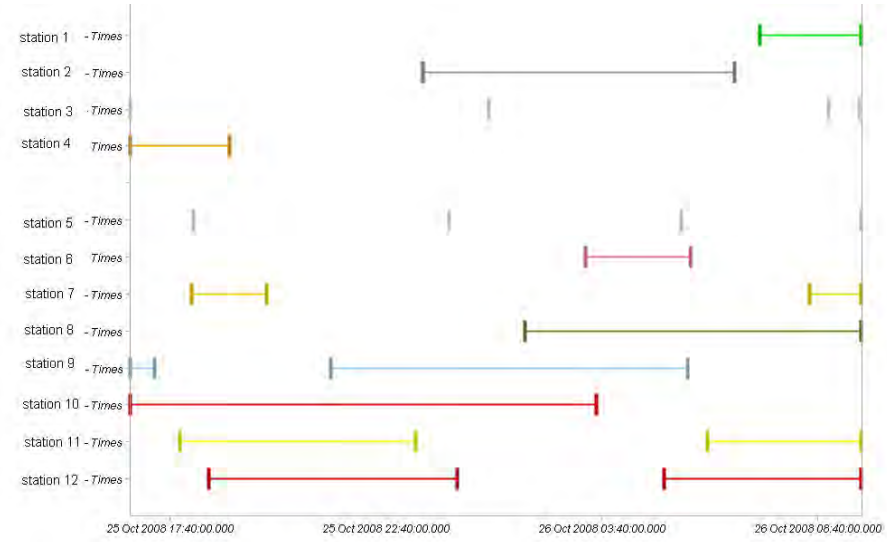

Figure 4.3: Ground Stations in View of the Satellite When the Anomaly Occurred

As can be observed in Fig. 4.3, obtained with a special routine developed for this analysis, when the frequency change occurred 12 ground stations could access the satellite. The graph in Fig. 4.4 shows that a minimum of 3 and a maximum of 7 stations were in view of the satellite at the same time:

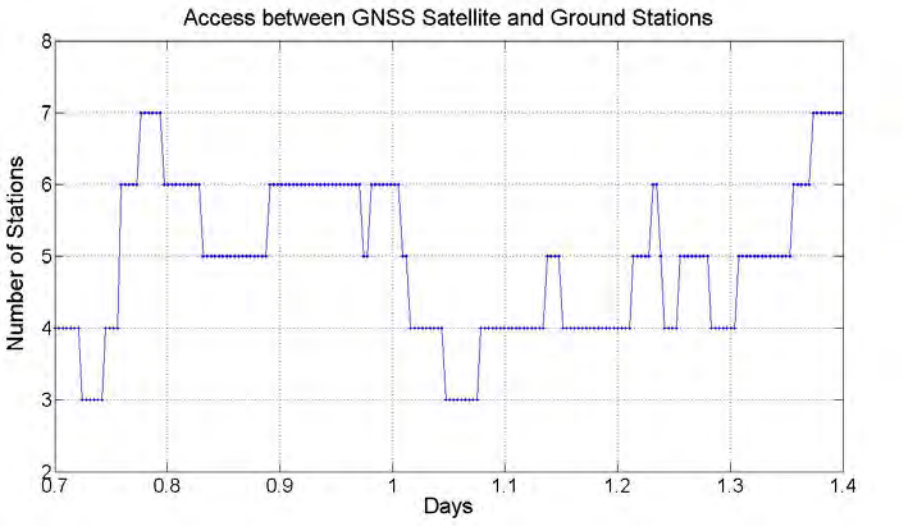

Figure 4.4: Number of Stations Simultaneously in View of the Satellite When the Anomaly Occurred, According to the STK Tool

The number of stations collecting simultaneously satellite data is therefore not critical (as the minimum required number of stations for a proper clock estimate is 2).
The ground stations whose measurements were actually used in the algorithm generating the satellite clock solution can be identified from a special file reporting the details of the algorithm execution. In fact, not all the measures collected by the ground stations are used to obtain the on board clock estimates: when the quality of the measures does not reach the expected standard, the algorithm could avoid to use those data.
Processing such file with a special routine that I created with this purpose, the stations employed in the algorithm at the different time instants are showed in Fig. 4.5. Each station is represented with a different color.

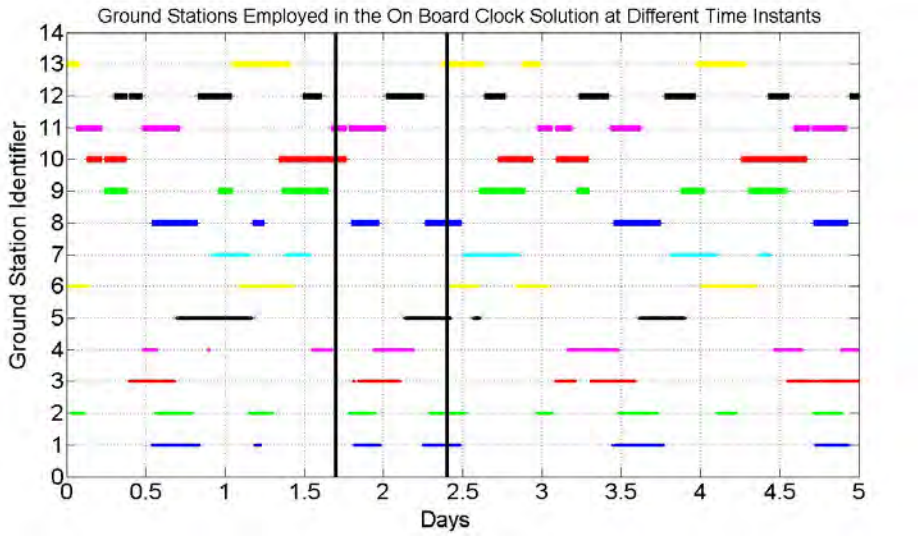

Figure 4.5: Ground Stations Employed to Produce the On Board Clock Solution at Different Time Instants. Case Study 1

As it can be derived observing Fig. 4.5, where the black vertical lines delimit the period of the frequency change, the number of stations whose measurements were actually used to compute the satellite clock estimates is then less than the one detected with the STK Access Tool; it oscillates from a minimum of 0 towards a maximum of 6, as reported in Fig. 4.6:

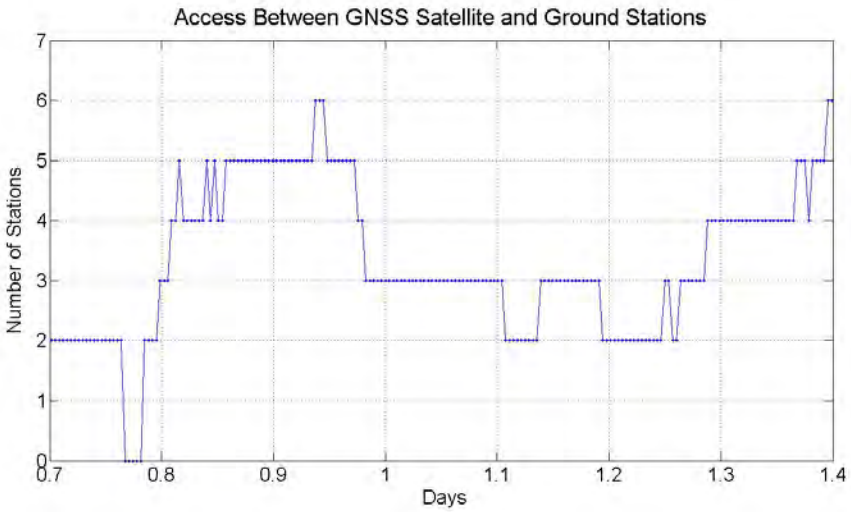

Figure 4.6: Number of Stations Actually Employed to Produce the On Board Clock Solution When the Anomaly Occurred

It can be noted that there is a short period, between day 0.7 and 0.8, in which no stations were used to estimate the satellite clock: however the anomaly in the clock frequency occurred in the second half of the second day of the analyzed period, hence the exiguous number of collected measures could not be the cause of the frequency change.
A comparison among the clocks of the stations in view of the sample satellite during the analyzed period has been performed: the time offset of the different station clocks with respect to a common reference is shown in Fig. 4.7:

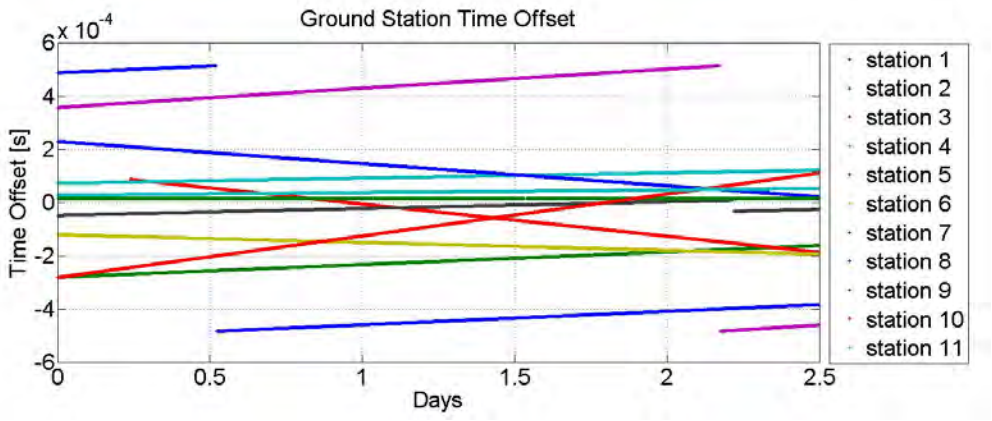

Figure 4.7: Time Offset of the Ground Stations' Clocks. Case Study 1

Three stations experienced a jump in the time offset: the blue, the violet and the grey lines. In the first two cases, the jump is due to a clock synchronization (routine maintenance operation), while in the third case the cause is a change in the Inter-System Bias (ISB) of the station [42].
Again, none of the observed events could be the cause of the frequency jump on the sample satellite, since the clock frequency started changing in the second half of the second day, when none of the stations having jumps in the time offset, due to maintenance operations was used.
Fig. 4.8 shows the frequency offset evolution of the ground stations' clocks, after the removal of a linear frequency drift (the frequency offsets of the stations whose clocks experienced maintenance operations are not reported, for graphical purpose):

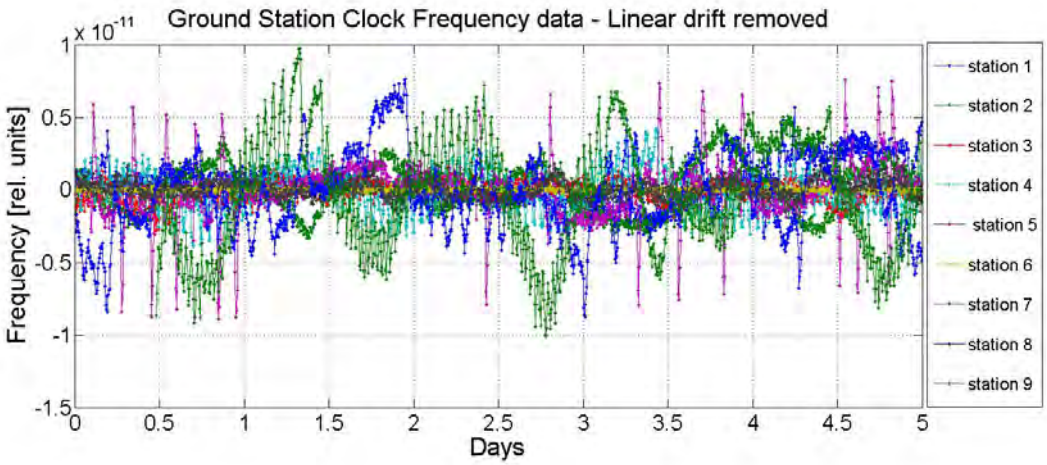

Figure 4.8: Frequency Offset of the Ground Stations' Clocks. Case Study 1

A zoom around the period of the frequency change is reported in Fig. 4.9

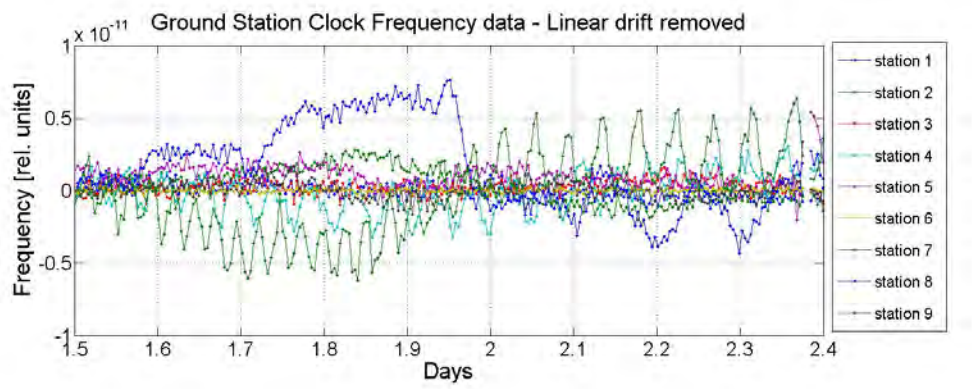

Figure 4.9: Frequency Offset of the Ground Stations' Clock: Zoom Around the Period of the Anomaly

The frequency of the ground stations' clocks show periodic fluctuations as well as jumps or abrupt changes. However, no particular anomalies are observed.
To better evaluate the station clock frequency potential impact on the satellite apparent clock estimation, the frequency evolution of the ground clocks only when those stations were used in the orbits and clocks estimation process have been evaluated. Results are reported in Fig. 4.10 (where a linear drift has been removed from frequency data): each color corresponds to the restitution of the onboard apparent clock with respect to a given ground station.
The period of the frequency change is highlighted by black vertical lines:

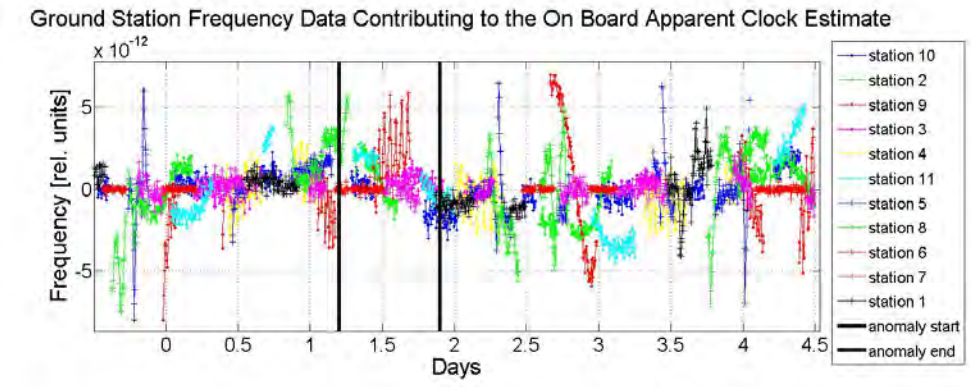

Figure 4.10: Ground Clocks' Frequency Evolution, only when Contributing to the On Board Clock Estimate. Case Study 1

From the frequency plot in Fig 4.10 no clear correlation between ground clocks' frequency behaviour and the satellite apparent clock estimation, even if the ground station clock frequency isvarying considerably.

4.1.2 Non-nominal Behaviour On Ground Station Clock: Search of the Possible Impact on Satellite Apparent Clock

In the example reported in this paragraph, the case study is the potential impact on the space clock solution due to a change in the inter-system bias in one of the ground stations. The ground station affected by an ISB change is here indicated as station n.6.
An inter-system bias change in the ground station receiver causes a jump in the time offset of the ground station's clock, as the one reported in Fig. 4.11:

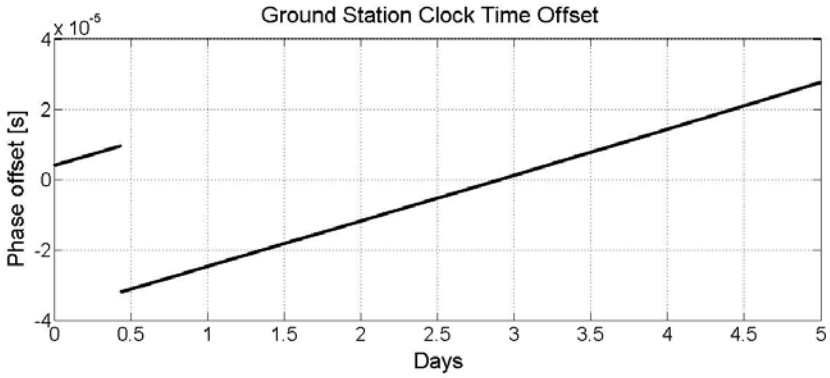

Figure 4.11: Ground Station Clock Time Offset Affected by an ISB Change

To determine whether this jump, of about 40μ s amplitude, present on the clock time offset of one of the ground station clocks used to estimate the satellite apparent clock could have any influence on the on board clock solution, an analysis has been performed considering one GNSS satellite tracked by the considered station.
Fig. 4.12 shows the satellite clock time offset (after quadratic drift removal) in the period the ISB changed. The vertical line indicates the instant in which the Inter-System Bias of the station changed:

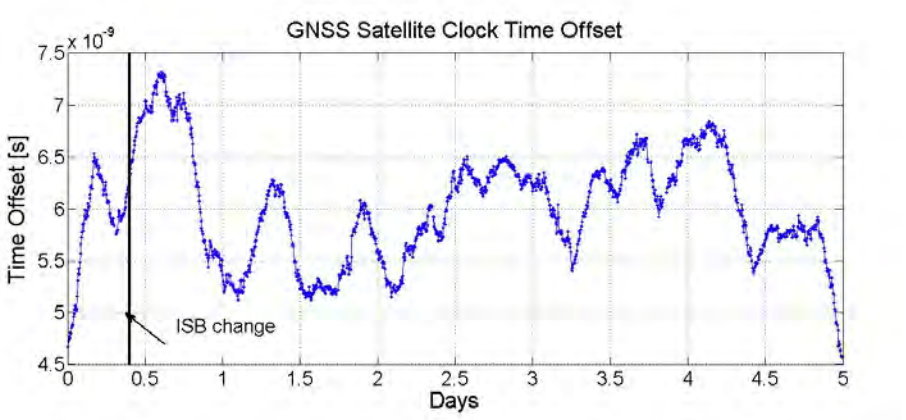

Figure 4.12: Satellite Clock Time Offset in the Period of ISB Change - Quadratic Drift Removed

The satellite clock frequency offset is illustrated in Fig. 4.13. Again the ISB change is indicated with a vertical line:

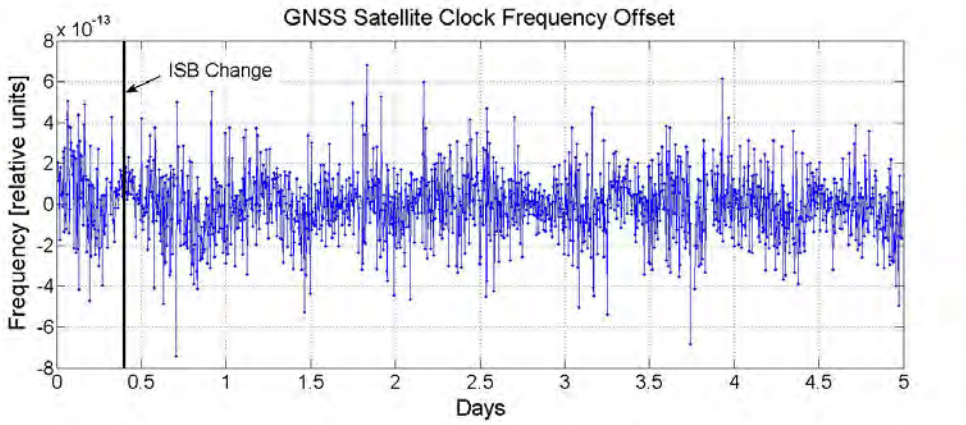

Figure 4.13: Satellite Clock Frequency Offset in the Period of ISB Change

No anomalies are observed on the apparent clock time offset (Fig. 4.12), nor in the apparent clock frequency estimates (Fig. 4.13).
The ground stations in view of the considered satellite when the ISB change occurred, identified using the STK Access Tool, are shown in Fig. 4.14.

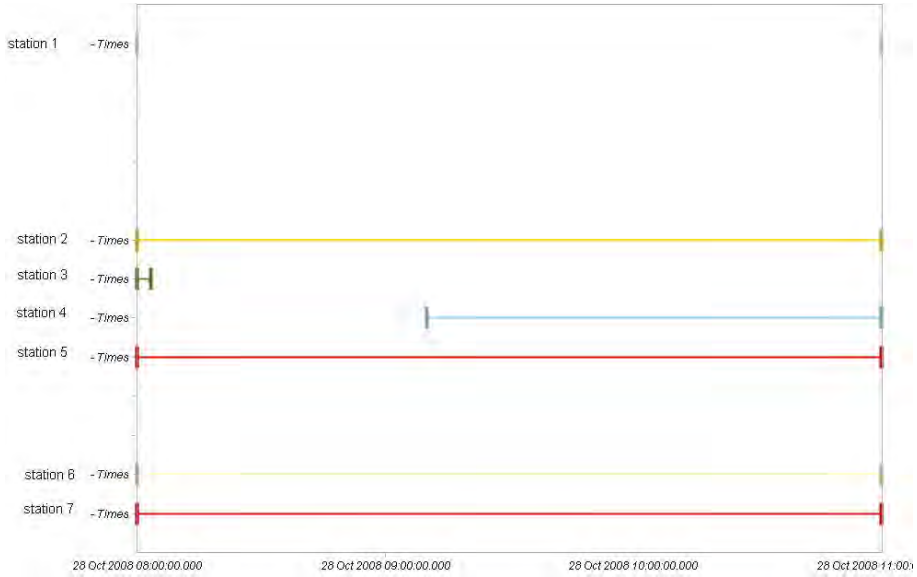

Figure 4.14: Ground Stations in View of the Satellite When the ISB Change Occurred

Fig. 4.15, illustrating which ground stations have been employed in the algorithm for the clock estimates, at different time instants, shows that, although the change in the ISB

(vertical line in the figure), the ground station n.6 has been used in the orbits and clocks estimation algorithm:

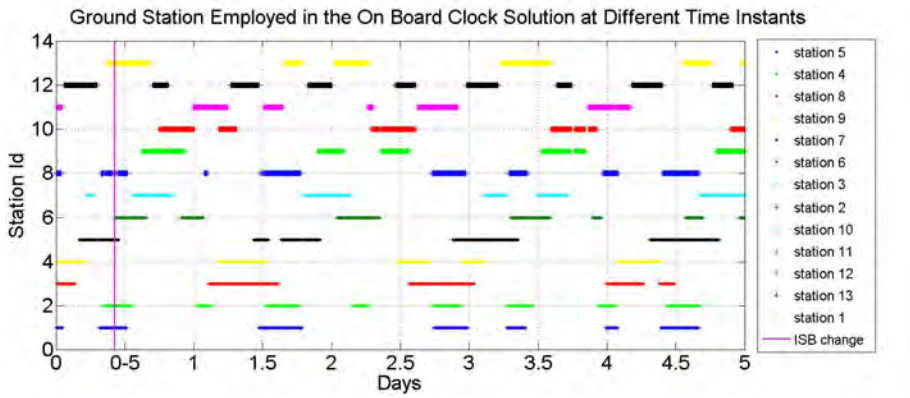

Figure 4.15: Ground Stations Employed To Produce the On Board Clock Solution at Different Time Instants. Case Study 2

Figures 4.16 and 4.17 shows the stations' time and frequency offset respectively:

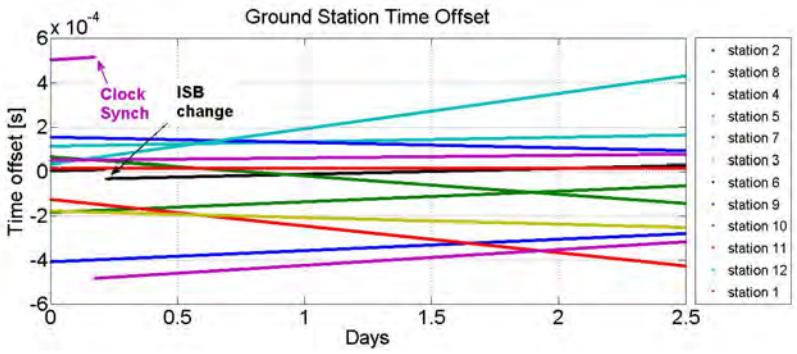

Figure 4.16: Time Offset of the Ground Stations' Clocks. Case study 2

As it can be noted in Fig. 4.16, station n.6 (black curve) is not the only station affected by a jump in the time offset: another station (pink curve) experienced a clock synchronization. The clock frequency offset for the two stations with a jump are not reported in Fig.4.17, where it can be seen that no anomalies are present in the frequency offset of the other stations at the time the ISB changed in station n.6 (black vertical line):

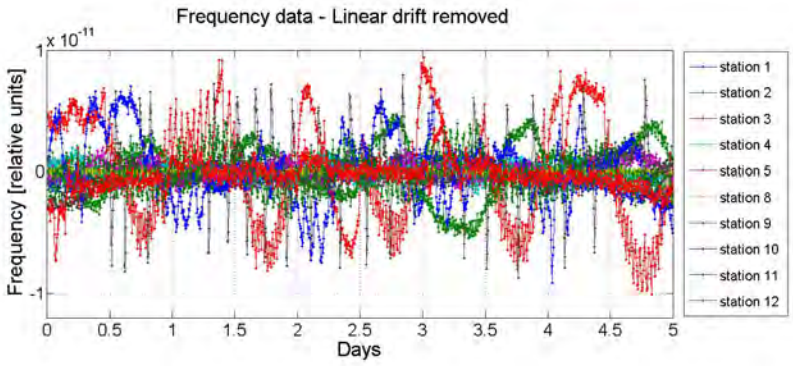

Figure 4.17: Frequency Offset of the Ground Stations' Clocks. Case Study 2

Again, the frequency evolution of the ground clocks only when used in the orbits and clocks estimation algorithm is illustrated in Fig.4.18. Station n.6 frequency is the black curve.

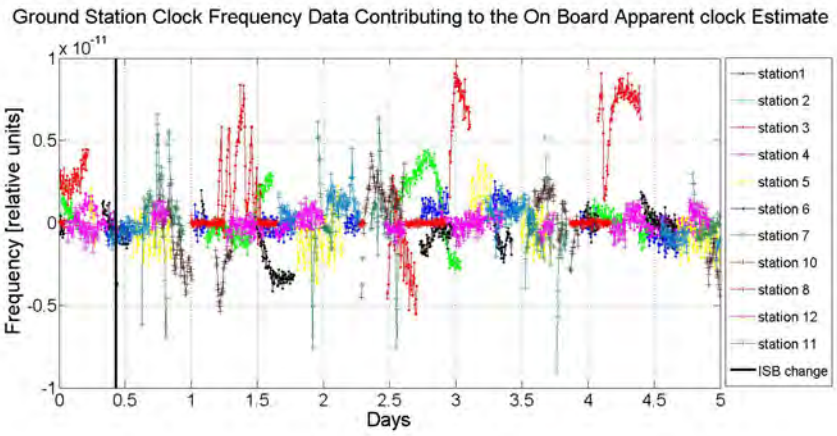

Figure 4.18: Ground Clocks' Frequency Evolution, only when Contributing to the On Board Clock Estimate. Case Study 2

Although station n. 6, at the moment of the ISB change, was in view of the GNSS satellite here considered and its measures were used in the process to obtain the on board clock estimates, it seems that the on board clock solution has not been affected at all by the jump in the ground apparent clock.

4.1.3 Conclusions on the Ground Clocks' Influence on the On Board Clock Solution

The analysis presented in the previous paragraphs was aimed at pointing out if any strange behaviour observed on the satellite apparent clock could be due to an analogous behaviour on some ground station clocks, particularly concerning the stations in direct view of the satellite. Similarly, the strange behaviours which sometimes is observed on the ground stations' apparent clocks, could be investigated in order to discover a possible impact on the on board clock solution.
For all the examined cases, including those reported in this thesis in which jumps, even well noticeable, are observed on clock time offset or frequency offset, no clear correlation could be pointed out between the ground stations' clocks and the on board clock estimates. This confirms the robustness of the Orbit Determination and Time Synchronizations algorithm in the on board clock estimation procedure. In fact, the algorithm should be able to automatically reject the station clock estimates whose quality is not sufficiently good to allow an adequate estimate of satellite clocks.

4.2 Clock Prediction and Prediction Error

As already mentioned, in real time navigation the users receive the predictions of satellite orbits and clocks through the navigation message and, when possible (ex. in Assisted-GNSS), also by means of external aids as ex. internet.
While the orbits predictions are pretty stable and accurate even over several days, it is quite difficult to have an accurate prediction for satellite clock phase. In fact, the quality and the accuracy of the clock prediction is strictly dependent not only on the clock itself but also on the potential jumps in the frequency source or on the effects introduced on the apparent clock by the algorithm applyed to get the clock solutions.
In present GNSS, the clock prediction error represents, for real time navigation, the main error contribution in the positioning for dual frequency users and the second contribution for single frequency users, after the ionosphere.
Clock technologies used in GNSS have strongly improved with respect to the ones of the early periods of satellite navigation: different types of clocks have been used in GNSS history: from the early Cesium technologies employed in GPS and GLONASS, to the different generations of space Rubidiums, GPS Block IIA and GPS Block IIR, until the Passive Hydrogen Maser (PHM) to be used in Galileo.
The clock prediction accuracy is intrinsically related to the age of data: the older is the prediction transmitted to the user, the worse is the accuracy. The rate of the dissemination of the information necessary to the user for the positioning depends on the Navigation

System: the update of the navigation message is nominally once per day in GPS, twice a day for GLONASS and it is planned to be 100 minutes for Galileo. The update rate is a function of the clock performance: the predictions of less stable clocks need to be updated more frequently.
In GPS as well as in Galileo, the satellite constellation is composed by a mixed configuration of clock families: Cesium and Ribidium for GPS, Rubidium and Passive Hydrogen Maser for Galileo...
In this section the clock prediction strategy foreseen for the Galileo system is presented, together with some tests on experimental data [63].
My personal contribution in this activity, conducted in the frame of the experimental phase of Galileo, the GIOVE Mission, consisted in the software implementation of the algorithm for clock prediction, on the analysis of the experimental data (presented at the 24^{th} European Time and Frequency Forum congress [63]) and on the evaluation of clock prediction error together with the related uncertainty in order to get a theoretical model for the prediction error.
A standard reference period without particular events has been selected for analysis reported [63]: it is the one month period from October 7^{th} to November 4^{th} of year 2009.

4.2.1 The Clock Prediction Technique

Different elements contribute to a robust and accurate clock prediction:

- The fitting model
- The choice of the fitting intervals for the model
- The data pre-processing and outliers treatment
- The update rate

Main attention is given hereafter to the fitting model, to the choice of data intervals for the model and to the adequacy to the 100 minutes maximum validity time foreseen for the Galileo system.

4.2.1.1 The Fitting Model

The clock prediction to be transmitted to the user is performed using a quadratic or linear model to fit the past clock estimates, using a least squares adjustment technique.
The general formula for fit $\widehat{x}(t)$ of clock phase data $x(t)$ is illustrated in Section 4.1:

$$\widehat{x}(t) = a_0 + a_1(t - t_0) + a_2(t - t_0)^2 + a_3 sin(\frac{2\pi t}{T} + \varphi) \tag{4.1}$$

Where:

- a_0, a_1 and a_2 are the polynomial terms: the intercept, the linear and quadratic term respectively
- a_3 and φ are respectively the amplitude and the initial phase of the periodic term
- T is the period of the periodic term
- t is the prediction time
- t_0 is the initial time of the prediction

In each navigation system, the fitting model is included in the proper space allocated in the navigation message. The Russian GLONASS, using only Cesium clocks, implements a linear prediction [1], estimating only a_0 and a_1. Both GPS and Galileo implement either a linear or a quadratic fit, estimating dynamically the a_2 term, necessary to describe the frequency drift of the Rubidium clocks, depending on the behaviour of each clock, in terms of drift.
The presence of periodic fluctuations on satellite clock phase is a well known feature [44]; in fact the IGS recommends the use of the periodic term in polynomial fit [83].
The time intervals Δt_2, Δt_1 and Δt_0 for the evaluation of each polynomial coefficient can be common to all the terms of the polynomial or can be different for each term.
A larger Δt_i allows to take benefit of a larger amount of data which permits to reduce the uncertainty on the coefficients estimate: it could be a worth solution for more stable clocks, whose behaviour is not changing considerably over time. On the contrary, a smaller Δt_i gives the opportunity to favour the local behaviour of the clock and mitigates the risk of a prediction influenced by older data which are no more representative of the current clock behaviour: this system could be more appropriate for clock which are more changeable over time. It can be reasonably expected that different clock technologies would require different prediction techniques.
A mixed configuration, as the one here adopted, would allow to gain from both the approaches.
The advantages and disadvantages of using different time intervals will be deepen in the next sections.

[1] since cesium clocks can be described with a linear model, see Section 1.2.1

4.2.2 Experimental Activity

The clock prediction included in the GIOVE navigation messages is computed using a common adjustment to the last 24 hours of clock phase data, therefore using $\Delta t_2 = \Delta t_1 = \Delta t_0 = 24h$. No pre-processing of the fitting data is foreseen.
On the contrary, the strategy used the in experimental activity and here reported uses different fitting intervals for the estimation of the different fit coefficients:

1. the quadratic coefficient a_2 is calculated by means of a parabolic fit on the clock estimates of the last 24 hours (Δt_2), using the least squares method

2. the linear term a_1 is evaluated with a least squares linear fit over the last 6 hours of clock estimates (Δt_1)

3. the a_0 coefficient is obtained as the linear fit over the last hour (Δt_0) of clock estimates, evaluated at the first prediction epoch, corresponding to the last measure epoch. In principle, being the stochastic behaviour mainly driven by white frequency noise, that is random walk on the phase, the best estimation for the intercept would be the last value of the past clock estimates. However, the last value of the fit is taken as a_0 in order to minimize the probability of selecting potential anomalous data.

The a_2, a_1 and a_0 coefficients obtained with the procedure described above are then used to predict the satellite clock phase for the subsequent 24 hours, extrapolating the polynomial fit function whose coefficients have been estimated over different time intervals (Δt_i):

$$x_p(t) = a'_2 t^2 + a'_1 t + a'_0 \tag{4.2}$$

Where $x_p(t)$ is the clock time offset prediction and a'_2, a'_1, a'_0 are the coefficients of the predicted time offset, obtained from those estimated on the past data.
It has to be reminded that an axis translation is required to consider the new origin of the time axis, that is the beginning of the prediction t_0: Naming T the new axis origin,

$$T = t - t_0$$

Hence,

$$t = T + t_0$$

The formula 4.2 can be written as:

$$x_p(T) = a_2(T + t_0)^2 + a_1(T + t_0) + a_0$$

$$x_p(T) = a_2(T^2 + t_0^2 + 2Tt_0) + a_1 T + a_1 t_0 + a_0$$

$$x_p(T) = a_2T^2 + a_2t_0^2 + 2a_2t_0T + a_1T + a_1t_0 + a_0$$

$$x_p(T) = T^2a_2 + T(2a_2t_0 + a_1) + (a_2t_0^2 + a_1t_0 + a_0)$$

Finally, we get

$$x_p(t - t_0) = \underbrace{a_2}_{a_2'}(t - t_0)^2 + \underbrace{(2a_2t_0 + a_1)}_{a_1'}(t - t0) + \underbrace{(a_2t_0^2 + a_1t_0 + a_0)}_{a_0'} \tag{4.3}$$

Where each term of the polynomial to be used for extrapolation not necessarily depends on only one coefficient of the fit. The quadratic term a_2' and the intercept a_0' are those evaluated with the fit strategy in the intervals Δt_2 and Δt_0 respectively, while the linear term a_1' depends on a combination of a_2 and a_1 estimated on Δt_2 and Δt_1 respectively.
This approach has been implemented on the whole experimental data set of GIOVE satellites from October 7^{th} to November 4^{th} of year 2009: the first 24 hours have been considered, the clock predictions for the subsequent 24 hours window have been evaluated, then we moved by 12 hours and started again the prediction calculation. There are therefore 12 hours overlapping between a prediction and the following one. Each prediction trajectory gives 24 hours predicted values and the procedure is repeated for the entire experimentation period, that is about one month: there are about 60 prediction trajectories.
The prediction error has been evaluated a posteriori as the difference between the prediction and the real clock estimates of the same period: there are about 60 series of prediction error for GIOVE-A and GIOVE-B.
Fig. 4.19 shows the prediction error for GIOVE-B satellite, together with the 2σ uncertainty [63]. Each line represents one prediction trajectory over 24 hours.

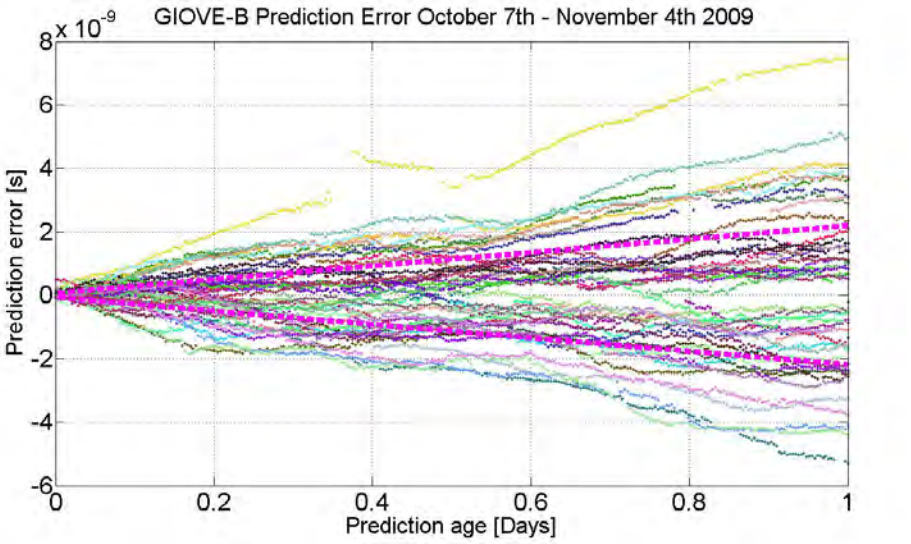

Figure 4.19: GIOVE-B (PHM) Clock Prediction Error, October 7th - November 4th 2009 [63]

As already mentioned, the quadratic term is flexibly used or rejected depending on the entity of the clock drift, that is on the clock technology. The importance of the quadratic term in the prediction of a Rubidium clock is shown in Fig. 4.20 which illustrates the prediction error if the a_2' coefficient is forced to zero when the satellite clock is a Rubidium Atomic Frequency Standard:

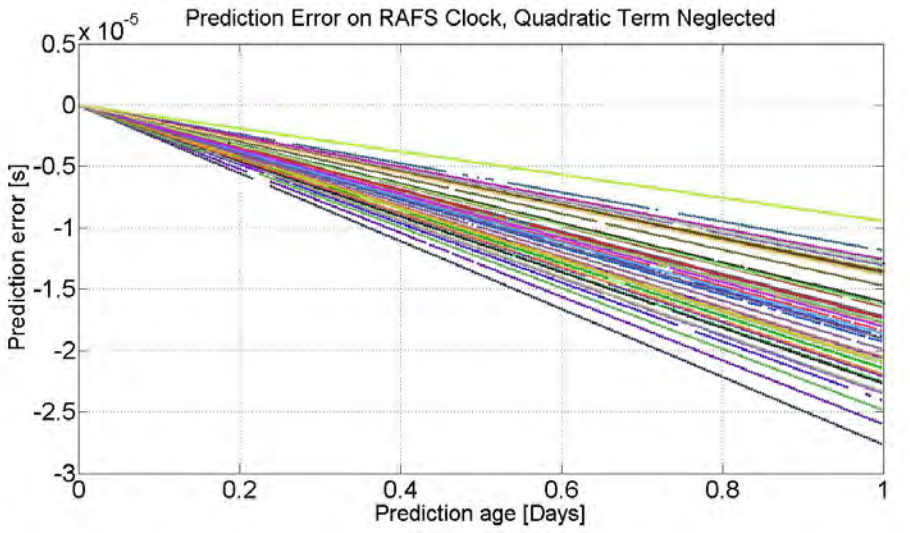

Figure 4.20: Clock Prediction Error of a RAFS when the Quadratic Term is Neglected [63]

Generally the prediction error is expected to grow with the prediction age, assuming equally positive and negative values, as in Fig. 4.19. On the contrary, the prediction error in Fig. 4.20 is clearly biased and reaches the level of tens of microseconds after 1 day, confirming that the prediction strategy was not appropriate to the clock technology.

4.2.2.1 Uncertainty Evaluation

A theoretical model has been evaluated for the prediction error, considering both the deterministic and stochastic contributions on the final budget. The resultant 2σ uncertainty is reported in Fig. 4.19 (pink dashed lines) together with the experimental results.
The main uncertainty factors taken into account are the following:

- The uncertainty related to the **polynomial fit** $(a_2t^2+a_1t+a_0)$ used to compute the predicted values, that is the uncertainty on the intercept a_0 (u_{a_0}), the uncertainty on the linear drift a_1, due to initial frequency offset (u_{a_1}) and the uncertainty on the quadratic term a_2 due to the linear frequency drift (u_{a_2}), when used
- The uncertainty related to the clock **stochastic components**, namely White Frequency Noise and Flicker Floor (u_ϵ)

- The uncertainty related to the **consistency of the overlapping day** between two consecutive ODTS Arcs (u_x)

The uncertainty on the prediction is obtained using the following equation, according to the law of propagation of uncertanties [59]:

$$u_{TOT}^2 = u_x^2 + u_{a_0}^2 + u_{a_1}^2(t-t_0)^2 + u_{a_2}^2(t-t_0)^4 + cov_{a_i,a_j} + u_\epsilon^2 \tag{4.4}$$

Where cov_{a_i,a_j} represents the coviarance between the different coefficients of the polynomial fit (see Eq. 3.26 for the complete expression). It has to be remarked that, even if in the present analysis the covariances have been taken into account, their values are typically very small with respect to the variances, especially if compared with the stochastic components, which is the dominant contribution, as illustrated in the next paragraphs.
Besides, considering that in the present analysis barycentric coordinates have been used (see Section 3.2.1.1.1), the only correlation term which is still present is σ_{a_0,a_2} (see Eq. 3.30).
In addition, the stochastic contributions to the uncertatiny were considered independent from the deterministic coefficients, being estimated over an historical data set, different from the one used to evaluate the polynomial fit.
In the following the contributions of the single factors listed in Eq. 4.4 are illustrated:

1. **Uncertainty Related to the Linear Fit ($\widehat{x}(t) = a_0 + a_1 t$)**
   When the frequency drift of the clock to be predicted is negligible, the prediction model is based on a linear fit of the last 6 hours for the a_1 coefficient and of the last hour for a_0. The choice of using different time intervals for the different coefficients, as anticipated in 4.2.1.1, allows to take benefit of the information about the local behaviour of the clock, and at the same time, of the recent past data.
   The uncertainty on the intercept a_0 and and the uncertainty on the linear drift a_1 are given by Eq. 4.5 and Eq. 4.6 respectively, according to the least squares method [54] and using baricentric coordinates:

$$u_{a_0}^2 = \frac{\sigma_{a_0}^2}{N_{a_0}} \tag{4.5}$$

$$u_{a_1}^2 = \frac{\sigma_{a_1}^2}{\sum_{i=1}^{N_{a_1}} t_i^2} \tag{4.6}$$

   Where N_{a_0} and N_{a_1} are the number of phase data used for the fit to evaluate a_0 and a_1 respectively, t_i are the considered epochs, while $\sigma_{a_0}^2$ and $\sigma_{a_1}^2$ are the variances of

the estimates, evaluated as the mean value of the squared residuals between the clock phase data estimated by the orbit determination and time synchronization algorithm and the corresponding fitted polynomial (See Eq. 3.3).

2. **Uncertainty Related to the Quadratic Fit ($\widehat{x}(t) = a_0 + a_1 t + a_2 t^2$)**
   When the frequency drift of the clock to be predicted is not negligible, the prediction model is based on a quadratic fit of the last 24 hours of clock phase data for the estimate of the a_2 coefficient, on a linear fit over the last 6 hours for the a_1 coefficient and over the last hour for a_0.
   Being a_1 and a_0 estimated through a linear fit, the equations for the related uncertainty are the same illustrated above. The uncertainty on the quadratic term a_2 is given by Eq. 4.7, according to the least squares method [54] and using baricentric coordinates:

$$u_{a_2}^2 = \frac{\sigma_{a_2}^2 \cdot N_{a_2}}{\sum_{i=1}^{N_{a_2}} t_i^4 - \left(\sum_{i=1}^{N_{a_2}} t_i^2\right)^2} \tag{4.7}$$

   Again N_{a_2} is the number of phase data used for the fit, t_i are the considered epochs and $\sigma_{a_2}^2$ is the variance of the estimates evaluated as the mean value of the squared residuals between the ODTS clock phase data and the corresponding fitted polynomial.

3. **Uncertainty Related to the Stochastic Components**
   The stochastic contribution on the uncertainty on clock prediction has been evaluated considering two types of noise: white frequency noise and flicker frequency noise, combined using the formula 4.8 recommended in [5]:

$$u_\epsilon^2 = \sigma_{y_{WF}}^2 (t - t_0)(t - t_0)^2 + \frac{\sigma_{y_{FF}}^2 (t - t_0)(t - t_0)^2}{ln2} \tag{4.8}$$

   Where t_0 is the instant at which the prediction starts, $\sigma_{y_{WF}}^2$ and $\sigma_{y_{FF}}^2$ are the Allan Variance of the clock noise given by the white frequency noise and flicker frequency noise respectively.
   For GIOVE-B the values of such noises have been taken from the specifications (Allan Deviation at 1 s is 10^{-12} for White Frequency Noise and $10^{-}14$ for Flicker Frequency Noise). For GIOVE-A the value of flicker frequency noise has been taken from the

specifications (Allan Deviation at 1 s is $3 \cdot 10^{-}14$) while for the white frequency noise the typical experimental value of $6 \cdot 10^{-12}$ has been considered, which is bigger than the value reported in the specs ($5 \cdot 10^{-12}$).

Combining the deterministic and the stochastic contributions, the 2σ total uncertainty is obtained, as shown in Fig. 4.21 for GIOVE-B satellite:

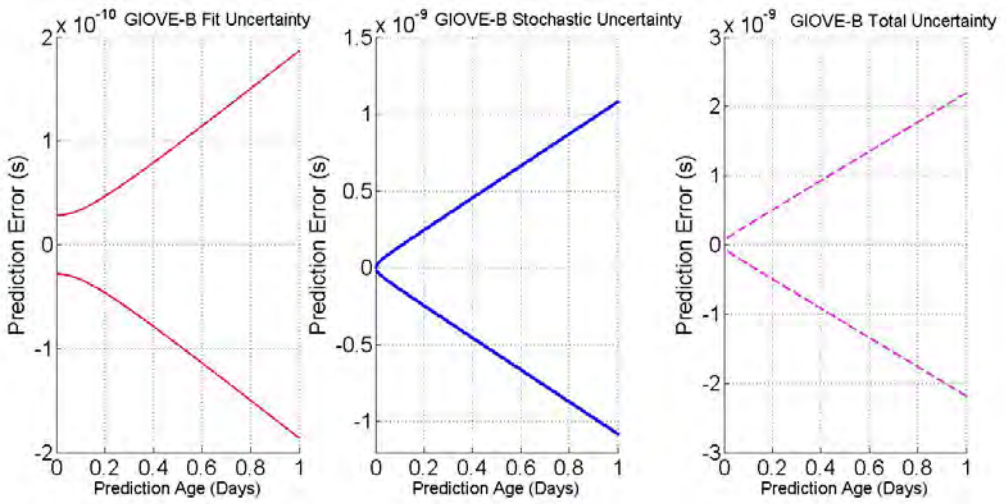

Figure 4.21: Contributions to the Uncertainty on Satellite Clock Prediction Error

Figure 4.22 illustrates the comparison between the deterministic and stochastic contribution on the clock prediction error uncertainty:

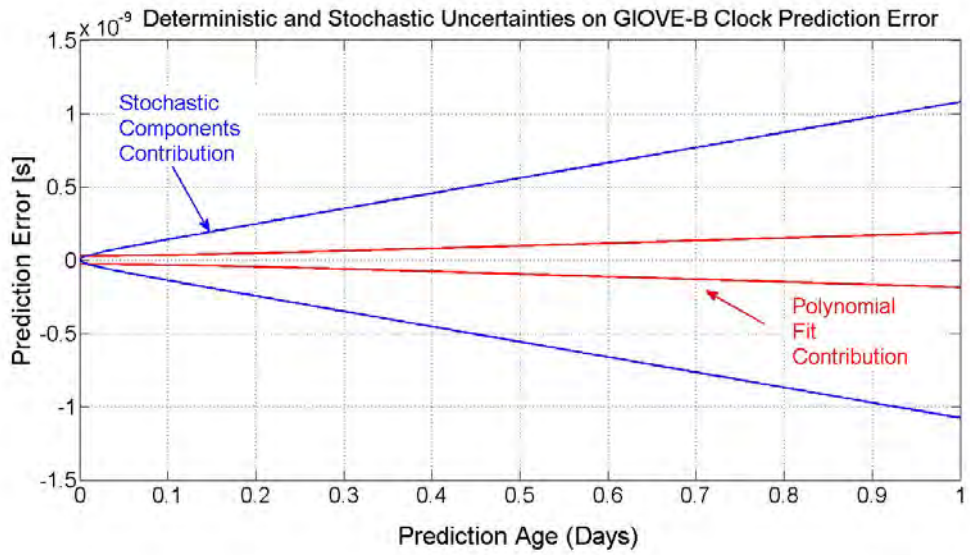

Figure 4.22: Deterministic and Stochastic Uncertainties on GIOVE-B Clock Prediction Error

It is clearly evident that the prevailing contribution is the one of the clock stochastic components.
The theoretical model applied to experimental data is the pink dashed line shown in Fig. 4.19 for GIOVE-A and GIOVE-B satellites respectively.
It can be noted that the theoretical model seems to be not suitable for the experimental data: many prediction error curves are not contained in the 2σ theoretical uncertainty. This could be related to the periodic fluctuation which is present on satellite clock data but which has not been taken into account in the prediction model.

Periodic Fluctuation

Periodic phase variations associated to clock estimations are very common in GNSS satellites [44]. From previous results it seems that the harmonic function can not be neglected without increasing the error.
In fact, in the presented prediction model the polynomial fit coefficients a_1 and a_0 are evaluated over the last 6 hours and over the last hour respectively: the resulting clock prediction is strictly dependent on the local behaviour of the data set.

Fig. 4.23 highlights the difference of a linear fit evaluated over 24 hours or over 6 hours of a simulated sinusoidal signal, with 24 hours period: in one case, over the whole period, the slope of the fitted line is negative while in the other case it is even positive.

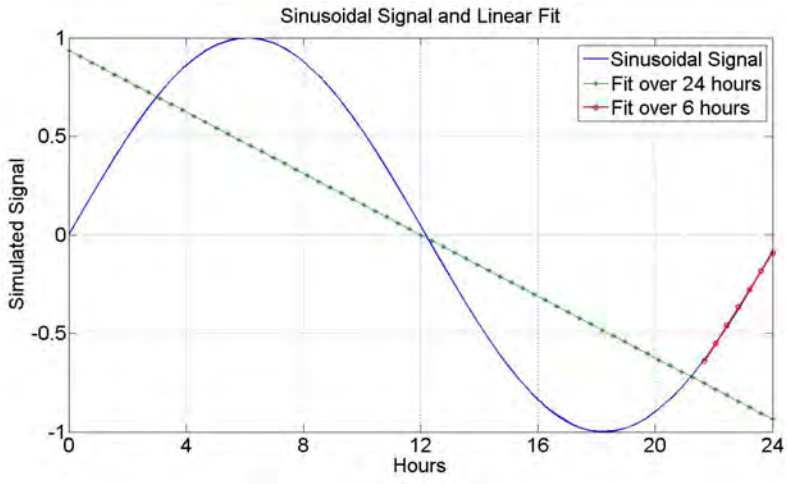

Figure 4.23: Linear Fit on a Simulated Sinusoidal Signal

In Fig. 4.24 are illustrated the results of the clock prediction model described in this paragraph, applied to simulated clock data in which the sinusoidal fluctuation, with period 14 hours, has been volunarily exaggerated:

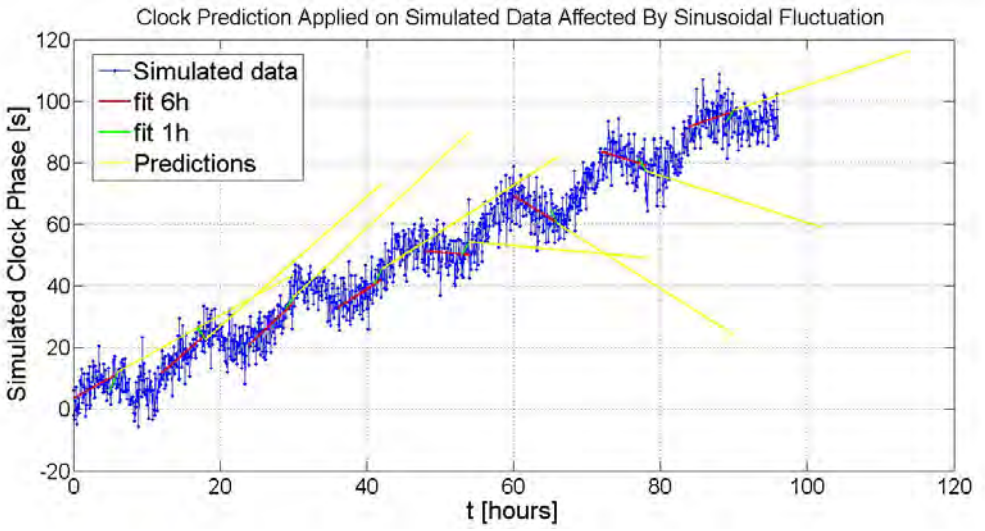

Figure 4.24: Clock Prediction on a Signal Affected by Sinusoidal Fluctuation

The yellow lines represent the linear predictions ($x_p(t) = a_1' t + a_0'$) for the next 24 hours evaluated using the a_1 coefficient of the linear fit over the last 6 hours (red lines) and the a_0 term of the fit estimated over the last hour (green lines): it is shown the impact of the error which can be made when fitting data affected by sinusoidal fluctuation if this latter is neglected. In fact, it can be seen that the predictions are not representative of the clock evolution when the coefficiets to be used in the clock model are evaluated over the descending part of the sinusoidal signal superimposed on the clock signal.
In the case of some RAFS clocks used in GNSS constellations, the amplitude of the sinusoid present on the apparent clock is about 4 ns peak to peak: estimating the a_1 coefficient over 6 hours and predicting for the next 24 hours would lead to an error up to 4×4 ns $= 16$ ns after 1 day; which is a considerable quantity, corresponding to a positioning error of about 5 meters if no corrections are applied.
The reason why the theoretical model in Fig. 4.19 does not contain the expected 95% of the experimental data could be ascribable to a similar phenomenon.
The solution to overcome or at least to mitigate the potential error on clock prediction when a periodic fluctuation is present on the apparent clock signal could be to include a sinusoidal fit in the model, as in Eq. 4.1: some experiments are described in [63].
An alternative and simpler solution is to estimate the a_2 and a_1 coefficients for the clock

prediction over a period multiple of the periodic fluctuation. The period T of the sinusoidal fluctuation could be estimated using some software tool for curve fitting over a representative set of experimental data, or could be even known a priori as in most cases the periodic fluctuation on the apparent clock signal is due to satellite orbital motion: strong harmonics of the 12 hours orbital periods are observed on GPS clocks [44]. The orbit period of GIOVE-B is about 14 hours [63].
If this approach is adopted, the clock prediction error is widely reduced, as can be noted in Fig. 4.25, in which the pink dashed lines representing the expected 2σ contain the majority of the experimental curves. In this case the linear coefficient a_1 has been estimated over an entire orbital period of the sinusoidal fluctuation while the quadratic term has been estimated over two periods of the fluctuation.

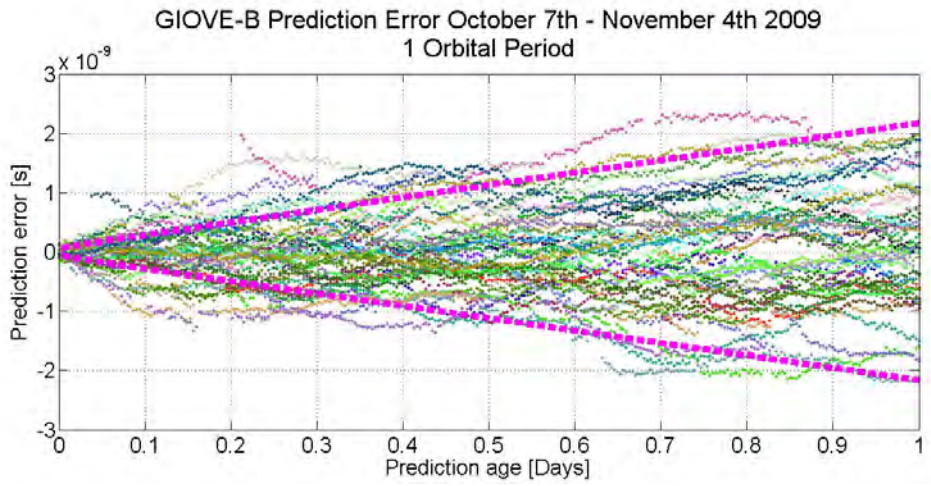

Figure 4.25: Clock Prediction Error on GIOVE-B Clock When a_1 is estimated over one orbital period and a_2 over two orbital periods

Further evidence of slight improvement is shown in Fig. 4.26, where both the quadratic and the linear coefficients have been evaluated over two entire satellite orbital periods:

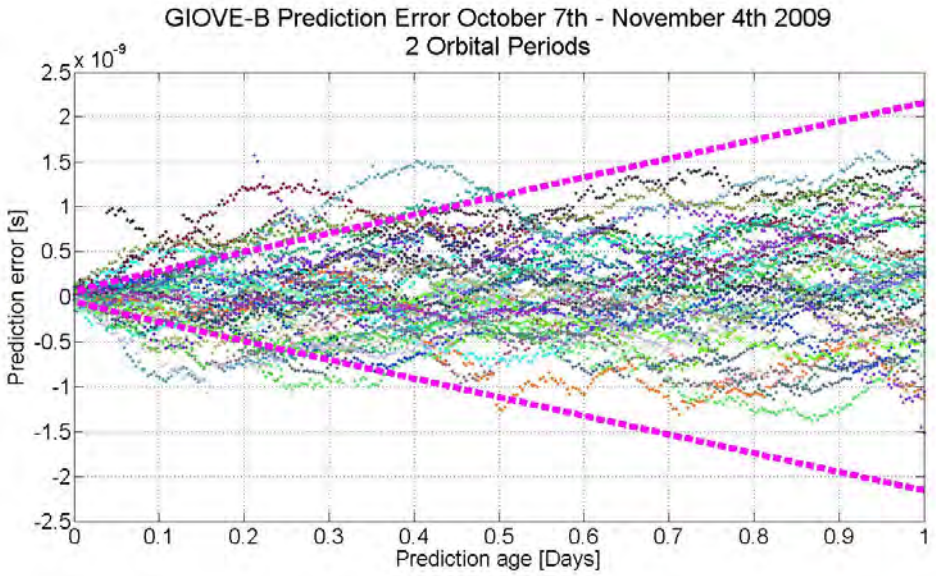

Figure 4.26: Clock Prediction Error on GIOVE-B Clock When a_1 is estimated over two orbital periods

If the size of the interval for a_1 estimation is increased to cover one more period of the periodic fluctuation (see Fig. 4.27), no benefit is observed:

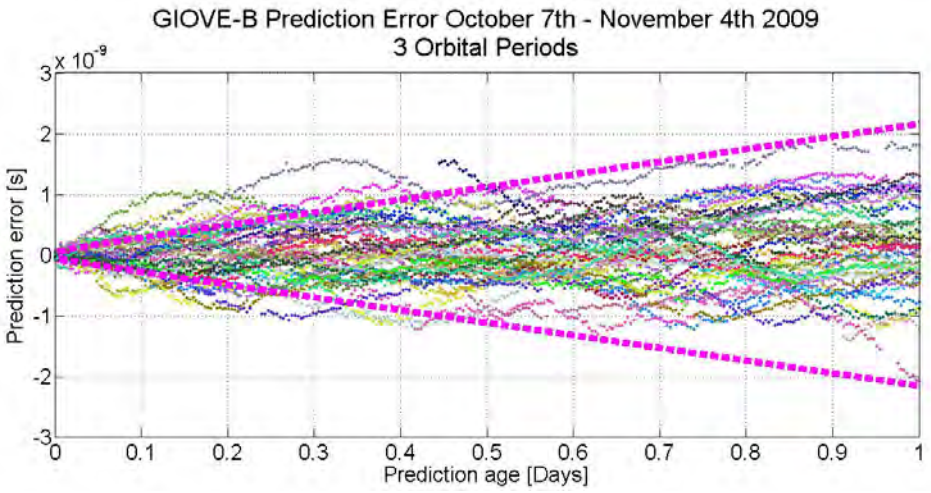

Figure 4.27: Clock Prediction Error on GIOVE-B Clock When a_1 is estimated over 3 orbital periods

Table 4.1 reports the peak to peak amplitude of the clock prediction error at 1 day, shown in Fig. 4.19, Fig. 4.25, Fig. 4.26 and Fig. 4.27:

Δt_1	Δt_2	**Peak to peak variation (ns)**
baseline (6h)	baseline (24h)	$[-5.2, 5.1]$
1 period (14h)	2 periods (28h)	$[-2.2, 1.97]$
2 periods (28h)	2 periods (28h)	$[-1.51, 1.50]$
3 periods (42h)	3 periods (42h)	$[-2.05, 1.81]$

Table 4.1: GIOVE-B peak to peak prediction error at 1 day

In the first column is reported the amplitude of the time interval in which is computed the linear coefficient of the clock model to be used for the prediction, while the second colum reports the quadratic term. Four different cases are illustrated: the first one is the baseline

solution described at the beginning of Section 4.2.2: a_2 is estimated over the last 24 hours of data, a_1 over the last 6 hours. The peak to peak error at 1 day is considerable, being about 10 ns. The potential inadequacy of the model is suggested also by the the fact that most of the experimental prediction error curves are not contained in the 2σ uncertainty (see Fig. 4.19).
In the second solution the coefficients of the clock model are evaluated over entire multiples of the orbit period: 1 period for a_1, 2 periods for a_2. In this case the peak to peak variation of the perdiction error at 1 day is considerably reduced from 10 ns to about 4 ns. Most likely it means that the periodic fluctuation present on the apparent clock cannot be neglected, but its effect can be limited through an appropriate choice of the fitting intervals Δt_i.
If then the Δt_1 is extended to include 3 entire periods of the sinusoidal fluctuation -while Δt_2 is not modified since the quadratic term is often negligible and hence not always used in the prediction-, the peak to peak error at 1 day is slightly reduced, probably gaining from the larger amount of data used in the fit rather than from the larger number of sinusoidal periods included in the estimate. In fact, if the coefficients are estimated over 3 entire periods of the sinusoidal fluctuation, as illustrated in the last experimental case, no improvement is observed: the peak to peak error at 1 day seems to be even increased with respect to the previous test. In this case too many data have been used in the fit and hence the advantage of considering mainly the local behaviour of the clock is lost.
When a periodic fluctuation is present, it is therefore convenient to evaluate the linear term of the polynomial to be extrapolated for the clock prediction over at least an entire period of the phenomenon, in order to avoid an erroneous estimate due to the non representative local clock behaviour. However does not seem so advantageous to extend the interval for the coefficient estimate to several periods of the periodic signal, also considering that the benefit of favouring the more recent data would be lost.
It can be observed that in both Fig. 4.26 and Fig. 4.27, despite a remarkable improvement, there is still a certain number of error curves which are not included in the $2-\sigma$ theoretical model, especially at short term: this is a consequence of the fact that, even if the polynomial coefficeints have been estimated over multiple periods of the observed fluctuation, the prediction does not include the sinusoidal term.

4.2.2.2 Prediction Error at Different Prediction Ages

The attention is now focused on the clock prediction error at some particular prediction ages:

- t = 0
- t = 100 minutes
- t = 12 hours
- t = 24 hours

For the Galileo system it is foreseen to refresh the clock prediction parameters every 100 minutes, while 24 hours is the refreshment rate currently employed in GPS.
The analysis is reported for the Rubidium clock on board GPS satellite G07 (SV 48), launched on March 15^{th} 2008 and belonging to satellite block IIR, since the results for GIOVE satellites not already published cannot be shown.
Fig 4.28 shows the clock prediction error as a function of the prediction age, for satellite G07. The prediction ages considered in the analysis are highlighted with red vertical lines:

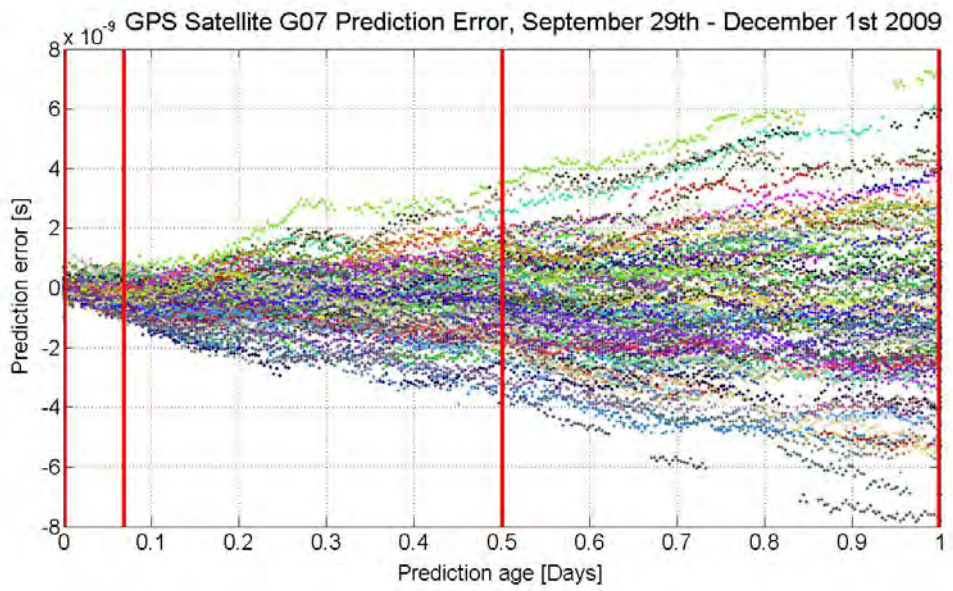

Figure 4.28: Clock Prediction Error on GPS Satellite G07 RAFS Clock, from September 29^{th} to December 1^{st} 2009

The peak to peak variation of the clok prediction error at the considered prediction ages are reported in Table 4.2, while Table 4.3 reports the standard deviation at the different time instants:

$t = 0$	t =100 min	$t = 12$ h	$t = 24$ h
[-0.98, 0.72] ns	[-0.96, 0.73] ns	[-3.53, 3.38] ns	[-7.80, 7.30] ns

Table 4.2: Peak to Peak Variation of GPS G07 Prediction Error for Different Prediction Ages

$t = 0$	$t = 100$min	$t = 12$h	$t = 24$h
0.23 ns	0.42 ns	1.45 ns	2.82 ns

Table 4.3: Standard Deviation of GPS G07 Prediction Error for Different Prediction Ages

It can be observed that the peak to peak variation and the standard deviation of the prediction error increases with the prediction age, reaching at 24 hours a value ten times bigger than the one at $t = 0$.
The following figures show the distribution of the prediction error at the different considered prediction ages, together with the corresponding Gaussian fit, computed using the standard deviation and the mean value of the prediction error at that specific time instant.

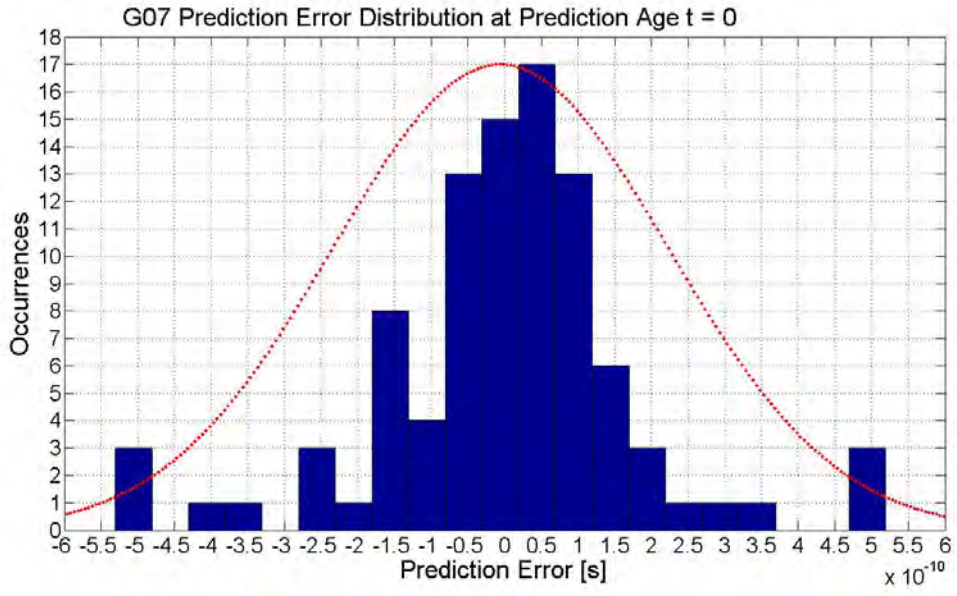

Figure 4.29: GPS G07 Prediction Error Distribution and Gaussian Fit at t=0

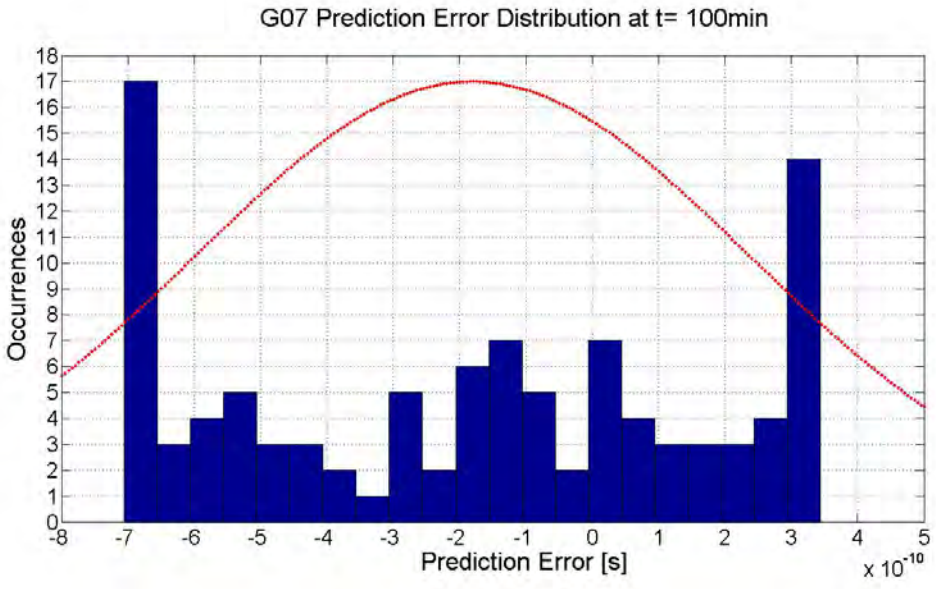

Figure 4.30: GPS G07 Prediction Error Distribution and Gaussian Fit at t=100 min

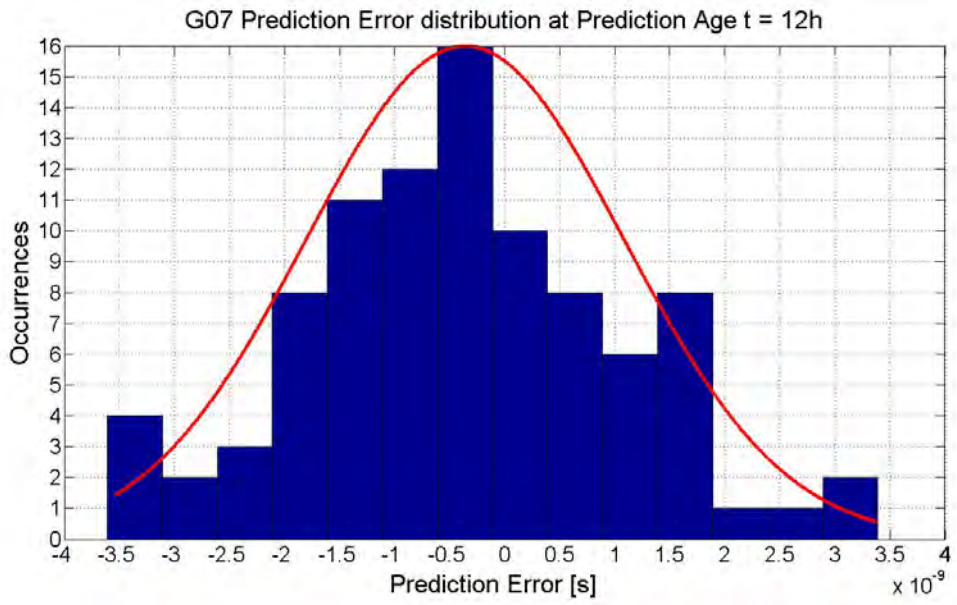

Figure 4.31: G07 Prediction Error Distribution and Gaussian Fit at t=12 h

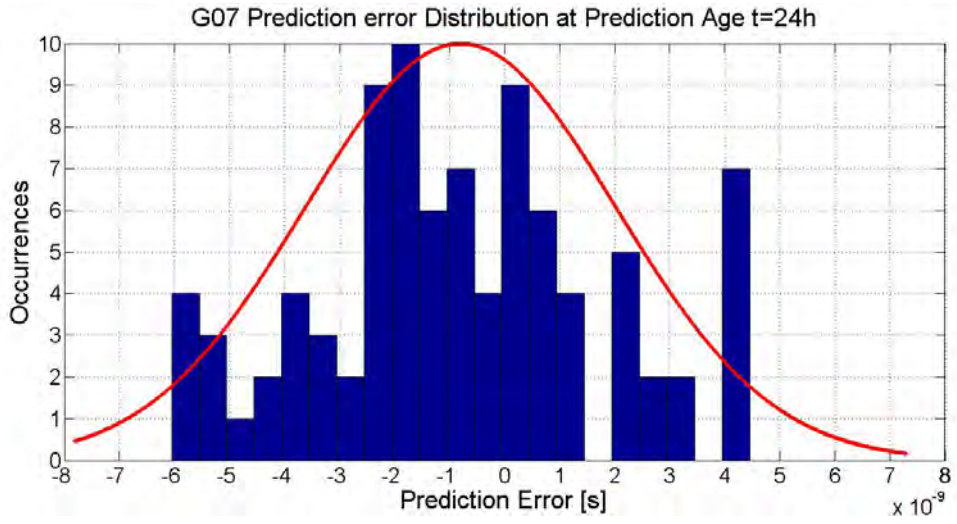

Figure 4.32: GPS G07 Prediction Error Distribution and Gaussian Fit at t=24h

From Fig. 4.29, Fig. 4.30, Fig. 4.31 and Fig. 4.32 it can be inferred that the prediction error has not exactly the Gaussian distribution which was expected, but this is probably due to the very limited number of available samples (two months of data for the present analysis).

A possible improvement for the clock prediction strategy could be the dynamic adaptation of the fitting intervals in case anomalies are detected in the clock signal, in order not to include the corrupted portion of data in the polinomyal fit, avoiding a prediction not representative of the overall clock behaviour.
Besides, the inclusion of a periodic term in the fitting model, as in Eq. 4.1, would improve the performances.

4.3 Feared Events Detection

A navigation system shall raise an alarm when an error is detected in the positioning solution or when a malfuncioning is identified in the satellite. The warning must be notified to the users within a limited time. GPS users are not informed in case of system failures. Galileo, on the contrary, is designed to ensure that users receive integrity data through the navigation signal, with a *time to alert* which shall not exceed 6 seconds, from the failure identification to the notification to users [32].
Undesired anomalies on clocks are generally called *feared events*. The most common on board clocks' feared events are frequency jumps, that are sudden changes in the apparent clock frequency, not predictable and which make erroneous the clock prediction provided to the users.
It is really important to detected such anomalies, to record them and to notify the users.
In literature frequency jumps are often indicated as frequency steps.
The causes of clock frequency jumps are not always clear. Although most of the frequency jumps can be attributed to the clock behaviour, in some cases they can be due to changes in the clock environment or to some operations such for example velocity changes in the satellite orbit to position the satellite in the desired location [48]. In addition, it has to be remarked that, for in orbit clocks, the measurements are not taken directly but have to pass through the chain which generates the broacast frequency, then are processed by the algorithm which produces the orbit and clock solutions elaborating the ground stations obsevations...
It is commonly known that Rubidium clocks generate frequency steps [48]. In some cases,

for Rubidium clocks, the observed frequency steps seem to be related to the excess of Rubidium, which is in the form of liquid droplets rather than vapor [84]. In these cases, it is expected to observe a decrease in the number of frequency steps with the age of the clock, since the excess of Rubidium could be redistributed or captured elsewhere.

Several different types of frequency jumps have been observed on satellite clocks. In particular, over 30 years of GPS experimental data it has been possible to notice several frequency jumps, characterized by different shapes [48]. Most frequency steps tend to persist in time. Others are characterized by a triangular frequency pattern in which a sudden jump is followed by a rapid decay of the frequency, which returns to the initial level. In other cases, a frequency step persists for a significant time, then it disappears.
In our experience with experimental data it has been possible to observe sudden frequency jumps, in which the phenomenon occurs in a few minutes and the frequency difference can be noted between the value of a frequency sample and the subsequent one, as well as slow frequency changes in which the final value of the frequency after the step is reached after a period up to several hours.
However, for the analysis reported in this paragraph, the term *frequency jump* will be used for all types of frequency steps: both instantaneous jumps and slow frequency changes, persistent or not persistent.

One of the activities regularly carried out at INRIM in the frame of the Galileo Project, and on which I was commissioned, is the detection of potential anomalies in clocks' behaviour.
The activity of frequency jump detection in the first experimental phases of the Galileo project has been carried out by visual inspection. It is currently under development the automatic method for anomaly detection [85].
The clock frequency is obtained converting the clock time offset estimates extracted from the received RINEX files and processed by the Clock Analysis software (described in Section 3.2). The detection of frequency jumps is then performed elaborating one of the output products of the Clock Analysis software, that is the clock frequency offset affected by frequency drift, after the outliers filtering.
at the time of the analysis, the feared events detection was done manually, by visual inspection, and using proper tools to average the frequency data over a smoothing window, in order to reduce the clock noise. Currently, in the frame of the Galileo Time Validation Facility (see Section 2.2.2.3), we are working at the automatization of the feared events detection [85]. The study of frequency anomalies consists in the evaluation of the entities of the frequeny jumps detected, and on the evaluation of other information related to the clock anomaly, such as the jump duration, the number of days elapsed from the last ob-

served anomaly, the number of days since the clock switch on, etc. All these information can be useful to obtain a more complete characterization of the clocks behaviour, in particular for what concerns the clock anomalies. The collected information can be used as input for further analysis to deepen the study of frequency jumps, with the aim of better understanding this phenomenon and maybe allowing to predict its coming and, as a consequence, to mitigate the impact on the timing performance of GNSS.
Furthermore, the possible causes of the anomalies are investigated. Sometimes frequency jumps are caused by particular events such as maintenance operations, power supply interruption etc.
In general, when a frequency jump is observed, all the possible causes are investigated. The satellite telemetry data are analyzed to look for any possible correlation with the detected anomalies. For example it is carefully studied the temperature of the environment in which the clock is located. Besides, the so called satellite *health parameters* are monitored in order to determine if the observed anomaly could be attributed to the clock physical package [86].

In the presented activity are considered as *frequency jumps* those jumps whose magnitude is at least five times the best level of noise of the apparent clock, as per clock manufacturer specifications, and which occur in a time span of a maximum of a few hours. Since the best level of stability of RAFS clock data, in terms of Allan Deviation without drift removal, is about 10^{-13}, then the frequency jumps whose magnitude is at the level of about $5 \cdot 10^{-13}$ are ascribed to an anomalous behaviour of the clock.
As already mentioned in Section 3.1, the clock measures in the RINEX files used in navigation systems have a sampling rate of 300 seconds (5 minutes): as a consequence they are quite sensitive to the measurement system noise. To smooth out that noise, an averaging operation is normally performed in order to simplify the jump detection; when averaging on a window of an hour it is possible to observe more easily the long term signal evolution. Fig. 4.33 shows an example of averaging operation performed on frequency data. Since GIOVE data are strictly confidential, the following picture has been obtained smoothing the frequency of the RAFS onboard GPS satellite G25:

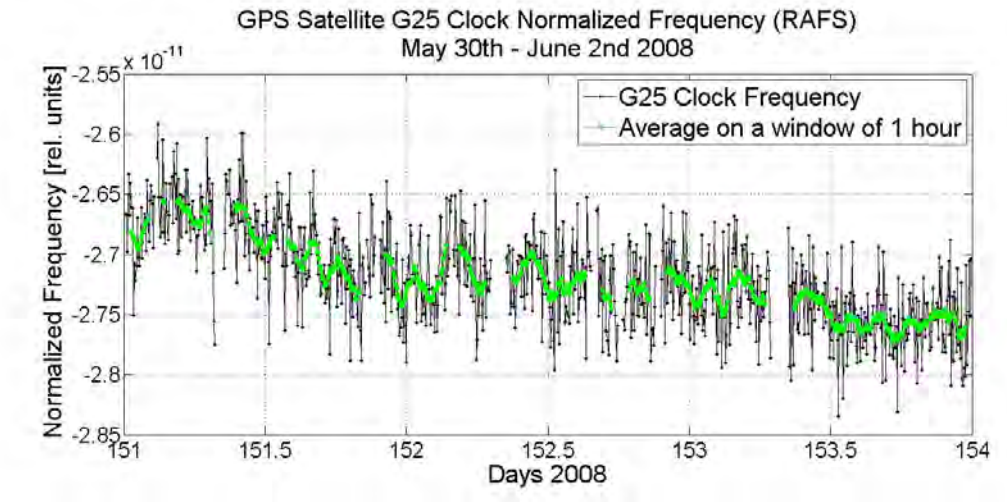

Figure 4.33: Example of averaging operation: GPS Satellite G25 (RAFS) May 30^{th} - June 2^{nd} 2008

Black points represent the estimated frequency values at 300s, while green points are the result of the averaging operation over a 1 hour window.
The averaging operation allows to perform an easier analysis of the frequency pattern, having mitigated the noisiness of the signal.
Fig. 4.34 shows an example of *sudden jump* observed on GPS satellite G31 RAFS clock, on June 8^{th} of year 2008

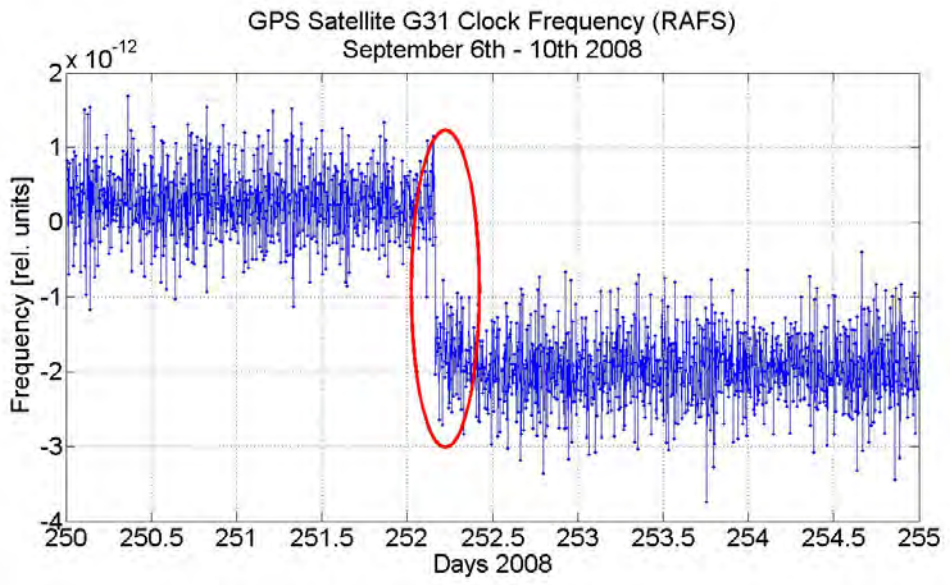

Figure 4.34: Example of sudden frequency jump: GPS Satellite G31 (RAFS) June 6^{th} - 10^{th} 2008

In this example, the apparent clock frequency has a jump of about $2 \cdot 10^{-12}$, then it remains at the level of $-2 \cdot 10^{-12}$.
Fig. 4.35 illustrates GIOVE-A apparent clock frequency from October 28^{th} to November 18^{th}, 2006, almost one year after the satellite launch [87]. The red lines indicate frequency jumps. These jumps occur in a few minutes and tend to persist in time.

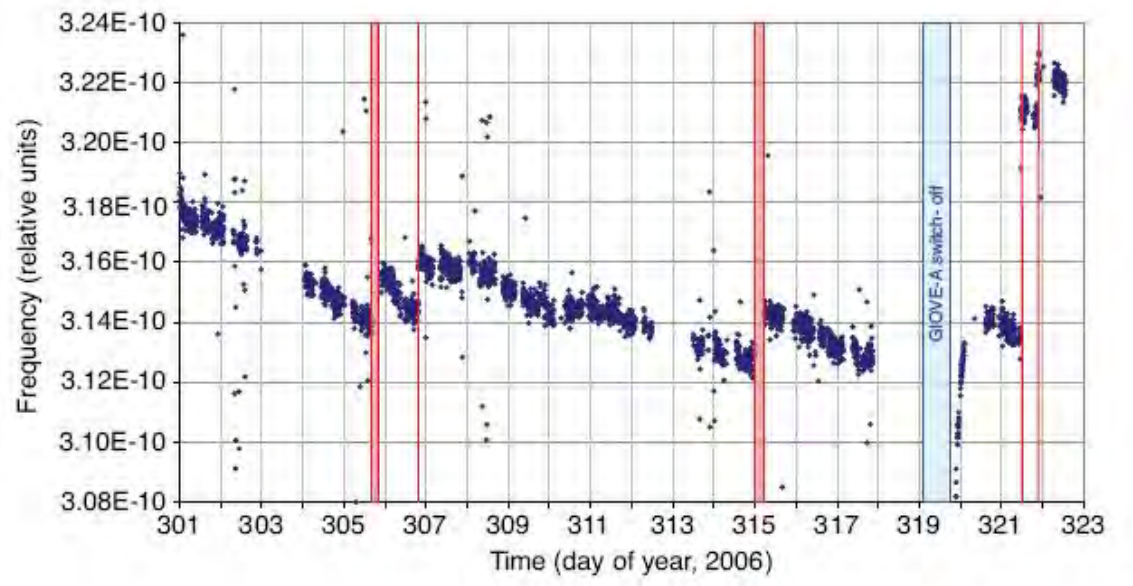

Figure 4.35: GIOVE-A Sudden Jumps [87]

Another type of frequency anomaly is represented by the *slow frequency changes*. In this case the apparent clock frequency changes slowly over time, and reaches its new frequency value after an interval of some hours or even some days.
An example of such behaviour is illustrated in Fig. 4.36, obtained through a simulation, where the jump duratin is 2 hours:

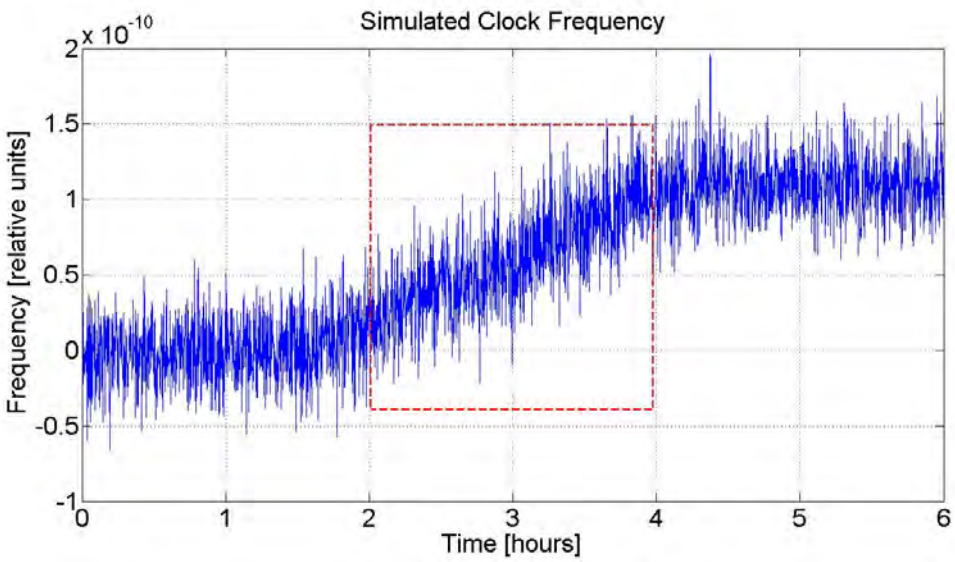

Figure 4.36: Simulation of Slow Frequency Change on Apparent Clock Frequency

A further example of anomaly on the clock normalized frequency is the presence of a sudden jump which is followed by a second jump of about the same entity but opposite in sign, as showed in 4.37:

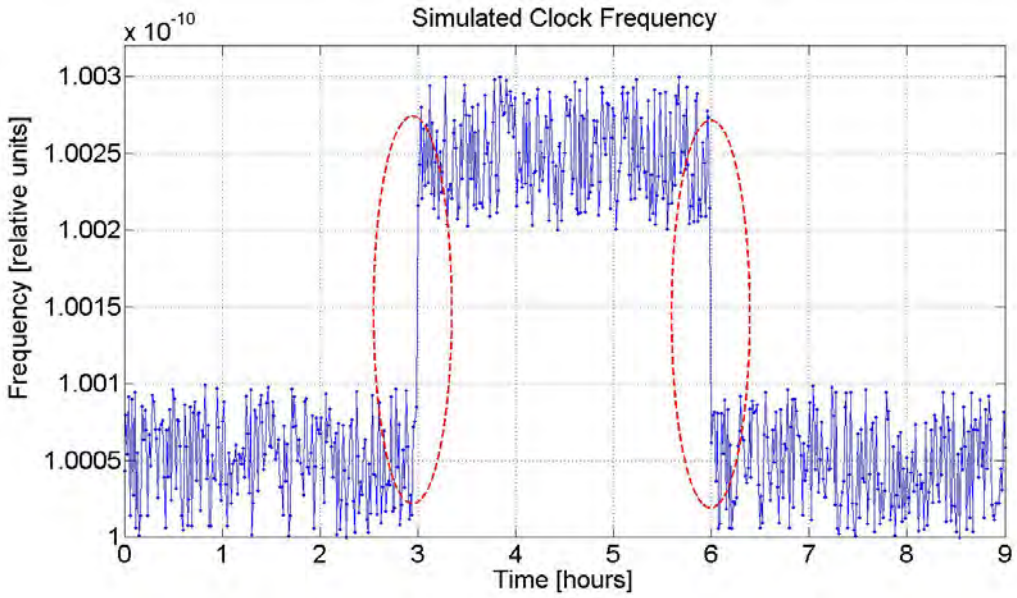

Figure 4.37: Simulation of Triangular Frequency Pattern on Apparent Clock Frequency

4.4 Statistical Analysis on Space Clock Feared Events

With the aim of evaluate the statistical distribution of the frequency jumps observed on GNSS onboard clocks, in order to derive some conclusions about the potential relationship between the clocks age and the jump occurrences and entity, an analysis has been performed on GIOVE and GPS satellites, analysing some years of experimental data. The results obtained from the analysis on the clocks on board GIOVE satellites will not be showed in this thesis because of the confidentiality of the data related to the Galileo project: analogous processing activities have been repeated on GPS clock data and the results will be illustrated in this section.

The RINEX files produced by IGS (see Section 3.1) have been processed and clock data have been analyzed using ad hoc created software programs as well as software routines commonly used at INRIM for clock characterization.

More than two years of GPS clock data have been processed: the analyzed period is January 2008 - May 2010.

For all the GPS satellites whose clock measures were present in the IGS RINEX files for the considered period the normalized frequency offset has been derived from time offset data and it has been observed in order to detect any frequency jump, with the visual inspection

method described in Section 4.3.
The data collected with the analysis of all the detected jumps have been processed by ad hoc created software routines to produce the results illustrated in this section.
Frequency jumps observed on Cesium or Rubidium clocks are analysed separately.
Usually, clocks on board satellites are switched on and off many times during their life, especially in the very first period after satellite launch. Therefore, many *operational lives* can be identified for each clock between two consecutive switch on.
In principle, the longer is the period of continuous operation, the larger is the probability to observe any anomaly on clock frequency. However it is possible that no anomalies are observed even in long clock lives.
One of the analysis carried out in the frame of the activity on clock feared events is the evaluation of the number of jumps observed in different periods after clock switch on. The objective is to understand, on the basis of the available experimental data, if most of the clock anomalies occur in the first periods of clock life in orbit or if they are a phenomenon which increase with the clock age.
Unfortunately no exhaustive information has been found on GPS satellite clock switch on and off.
The information about the type of clock on board different satelllites (RAFS os Cesium) and about the date of satellite launch can be found in the Web Site of the United States Naval Observatory (USNO) [88].
Therefore, even if it is not known exactly the date of the clock first switch on, the launch date is known: it is assumed that the payload switch on (then the clock first switch on) takes place not many days after satellite launch. In the next analysis we will consider the date of satellite launch, assuming that the clock switch on is close to that date.
Unfortunately, for GPS satellites, any clock switch ON/OFF operation after the satellite launch is not known.
In the analyzed period, from 2008 to 2010, on GPS constellation 25 RAFS and 7 Cesium Clocks were active as primary clock on board the satellites. On the experimental data collected for these two years, 15 among the 25 RAFS clocks and 4 of the 7 cesium clocks on board satellites experienced frequency jumps.
A total of 164 jumps has been observed on GPS satellite clocks, in two years of observations: 123 on RAFS and 40 in Cesium clocks.
All of these jumps took place in the same operational life of each clock since, from the information on the USNO FTP repository [88], none of the clocks has been switched off-on in the considered period.
In the following paragraphs there will be reported some statistics on the frequency jumps observed on GPS RAFS and Cesium satellite clocks respectively.

Only 8 of the 32 observed GPS satellites have been launched after year 2000, while most of space vehicles have been launched in the 90s. This means that unfortunately, differently on what could be observed on Galileo GIOVE data which can not be published, in the analysis on GPS clocks reported in this thesis it is not possible to observe the clock behaviour in the very first months or years after switch on. However it is interesting to observe the satellite clock behaviour when the system operates in ordinary conditions, several years after the launch.

4.4.1 GPS Satellite RAFS Clocks

4.4.1.1 Jumps Occurrence

In Fig. 4.38 is reported the number of occurrences of frequency jumps observed on different groups of 50 days after satellite launch:

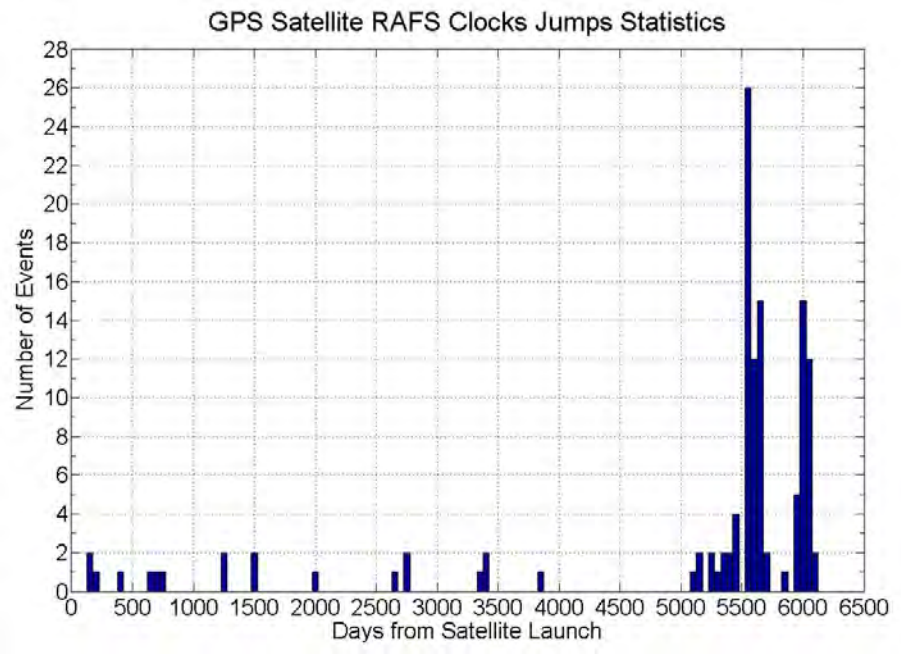

Figure 4.38: GPS RAFS Clocks: Frequency Jumps Occurrence After Satellite Launch Observed from 2008 to 2010

The first jump observed in the considered period occurs 120 days after satellite launch. It can be noted that the frequency anomalies seem to be sporadic, distributed along the whole life of satellite clocks.
It has to be remarked that Fig. 4.38 shows the occurrence of frequency jumps on all GPS satellites carrying RAFS clocks as primary reference: therefore it comprises both satellites relatively recently launched and satellites which are in orbit since more than 15 years.
The peak of 26 events is observed in the period between 5530 and 5570 days after satellite launch. Many frequency anomalies occur around 6000 days after the launch: it seem that, on the whole, most of the events happen after 15-16 years of satellite continuous operation.
The cumulative distribution of GPS satellite RAFS clocks is shown in Fig. 4.39:

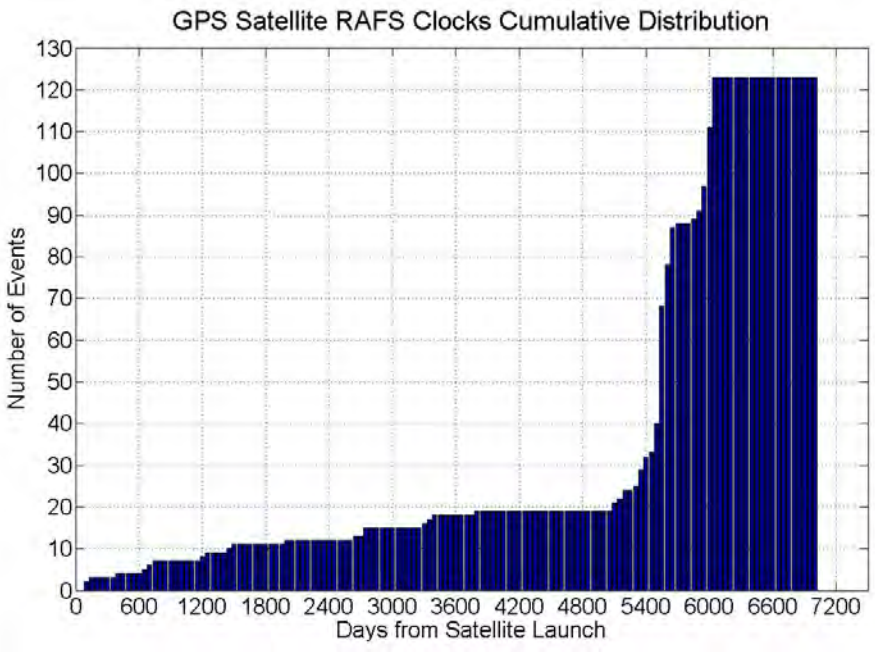

Figure 4.39: GPS RAFS Clocks: Cumulative Distribution of Frequency Jumps Observed from 2008 to 2010

4.4.1.2 Interval Between Jumps

Also the experimental distribution of the interval between two consecutive jumps has been considered and it is illustrated in Fig. 4.40. In the x-axis is reported the number of days

one has to wait to observe the next jump; there are several classes: from 0 to 5 days, from 5 to 10 days, etc. In the y-axis is reported the number of jumps observed with that delay with respect to the previous one.
The aim is to check if the frequency jumps observed in GNSS satellite clocks can be modelled as a Poisson process, in which the inter arrival times follow an exponential distribution.

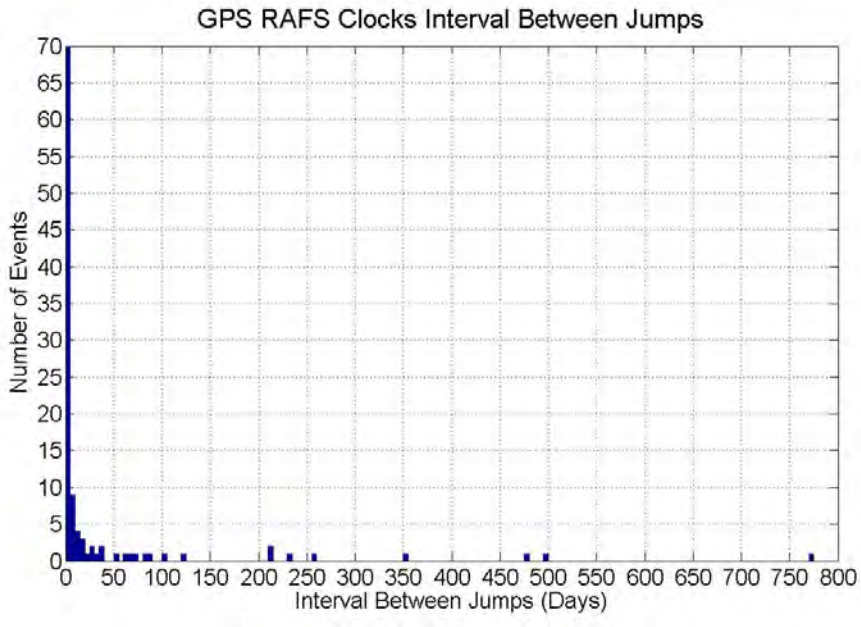

Figure 4.40: GPS RAFS Clocks: Interval Between Consecutive Jumps Observed from 2008 to 2010

Fig. 4.41 is a zoom of Fig. 4.40, reporting the distribution of the interval between consecutive jumps for the first 100 days:

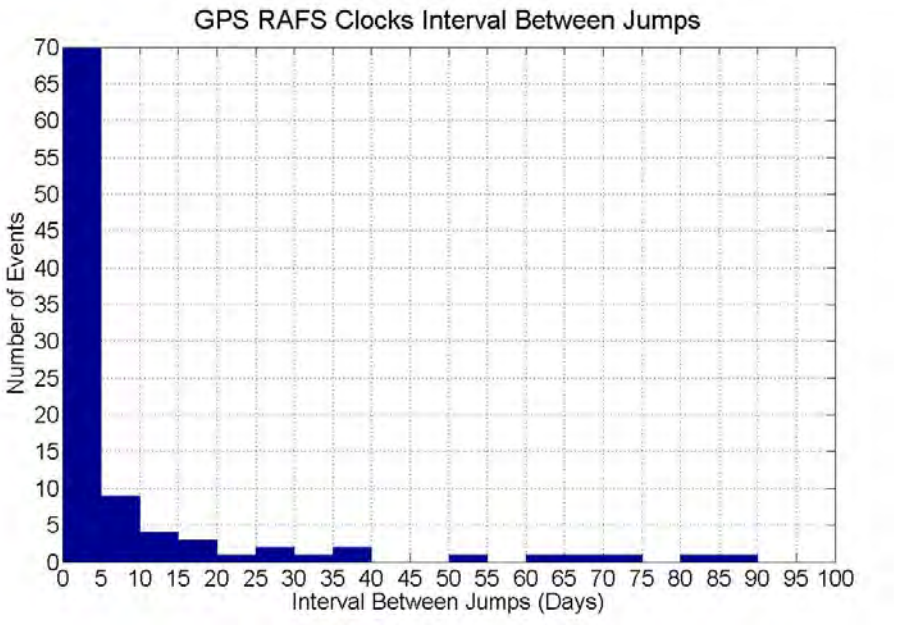

Figure 4.41: GPS RAFS Clocks: Interval Between Consecutive Jumps Observed from 2008 to 2010, Zoom on the First 100 Days

From the experimental data available for the period 2008-2010, it seems that most of the jumps (70 in the example in Fig. 4.41) occur less than 5 days after the previous event has occurred.

4.4.1.3 Jumps Magnitude

The link between jumps' age since satellite launch and jumps' magnitude has been examined. Fig 4.42 shows the absolute value of the jumps' magnitude observed on GPS satellites carrying RAFS clocks with respect to the days elapsed since satellite launch:

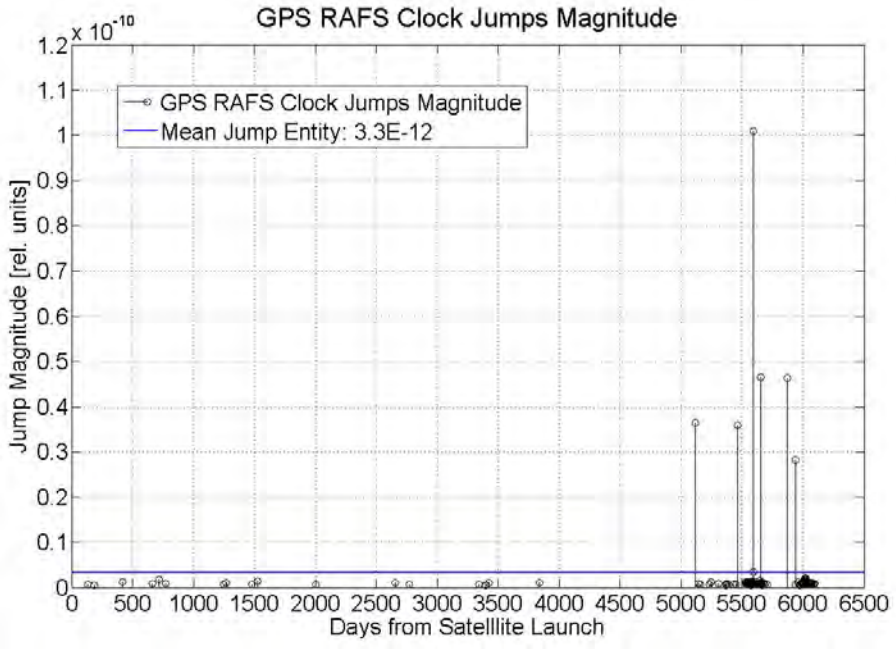

Figure 4.42: GPS RAFS Clocks: Magnitude (Absolute Value) of Frequency Jumps Observed from 2008 to 2010

The blue horizontal line is the mean value of the entity of frequency jumps observed on RAFS clocks of the GPS constellation from 2008 to 2010. The mean jump magnitude observed on the experimental data is $3.3 \cdot 10^{-12}$ relative units. It can be seen in Fig 4.42 that few jumps are much bigger than the others, being at the level of 10^{-11}, exceeding considerably the mean value. All of these big jumps appeared more than 10 years after satellite launch.

Fig. 4.43 shows the magnitude of GPS RAFS clocks, excluding the 6 big jumps present in Fig 4.42:

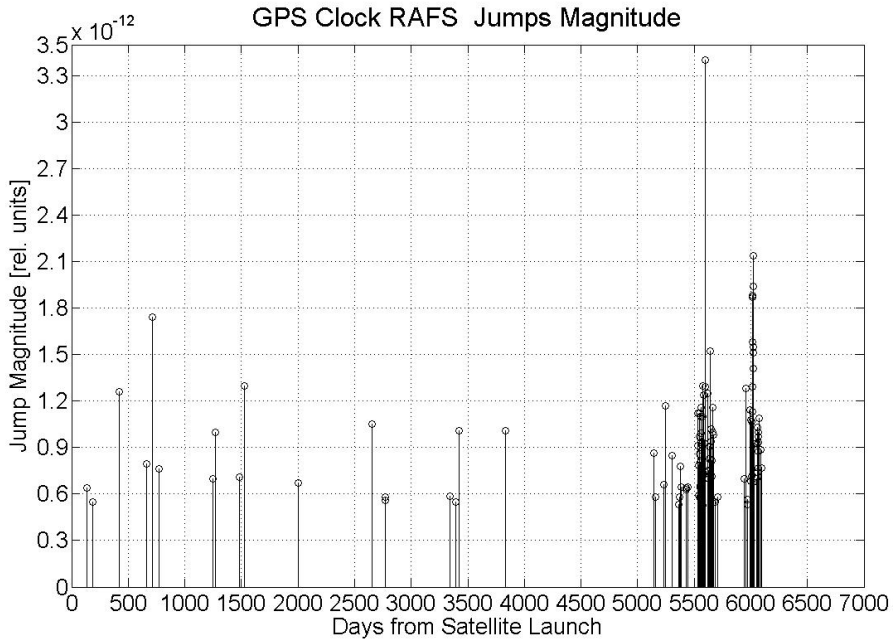

Figure 4.43: GPS RAFS Clocks: Magnitude (Absolute Value) of Frequency Jumps Observed from 2008 to 2010, biggest jumps removed

From the reported graphic it can be noted again that most of the jumps seem to concentrate around 5500-6000 days after satellite launch, that is 15-16 years after clock first switch on.
Seemingly, there is no remarkable difference in the jumps' entity for the events happening during the first years of satellite operations or those relating to the most recent periods.

4.4.2 GPS Satellite G05 (RAFS) Clocks

As mentioned, for the previous analysis on RAFS clocks, the complete constellation of GPS satellites has been considered: the results comprises both satelliets recently launched and vehicles in orbit since the 90s. To have a statistics of the feared events on a single space clock, a specific GPS satellite has been chosen: satellite labeled with PRN G05, launched on Space Vehicle 35 on August 30th 1993.

4.4.2.1 Jumps Occurrence

Fig. 4.44 reports the histogram with the jumps occurrence from 2008 to 2010, as a function of the days elapsed from satellite launch:

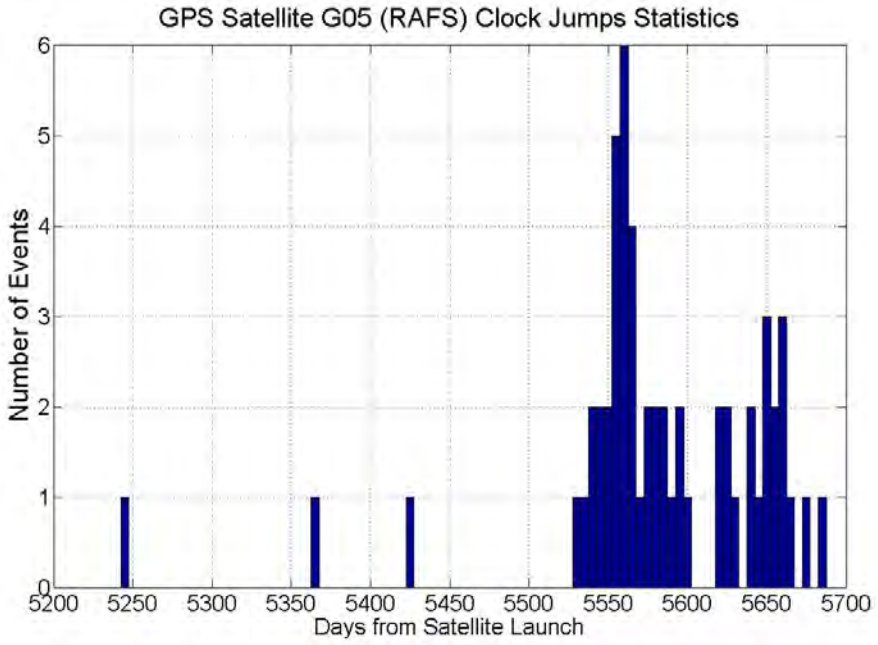

Figure 4.44: GPS G05 (RAFS) Clock: Jumps Occurrence from 2008 to 2010

The number of events in the observation period is too limited to drive general conclusions, however in the population of frequency anomalies of satellite G05 from 2008 to 2010 there is a prevalence of jumps arising more than 5500 days after the launch (15 years).

4.4.2.2 Interval Between Jumps

In Fig. 4.45 is shown the statistics of the intervals between consecutive jumps:

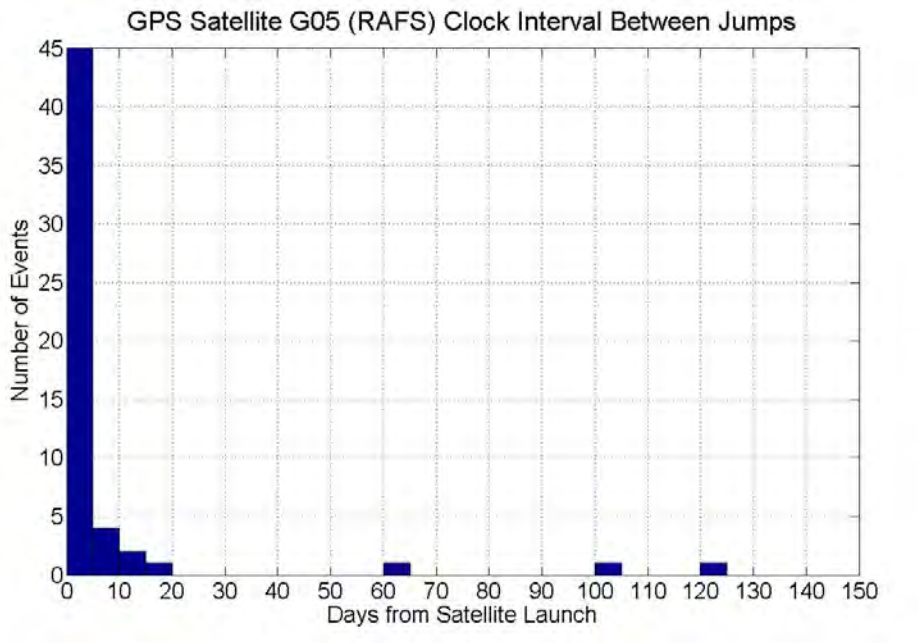

Figure 4.45: GPS G05 (RAFS) Clock: Interval Between Consecutive Jumps from 2008 to 2010

Again most of the jumps occur during the first 5 days after the previous event.

4.4.2.3 Jumps Magnitude

The entity of the observed jumps is reported in Fig. 4.46. The mean value is $8.81 \cdot 10^{13}$.

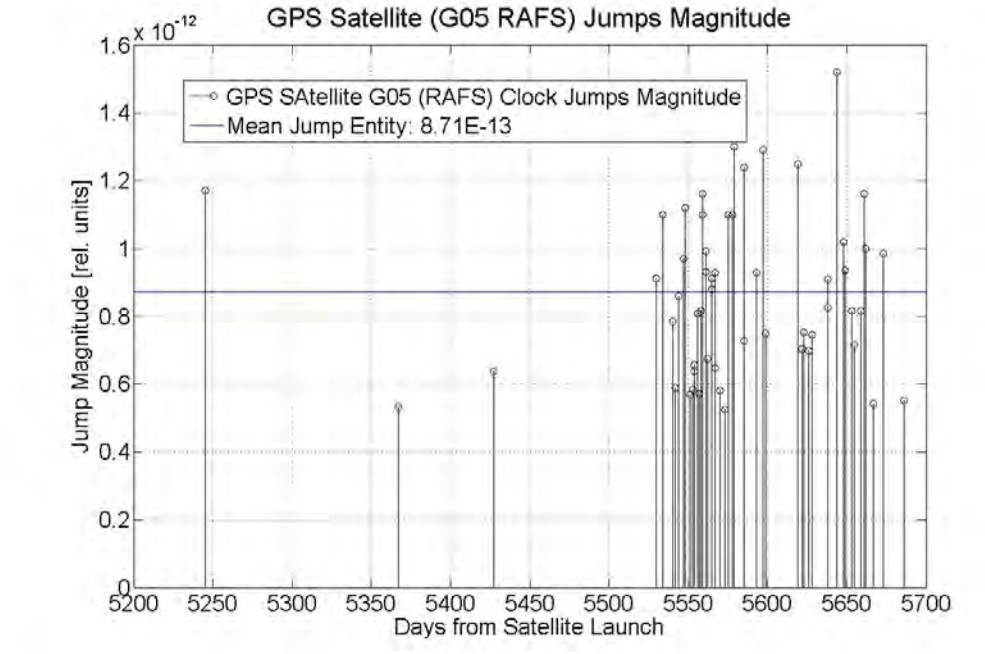

Figure 4.46: GPS G05 (RAFS) Clock: Magnitude (Absolute Value) of Frequency Jumps Observed from 2008 to 2010

As for the whole GPS constellation, also for the clock on board satellite G05 there is not any substantial difference in the jumps entity in different periods, even if the biggest happens after 5600 days since satellite launch.

4.4.3 GPS Satellite Cs Clocks

4.4.3.1 Jumps Occurrence

The histogram reporting the jumps occurrence on GPS Cesium clocks is reported in Fig. 4.47:

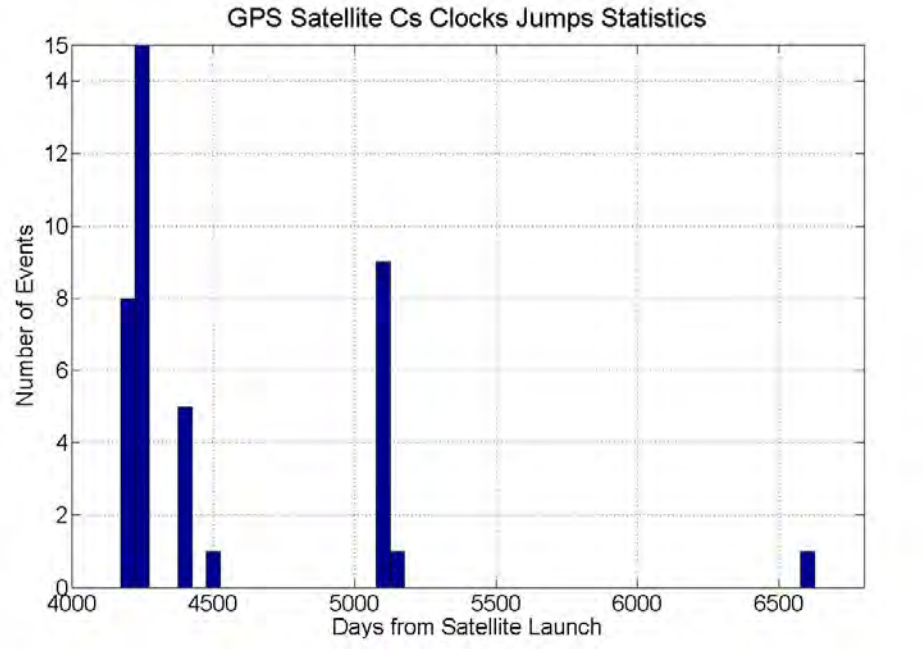

Figure 4.47: GPS Cs Clocks: Frequency Jumps Occurrence After Satellite Launch Observed from 2008 to 2010

The number of events is really limited. The peak of 15 observed frequency jumps is around 4200 days after satellite launch.
The cumulative distribution is showed in Fig. 4.48:

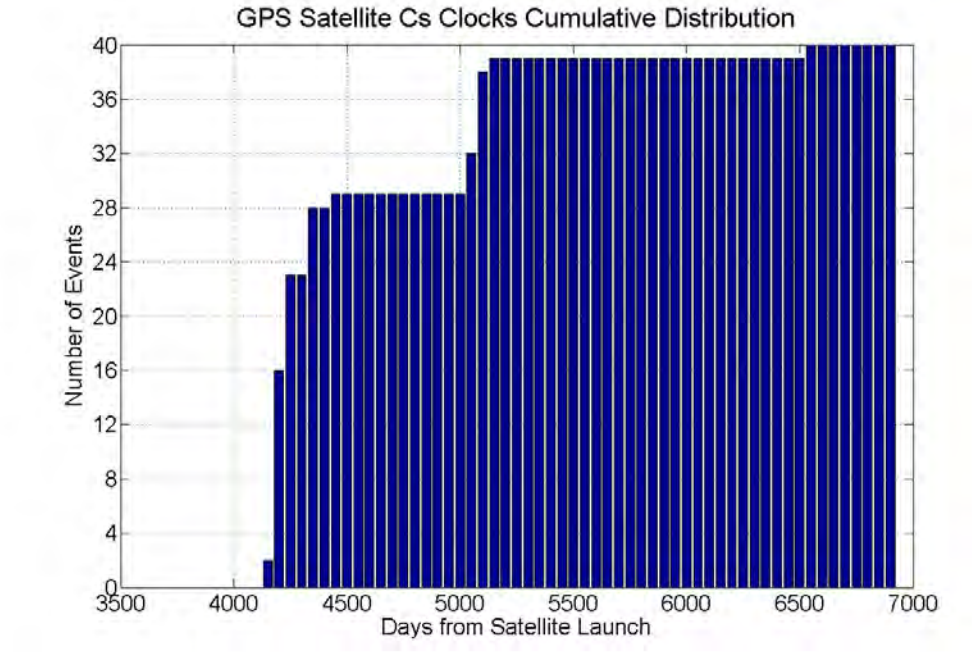

Figure 4.48: GPS Cs Clocks: Cumulative Distribution of Frequency Jumps

4.4.3.2 Interval Between Jumps

Fig. 4.49 illustrates the distribution of the interval between consecutive jumps for GPS Cesium clocks. A zoom limited to the first 100 days after the launch is reported in Fig. 4.50:

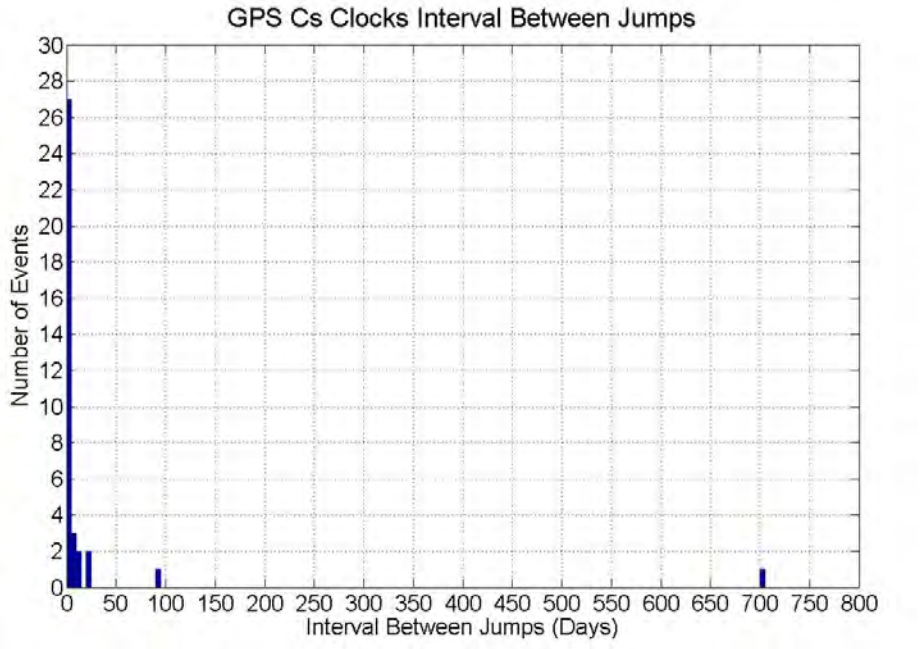

Figure 4.49: GPS Cs Clocks: Interval Between Consecutive Jumps from 2008 to 2010

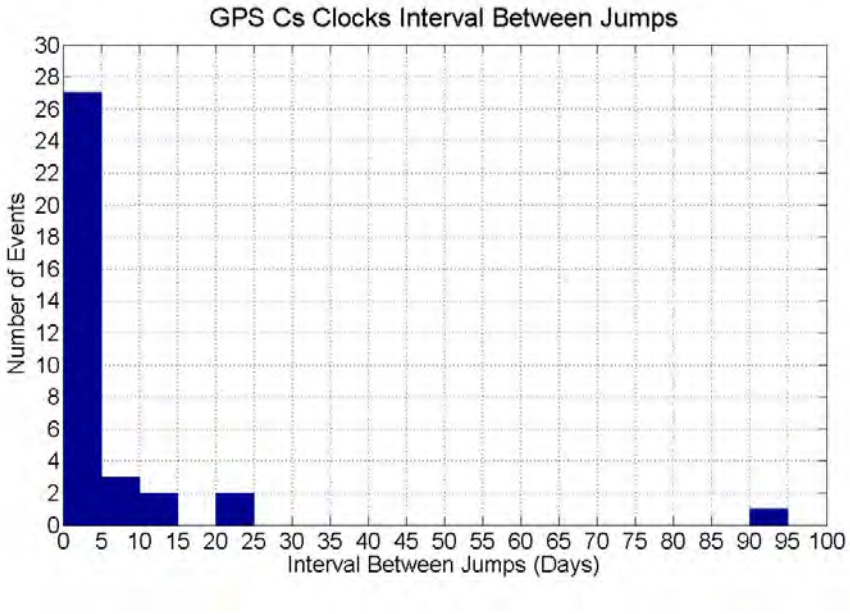

Figure 4.50: GPS Cs Clocks: Interval Between Consecutive Jumps from 2008 to 2010, Zoom on the First 100 days

Despite the number of observed events is too limited to allow a representative generalization, one can notice that once again most of the jumps occur in the first 5 days after the last event.

4.4.3.3 Jumps Magnitude

The jumps' magnitude and the respective mean value is shown in Fig. 4.51:

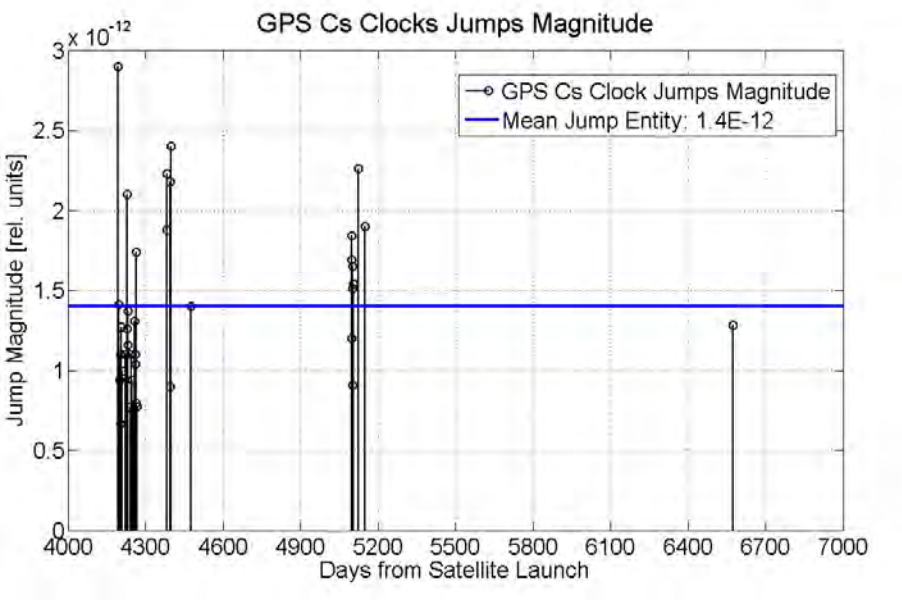

Figure 4.51: GPS Cs Clocks: Magnitude (Absolute Value) of Frequency Jumps Observed from 2008 to 2010

The mean jump entity for the analysed GPS Cesium clocks is $1.4 \cdot 10^{-12}$. From the available experimental data it can be noted that most part of the observed jumps exceeding the mean value is concentrated in the first 4600 days after atellite launch, but it is quite evident since actually the most part of events are concentrated exactly in that period.

4.4.3.4 Conclusions on GPS Satellite Frequency Jumps Statistics

The number of experimental data available in the analysed period 2008-2010 is clearly not sufficient to draw general conclusions about the behaviour of different on board clock types, nor on the behaviour of a specific clock technology in the different phases of its life. Furthermore, it has to be remarked that the analysis here reported is focused on a time period of two years, for most of clocks related to the last years of the operational life, being most of satellites launched in the early 90s.
In addition, this analysis comprises all the GPS constellation, including both satellite recently launched and satellites in orbit since more than 10 years. This allow to have a general

idea of the navigation system status in nominal conditions, since it is common to have a mixed constellation of old and new satellites, but prevent to assess the clocks behaviour in the different phases of their operational lives, starting from the clock switch on until the satellite grave yarding.
However, on the basis of the statistics performed on GPS satellite clocks in the considered period, it can be noted that:

- The occurrence of frequency jumps, both from the analysis of the complete GPS constellation and of a specific satellite, seems to be sporadic and distributed during the whole clock life, even if apparently there is a major concentration of events at a distance of 15-16 years from the satellite launch. It could be due to the clock aging, but it is difficult to say, due to the unsufficient amount of data.

- It appears that frequency jumps tend to happen in groups, since the difference between consecutive jumps is mainly 5-10 days. This consideration is common to RAFS and Cesium clocks. The agreement of the distribution of the interval between jumps and the Poisson Process cannot be confirmed due to the unsufficient amount of data.

- From the analysis of the potential connection between clock's age and jump magnitude it seems that there is no remarkable difference between the entity of jumps occurring in relative recent clock life and the jumps belonging to the period of 15 years after satellite launch. Apparently it seems that the most part of jumps exceeding the mean value happens after 5600 days since satellite launch, but the number of experimental data is too limited to draw conclusions on this topic.

Conclusions

The present work is the result of the experimental activity carried out during my PhD at the National Institute of Metrological Research (INRIM), at the Time & Frequency department. The research topic is the application of atomic clocks and time scales to Global Navigation Satellite Systems.
The research activity has been carried out mainly in the frame of the experimental phases of the Galileo project: firstly the *GIOVE Mission*, and the *In Orbit Validation* phase in the last period of doctorate.
The objective was the assessment of the metrological characteristics of the timing system, in order to verify its adequacy to the positioning and dissemination service foreseen for satellite navigation systems users.
During these years it has been necessary to develop proper algorithms and software routines in order to analyse satellite experimental data, to study the peculiar aspects of the timing infrastructure in navigation systems, some well known, others new.
One of the objectives was to give a contribution to the development of the new satellite system Galileo, taking advantage of the knowledge of GPS history and making use of the experience gained during the experimental phases with GIOVE satellites.
Particular attention has been given to the atomic clocks flown on board satellites, being one of the most critical aspects of navigation systems, and also, in case of Galileo, one of the most innovative features since the Passive Hydrogen Maser on board GIOVE-B is the first ever flown in the space.
One of my contributions has been the study and the characterisation of clocks deterministic and stochastic behaviour, as well as some activities on the clock sensitivity to environment. To this purpose, some existing processing routines have been re-adapted and some new software has been developed. In particular, in the frame of the Galileo Time Validation Facility project, for the Galileo In Orbit Validation phase, I developed a tool for the automatic generation of timing products necessary for the analysis of the performances of atomic clocks and time scales: such products have then been used for the activity of clock characterization. With this aim, I collected the available algorithms, integrated new

features and functions, giving raise to a complete software for clock validation.
The tool has been optimized for GNSS applications, applying ad hoc methods and techniques which allow to study and characterize the space clock behaviour.
The Clock Analysis Tool presented in Section 3.2.4 has been used by the INRIM staff to perform the characterization of the atomic clocks employed in the frame of the experimental phase of the Galileo Project named GIOVE Mission. The tool has been used for the analysis of the clocks flown on board the first two experimental satellites of the Galileo Project, GIOVE-A and GIOVE-B, as well as for the characterization of the clocks of the ground stations. Moreover, it has been used to analyse the data coming from the first Galileo satellites launched in October 2011.
In fact, most of the activities carried out in the last year of doctorate consisted in the design and implementation of an automatic infrastructure deputed for the generation of products to be used for the evaluation of system clock performances. Such infrastructure is part of the Galileo Time Valiadation Facility installed at INRIM in the frame of the preparation of the In Orbit Validation phase, and it has been used to characterize satellite and ground station clocks as well as the system time scale Galileo System Time.
In this framework, it has been noted the importance of having a structure as much as possible configurable, allowing to manage a variety of situations which could be even not expected initially. On the other hand, the report files with the details of the processing, especially the notifications of warnings and alarms, have been really precious to localize the issues and find a rapid solution.
In general, from the different activities carried out on space clocks some considerations can be derived.
First, the treatment of space clock data should be different from the one normally used when dealing with clocks employed in timing laboratories or time scales, because of the peculiar features of the clock technology, of the special environment and of the measurement system. For example, it is hence fundamental the development and the employment of ad hoc algorithms.
The satellite normalized clock frequency is strongly dependent on the temperature: it is indeed really important the thermal control of the environment in which the clock operates. However, in case residual effects are observed on the clock estimaqtes, they have to be taken into account and treated correctly . On the other hand, the correlation with solar radiation is not yet confirmed: no particular influence has been observed since rarely relevant radiation peaks appear.
In addition, the frequency drift of satellite clocks could be quite variable, assuming both positive or negative values, depending on the period in which it has been evaluated. The drift entity depends on the clock technology: a couple of orders of magnitude can exist

between a RAFS and a PHM clock. The frequency drift is strongly influenced by the local behaviour of the clock: frequency jumps and outliers can seriously affect the estimate. It has been noted that it is better to etimate the drift over several weeks. Besides, in the reference clock should be chosen properly in order to get a representative estimate of satellite clock drift.

The system noise is an important element to determine the quality of the analysis which are performed. From the experience gained it appears that the system noise generally allows to estimate the satellite clocks, but in the Galileo experimental infrastructure it has still to be improved with the increase of the ground stations employed in the network algorithm to generate the clock solutions, since it is currently limiting the characterization of the Passive Hydrogen Masers.

It has been likewise observed the importance of the study of the reference clock employed in the clock characterization activity, in order to be able to distinguish the behaviour of the clock being analyzed from what instead can be attributed to the reference.

On the other hand, from the study on the possible influence of ground station clocks on the satellite clock estimate, it seems that the algorithm for orbit and clocks determination developed in the Galileo project seems sufficiently robust to be not affected by potential anomalies present on single ground clocks at certain istants. In fact, ground station clocks anomalies or failures seem to be not mapped on the spacecraft apparent clocks: this demonstrates the effectiveness of the clock estimation algorithm against undesired events.

Besides, in GNSS is fundamental to notify to users any satellite malfunctioning, in a very limited time: considering the timing aspects of a navigation system, the anomalies on satellite clocks have to be detected and reported. Hence, the study and characterization of these events is useful to better understand the phenomenon and these kind of analysis are also useful for clock manufacturers who can consider the possible improvements of the clock technology.

From the experience gained in these years of doctorate and from the experimental study on satellite clock anomalies reported in this thesis, it seems that the frequency jumps are distributed over the whole satellite life, but are seemingly more concentrated after 15-16 years after satellite launch. Besides, since the time elapsed between two consecutive jumps is mainly 5-10 days, it seems that clock anomalies tend to appear in groups: it means that if one anomaly is observed, it is quite probable to observe the next one in the next 5 days. Finally, there is no evident correlation between the jump magnitude and clock age, even if the most part of big jumps occur more than 10 years of satellite life.

In this particular activity, as besides in general for the satellite clock characterization, it has been fundamental the access to satellite information such as telemetry measures about satellite payload and clock physical package, notification of clock switch-on and switch-

off...It is really difficult to drive conclusions about clocks behaviour without a complete view of satellite situation. In fact, in case of GPS,one of the major troubles encountered in these years has been the lack of information mainly due to the restricted access to certain data and documents. One example is the absence of notification about GPS satellite clock switch on or generally on the operations performed on board. In case of Galileo instead, being involved in the team developing the system, the availability of information was ensured and fundamental.
The algorithms of clock prediction are essential in GNSS since the positioning is based on the predictions received within the navigation message. Any anomaly in the clock could generate an error in the prediction: it has been observed how much a step in the clock phase or normalized frequency can impact the prediction error. Besides, the clock model to be used in the prediction shall be dynamically adaptable to the different clock technologies, which could require a linear or quadratic model (Cesium and Passive Hydrogen Maser clocks or Rubidium Atomic Frequency Standards respectively), and shall include also terms able to decribe behaviours not necessarily due to the clock itself, such as the periodic fluctuations often observed on the satellite apparent clock.
Because of the confidentiality of the results obtained in the frame of the Galileo project, most of the graphics present in this thesis are the result of simulations or come from the analysis performed on GPS data.

Acronym List

ADEV Allan Deviation

BIPM Bureau International des Poids et des Measures

CEDEX Cosmic Ray Energy Deposition Experiment

CS Commercial Service

CV Common View

DOC Depth Of Coverage

DoD Department Of Defense

E-OSPF Experimental Orbitography and Synchronization Processing Facility

ERIS External Region Integrity Systems

ESA European Space Agency

FOC Full Operational Capability

GESS Galileo Experimental Sensor Station

GIOVE Galileo In Orbit Validation Element

GCS Ground Control Segment

GMS Ground Mission Segment

GNSS Global Navigation Satellite System

GOES Geostationary Operational Environmental Satellite

GPC Giove Processing Center

GPS Global Positioning System

GST Galileo System Time

GSTB Galileo System Test Bed

IGS International GNSS Service

IPF Integrity Processing Facility

ISB Inter System Bias

MAD Median Absolute Deviation

MASER Microwave Amplification by Stimulated Emission of Radiation

MEO Medium Earth Orbit

MCS Mission Control Facility

MCS Master Control Station

NAVSTAR Navigation System with Timing And Ranging

NESDIS National Environmental Satellite Data and Information Service

NOAA National Oceanic and Atmospheric Administration

ODTS Orbit Determination and Time Synchronization

OS Open Service

OSPF Orbit Synchronization and Processing Facility

PHM Passive Hydrogen Maser

PPS Precise Positioning Service

PRN Pseudo Random Noise

PRS Public Regulated Service

PTF Precise Time Facility

PVT Position Velocity and Time

RAFS Rubidium Atomic Frequency Standards

Rinex Receiver INdependent EXchange

SA Selective Availability

SAR Search And Rescue

SCF Service Control Facility

SoL Safety of Life

SPF Service Product Facility

SIS Signal In Space

SISA Signal In Space Accuracy

SPS Standard Positioning Service

SREM Standard Radiation Environment Monitor

SRP Solar Radiation Pressure

SV Space Vehicle

SVN Space Vehicle Number

TAI Temps Atomique International

TEC Total Electron Content

TOA Time Of Arrival

TVF Time Validation Facility

TWSTFT Two-Way Satellite Time and Frequency Transfer

UERE User Equivalent Ranging Error

ULS Up Link Station

USNO United States Naval Observatory

UTC Universal Time Coordinated

Bibliography

[1] F. Dovis , P. Mulassano, *Introduction to Global Navigation Satellite Systems*, Politecnico di Torino Lecture Notes, 2008

[2] www.gpsscales.com/intro.htm

[3] Parkinson, Spilker, *Global Positioning System: Theory and Applications*, 1996

[4] E.D.Kaplan, C.J.Hegarty, *Understanding GPS: principles and applications*, Second Edition, Artech House, Norhood, MA, 2006

[5] D.W Allan, *Characterization, Optimum Estimation and Time Prediction of Precision Clocks*, IEEE Transaction on ultrasonics, ferroelectrics, and frequency control. vol UFFC-34, NO. 6, Nov 1987. pp. 647-654.

[6] D.W Allan, *Tutorial: Clock and Clock Systems Performance Measures*, Proceedings of the 27th Annual Precise Time and Time Interval (PTTI) Application Planning Meeting, San Diego, California, USA, November 29th - December 1st, 1995

[7] J. Vanier, *Recent Advances in Metrology and Fundamental Constants*, Proceedings of the International School of Physics Enrico Fermi Course CXLVI, held at Verenna on Lake Como, Villa Monastero, July 25 - August 4, 2000, Part of the Italian Physical Society series. Edited by T. J. Quinn, S. Leschiutta, and P. Tavella. Published by IOS Press, Ohmsha, Amsterdam, The Netherlands, 2001, pp 397-428

[8] C.Audoin, J. Vernier, *Atomic Frequency standards and Clocks*, J.Phys. E 9, pp.697-720, 1976.

[9] *Le Systeme International d'Unites SI*, 8th ed., Paris, France: BIPM, 2006

[10] *Time and Frequency from A to Z: An illustrated glossary*, National Institute of Standard and Technology web site, http://www.nist.gov/pml/div688/, retrieved November 2011

[11] Various Authors, *Recommendation ITU-R TF.686-2: Glossary and definitions of time and freqeuncy terms*, 2002

[12] Riley, Wti, *Rubidium Atomic Frequency Standards for GPS Block IIR*, Proceedings of the 5th International Technical Meeting of the Satellite Division of The Institute of Navigation (ION GPS 1992), Albuquerque, NM, September 1992, pp. 537-545

[13] R.Markowitz, R.Hall, L.Essen, J.Parry *Frequency of Cesium in terms of ephemeris time*, Phys. Rev. Letters, 1, 105-7, 1958

[14] G.Panfilo, F.Arias, *Algorithms for International Atomic Time*, IEEE Transactions on Ultrasonics, Ferroelectrics and Frequency Control, Vol.57, No.1, January 2010

[15] Allan, *Time and Frequency (Time-Domain) Characterization, Estimation, and Prediction of Precision Clocks and Oscillators*, IEEE transaction on ultrasonics, ferroelectrics, and frequency control, VOL. UFFC-34, N.6, November 1987

[16] Bureau International des Poids et Mesures Web Site *http://www.bipm.org/en/scientific/tai/*, accessed on February 2012

[17] *BIPM Circular T: monthly*, $http://www.bipm.org/jsp/en/TimeFtpTimeFtp.jsp?TypePub = publication$

[18] D.W.Allan, N.Ashby, C.Hodge, *The Science of Time Keeping. Application Note 1289*, Hewlett Packard

[19] D.McCarthy, C.Hackman, R.Nelson, *The Physical Basis of the Leap Second*, The Astronomical Journal, 2008 November,

[20] *http://tycho.usno.navy.mil/leapsec.html*

[21] A. Bauch, A. Sen Gupta, E. Staliuniene, *Time Scale Prediction Using Information From External Sources*, Proceedings of the 19th European Frequency and Time Forum, Besancon, France, March 21-24 2005, p.442-8

[22] , R.Zanello, M.Blanchi, E.Detoma, D.Villabruna, *Precise Timing Facility: the Time Scale for Galileo*, Proc. if the 2nd International Colloquium - Scientific and Fundamental Aspects of the Galileo Programme, Padua (Italy), October 14th-16th 2009

[23] M.Suess, A.Moudrak, E.Frolova, *Ensamble Time In GNSS - Performance Requirements and Algorithm Tests*, Proceedings of 39th Annual Precise Time and Time Interval (PTTI) Meeting, November 26th - 29th 2007, Long Beach, California (USA)

[24] Recommendation ITU-R TF.1153-3, *The operational use of two-way satellite time and frequency transfer employing PN time codes*, ITU, Radiocommunication Study Group, Geneva, March 2010.

[25] Z. Jiang, G. Petit, *Time transfer with GPS satellites All-in-View*,Proc. ATF2004, 236, 2004.

[26] D.W. Allan, C. Thomas, *Technical Directives for Standardization of GPS Time Receiver Software*, Metrologia, 1994, 31, pp.67-79

[27] G.Panfilo, P.Tavella, *Preliminary test on the steering algorithm for keeping a time scale synchronized to UTC*, Proceedings of the 2003 IEEE International Frequency Control Symposium and PDA Exhibition Jointly with the 17th European Frequency and Time Forum, Tampa, FL, USA

[28] W.Lewandowsky, F.Arias, *GNSS times and UTC*, Metrologia Vol. 48 (2011) S219-S224, doi:10.1088/0026-1394/48/4/S14

[29] U.S Coast Guard NAvigation Center *http://www.navcen.uscg.gov/*, Accessed December 29th 2011

[30] Naval Oceanography Portal, *http://www.usno.navy.mil/USNO/time/gps/*, Accessed December 29th 2011

[31] NAVSTAR Global Positioning System Joint Program Office, Interface Specification IS-GPS-200 Rev.D, IRN-200D-001, March 7th 2006, *www.navcen.uscg.gov/gps/modernization/*

[32] European Space Agency Galileo Web Site, *http://www.esa.int/esaNA/*, Last Updated August 31st 2011, Accessed January 2nd 2012

[33] G.Gatti, M.Falcone, V.Alpe, M.Malik, T.Burger, M.Rapisarda, E.Rooney, *GIOVE-B Chilbolton In Orbit Test: Initial Results from the Second Galileo Satellite*, InsideGNSS, September/October 2008

[34] European Space Agency Galileo Brochure, *The First Galileo Satellites*, BR-251, 2nd imprint, August 2006,ISSN: 0250-1589, ISBN: 92-9092-497-7

[35] European Space Agency Galileo Brochure, *Galileo The European Programme for Global Navigation Services*, BR-186, 2nd Edition, January 2005, ISSN: 0250-1589, ISBN: 92-9092-738-0

[36] J.Benedicto, S.E.Dinwiddy, G.Gatti, R.Lucas, M.Lugert, *GALILEO: Satellite System Design and Technology Developments*, Galileo World Paper, European Space Agency, November 2000

[37] European Commission Website, Directorate General Energy and Transport, Galileo European Satellite Navigation System, *http : //ec.europa.eu/dgs/energy$_t$ransport/galileo/index$_e$n.htm*

[38] W. Gurtner , *RINEX, the Receiver Independent Exchange Format*, November 2007, avilable at *http://ftp.igs.org/igscb/data/format/rinex300.pdf*

[39] International GNSS Service Web Site, *http://igscb.jpl.nasa.gov/*

[40] *NASA Space Flight Center Website*, *http : //cddis.nasa.gov/gnss_summary.html*

[41] European Space Agency *GIOVE Experimentation Results: A Success Story*, ESA SP-1320, October 2011, ESA Communications

[42] R.Piriz, M.Cueto, V.Fernandez, P.Tavella, I.Sesia, G.Cerretto, J. Hahn, *GPS/Galileo Interoperability: GGTO, Timing Biases, and GIOVE-A Experience*, Proceedings of the 38th Annual Precise Time and Time Interval (PTTI),Washing, DC, USA, December 7th - 9th 2006

[43] I.Sesia, P.Tavella, *Estimating the Allan variance in the presence of long periods of missing data and outliers*, Metrologia, 45, December 2008, pp.S134-S142

[44] K.L Senior, J.R Ray, L.R Beard, *Characterization of periodic variations in the GPS satellite clocks*, GPS Solutions, Springer-Verlag 2008

[45] I. Sesia, *Metrological characterization of clock and time scales in satellite applications*, PhD Thesis, Politecnico of Turin (Italy), May 2008

[46] I. Sesia, L. Galleani, P. Tavella, *Monitoring clocks in space systems with the dynamic Allan variance*, IEEE Transactions on Aerospace and Electronic Systems, in press

[47] J.Camparo, *Frequency Equilibration and the Light Shift Effect for Block IIR GPS Rubidium Clocks*, Proceedings of the 36th Annual Precise Time and Time Interval (PTTI) Meeting, Washington DC, December 7-9 2004

[48] M. Epstein, T. Dass, J. Rajan, P.Gilmour, *Long Term Clock Behaviour of GPS IIR Satellites*, Proceedings of 39th Annual Precise Time and Time Interval (PTTI) Meeting, November 26th - 29th 2007, Long Beach, California (USA)

[49] J.Camparo, *A Partial Analysis of Drift in the Rubidium Gas Cell Atomic Frequency Standard*, Proceedings of the 18th Annual Precise Time and Time Interval (PTTI) Meeting, December 2nd - 4th 1986, Washington, D.C, (USA)

[50] J.A.Barnes, *The Measurement of Linear Frequency drift in Oscillators*, Proceedings of the 15th Annual Precise Time and Time Interval (PTTI), Naval Research Laboratory, Washington, DC, December 6-8 1983

[51] L.A Breakiron, *A Comparative Study of Clock Rate and Drift Estimation*, Proceedings of the 25th Annual Precise Time and Time Interval (PTTI) Meeting, Marina Del Rey, CA, USA, November 29-December 2, 1993

[52] R. Willink, *Estimation and uncertainty in fitting straight lines to data: different techniques*, Metrologia, 45, May 2008, pp. 290-298, doi:10.1088/0026-1394/45/3/005

[53] A. Cernigliaro, I. Sesia, *INRIM Tool for Satellite Clock Characterization: Frequency Drift Estimation and Removal*, Accepted for publication on February 20th 2012 on MAPAN-Journal of Metrology Society of India, special Issue on Advanced Frequency Standards

[54] C.Radhakrishna Rao, *Linear statistical inference and its applications*, Second Edition, John Wiley and Sons, New York, 1972, ISBN 0 471 70823-2

[55] Press, Teukolsky, Vetterling, Flannery, *Numerical Recipes: The Art of Scientific Computing* (3rd ed.), New York: Cambridge University Press. ISBN 978-0-521-88068-8

[56] D. Gluenberger,*Optimization by Vector Space Methods*, New York: Wiley, 1997.

[57] S. Weisberg, *Applied Linear Regression*, John Wiley and Sons, USA, 2005, pp.19-46

[58] D.C. Montgomery, and G.C Runger, *Applied statistics and probability for engineers*, John Wiley & Sons New York, 1994.

[59] Joint Committee for Guides in Metrology,*Evaluation of Measurement Data - Guide to the Expression of Uncertainty in Measurement*, JCGM 100:2008

[60] H. Wodsworth, *Handbook of statistical methods for engineers and scientists*, McGraw-Hill Professional, USA, 1989

[61] Priestley M., *Spectral analysis and time series*, Academic Press, London, 1989

[62] G. Durando , G. Mana , *Propagation of error analysis in least-squares procedures with second order auto-regressive measurements error*, Measurement Science and Technology, September 2002, pp. 1505-1511

[63] F.Gonzalez, A.Cernigliaro, P.Tavella, J.P Boyero, *Clock Strategy Experimentation with GIOVE Clocks*, in Proc. of the 24th European Frequency and Time Forum (EFTF), April 13th-16th 2010, ESTEC; Noordwijk, The Nederland.

[64] C.Audoin, *Frequency Metrology*, Metrology and Fundamental Constants (A. Ferro Milone and P. Giacomo, eds.), North Holland, Amsterdam, 1980, pp. 169-222. 2

[65] Cordara, Mannucci, Pettiti, Tavella, *Misurare il tempo e la frequenza*, Ed. Il Rostro, Milano, 1997

[66] Cardinal Components Inc. Applications Brief No. A.N 1006, *Clock Oscillator Stability*

[67] J.A.Barnes, *Atomic timekeeping and the statistics of porecision signal generators*, in Proceedings of the IEEE, special issue on frequency stability, Vol. 54, N.2, pp.204-220, February 1966

[68] Barnes, Chi, Cutler, Healey, Lesson, McGunigal, Mullen, Smith, Sydnor, Vessot, Winkler, *Characterization of frequency stability*, Proceedings IEEE tran. on instrumentation and measurement, IM-20, 105, NBS Technical Note 394, 1971

[69] National Institute of Standards and Technology (NIST) website: $http://tf.nist.gov/$

[70] S. Hutsell, *Operational use of the Hadamard variance in GPS*, PTTI 1996

[71] D.N.Baker, *What is Space Weather?*, Adv. Space Res. Vol. 22, No.1, 1998, pp.7-16

[72] *NASA image*, $http://planetfacts.org/$

[73] B.Taylor, C.I. Underwood, H.Evans, K.Ryden, D.Rodgers, E.Daly, G.Mandorlo, M.Falcone, P.A.Morris, R.G.Prieto, *Results from the Galileo GIOVE-A Radiation Monitors and Comparison with Existing Radiation Belt Models*, IEEE Transaction on Nuclear Science, Vol. 54, N. 4, August 2007

[74] D. Marinov, W. Hajdas, L. Desorgher, H. Evans, P. Nieminen, *Space weather observations with four SREM radiation monitors*, 21st European Cosmic Ray Symposium, Kosice, Slovakia, September 9-12, 2008

[75] P.Galeotti, *Elementi di probabilita e statistica*, Levrotto & Bella, 1983

[76] National Oceanic and Atmospheric Administration Space Weather Prediction Center website *http://www.noaa.gov/*

[77] NOAA Satellite and Information Sevice, *http://www.goes.noaa.gov/*

[78] A.Cernigliaro, I.Sesia, *Satellite Clocks Characterization and Monitoring for Global Navigation Satellite Systems*, in Proceedings of the XXX URSI General Assembly and Scientific Symposium of International Union of Radio Science, August 13th-20th 2011, Istanbul, Turkey

[79] G. Cerretto, N. Guyennon, I. Sesia, P.Tavella, F. Gonzalez, J. Hahn, V. Fernandez, A. Mozo, *Evaluation of the ODTS system noise in the GIOVE mission*, Proceedings of the European Frequency and Time Forum (EFTF), Toulose, France, April 22nd -25th 2008

[80] IGS Tracking Network Web Site,*IRKT Log*, http://igs.org/network/site/irkt.html

[81] IGS Tracking Network Web Site,*IENG Log*, http://igs.org/network/site/ieng.html

[82] AGI Web Site *http://www.agi.com/products/by-product-type/applications/stk/*

[83] J.Ray *[IGSMAIL-2962]: USNO Ultra-rapid clock predictions.31 Jul 2000. http://igscb.jpl.nasa.gov/mail/igsmail/2000/msg00301.html*

[84] J. Camparo, *Does the Light shift Drive Frequency Aging in the Rubidium Atomic Clock?*, IEEE Transactions on Ultrasonics, Ferroelectrics, and Frequency Control, vol.52, No.5, Oct.2005, pp.1873-1880.

[85] L.Galleani, P.Tavella *An algortihm for the detction of frequency jumps in space clocks*, in Proceedings of the 42^{th} Annual Precise Time and Time Interval (PTTI) Meeting, November 15th-18th 2010, Reston, Virginia, USA.

[86] C.H. Volk, R.P, Frueholz, *The role of long-term lamp fluctuations in the random walk of frequency behaviour of the rubidium frequency standard: A case study*, Journal of Applied Physics, Volume 57, Issue 3, 1985, ISSN:1089-7550

[87] Cerretto, Cueto, Delporte, Droz, Falcone, Fernandez, Gandara, Hahn, Hannes, Langley, Mandorlo, Navarro, Piriz, Rochat, Sesia, Tavella, Waller, *Time for GIOVE-A, the Onboard Rubidium Clock Experiment*, GPS World, pp 64-69, May 2007

[88] United States Naval Observatory FTP repository, *ftp://tycho.usno.navy.mil/pub/gps/*